UNIVERSITY OF SOUTHAMPTON

Circuit Rating Methods for High Temperature Cables

by

James A Pilgrim

A thesis submitted for the
degree of Doctor of Philosophy

in the
Faculty of Engineering, Science and Mathematics
School of Electronics and Computer Science

June 2011

UNIVERSITY OF SOUTHAMPTON

ABSTRACT

FACULTY OF ENGINEERING, SCIENCE AND MATHEMATICS
SCHOOL OF ELECTRONICS AND COMPUTER SCIENCE

Doctor of Philosophy

by James A Pilgrim

For the safe and efficient operation of power transmission systems, each system component must have an accurate current rating. Since the advent of formal power networks a wide variety of methods have been employed to calculate the current carrying capacity of power cables, ranging from simple analytical equations to complex numerical simulations. In the present climate of increasing power demand, but where finance for large scale network reinforcement schemes is limited, providing an accurate rating becomes paramount to the safe operation of the transmission network.

Although the majority of the transmission network in the United Kingdom comprises overhead lines, many vital links make use of high voltage cable circuits. Advances in our ability to manipulate the properties of dielectric materials has led to increased interest among the cable community as to whether new cables could be designed which could deliver improved power transfer performance in comparison to traditional technologies. One way in which this might be possible is if the existing conductor temperature limit of 90°C common to XLPE based cable systems could be lifted. At the present time a number of polymer systems exhibit potential in this area - however prior to investing significant resources in their development, it would be valuable to scope out the magnitude of the benefits that such cable systems could deliver to a network operator.

In order to determine the scale of the operational benefit available, a comprehensive rating study would need to be undertaken. However most existing cable rating methodologies were not designed for situations with conductor temperatures in excess of 100°C and may not be suitable for the task. To allow a quantitative analysis of the benefits available from permitting higher cable conductor temperatures, cable rating techniques for all major installation types have been reviewed and improved.

In buried cable systems high temperature operation can lead to significant problems with moisture migration which is not easily modelled by traditional calculations. To overcome this a full dynamic backfill model has been created which explicitly models moisture movement and allows its impact on the thermal profile around a high temperature cable

circuit to be established. Comparison is also made to existing forced cooling techniques to benchmark the scale of the benefits attainable from high temperature operation. Cable joints become critical in such forced cooled systems - to ensure that the joint temperatures do not exceed acceptable levels a full finite element based modelling process has been developed, allowing detailed rating studies to be undertaken.

It is not always possible to bury cable circuits, for instance where they are installed in surface troughs or tunnels in urban areas. By applying modern computational fluid dynamics methods it is possible to develop more comprehensive rating methodologies for these air cooled cable systems, allowing the benefits of high temperature operation in such circumstances to be demonstrated.

By utilizing these techniques for an example cable design it has been possible to provide an in depth discussion of the advantages available from high conductor temperature operation, while simultaneously noting the potential problems which would need to be mitigated should such a cable design be deployed in an operational setting.

Contents

List of Figures

List of Tables

Symbols and Abbreviations

A	Area (m^2)
A_f	Tunnel Cross-sectional Area for Air Flow (m^2)
A_s	Surface Area (m^2)
a	Soil suction at air entry value (kPa)
C	Volumetric specific heat capacity ($kJm^{-3}{}^{\circ}\mathrm{C}^{-1}$)
C_d	Capacitance of Dielectric (F)
C_j	Thermal Capacitance at Radial Node j (J/K)
C_p	Specific Heat Capacity ($kJ/kg.K$)
c	Vapour flux (kgm^{-3})
c_{qs}	Specific heat of quartz
c_w	Specific heat of water
D_{atm}	Molecular diffusivity of saturated water vapour (m^2s^{-1})
D_e	Cable Outer Diameter (m)
D_T	Thermal diffusivity ($m^2s^{-1}{}^{\circ}\mathrm{C}^{-1}$)
D_{TL}	Thermal liquid diffusivity ($m^2s^{-1}{}^{\circ}\mathrm{C}^{-1}$)
D_{TV}	Thermal vapour diffusivity ($m^2s^{-1}{}^{\circ}\mathrm{C}^{-1}$)
D_θ	Isothermal diffusivity (m^2s^{-1})
$D_{\theta L}$	Isothermal liquid diffusivity (m^2s^{-1})
$D_{\theta V}$	Isothermal vapour diffusivity (m^2s^{-1})
D_{tun}	Tunnel Diameter (m)
F_{cc}	Cable to Cable Radiation Viewfactor
F_{cw}	Radiation Viewfactor from Cable to Wall
f	Frequency (Hz)
f_c	Coolant volumetric flow rate (m^3/s)
Ga	Air shape factor
h	Relative humidity
h_{cab}	Cable Convective Heat Transfer Coefficient (W/m^2K)
h_r	Soil suction at residual water content (kPa)
h_{wall}	Tunnel Wall Convective Heat Transfer Coefficient (W/m^2K)
K_c	Hydraulic conductivity (ms^{-1})
Ke	Kersten number
j	Diffusion of vapour flux ($kgm^{-2}s^{-1}$)

k	Thermal Conductivity (W/mK)
k_r	Relative permeability
k_{unsat}	Unsaturated hydraulic conductivity (ms^{-1})
I	Phase Current (A)
L	Volumetric heat of vaporisation (Jm^{-3})
m	Timestep Identifier
m	Function of residual water content (Fredlund calculation)
m_c	Mass of coolant (kg)
N	Total number of cables
Nu	Nusselt Number (dimensionless)
n	Number of Nodes
n	Function of rate of moisture extraction (Fredlund calculation)
P	Air pressure (kPa)
Pr	Prandtl Number (dimensionless)
p	Partial pressure of water vapour (kPa)
q	Heat flux (W/m^2)
q_L	Liquid flux diffusivity ($kgm^{-2}s^{-1}$)
q_m	Moisture flux density ($kgm^{-2}s^{-1}$)
q_v	Vapour flux density ($kgm^{-2}s^{-1}$)
Q_j	Heat Source at Radial Node j (W)
$\dot{Q}$	Heat Transfer Rate (W)
R	Ideal gas constant water vapour
R_{ac}	Resistance (a.c.) (Ω)
R_e	Reynolds Number
R_j	Thermal Resistance between Nodes j and j+1 (K/W)
T	Temperature (°C)
$\mathbf{T}$	Temperature (K)
T_f	Temperature of fluid (K)
$tan\delta$	Electrical loss factor
U	Phase Voltage (V)
$\mathbf{U}$	Liquid Water Velocity (m/s)
V	Bulk air velocity (m/s)
$\mathbf{V}$	Vapour Velocity (m/s)
V_c	Volume of coolant
V_g	Volume of gas (m^{-3})
V_l	Volume of liquid (m^{-3})
V_t	Total volume (m^{-3})
v	Moisture flux (ms^{-1})
W_c	Joule loss (W)
W_d	Dielectric loss (W)
W_s	Sheath loss (W)

y	Dummy variable of integration for the logarithm of soil suction
ϵ	Emissivity
ϵ	Porosity
ϵ_0	Permittivity
ϵ_r	Relative Permittivity
η	Dynamic viscosity of water (Pa.s)
θ	Volumetric moisture content
ω	Angular frequency
Λ	Equivalent flow area
λ	Thermal conductivity ($Wm^{-1\circ}\mathrm{C}^{-1}$)
λ_{dry}	Thermal conductivity of dry backfill ($Wm^{-1\circ}\mathrm{C}^{-1}$)
λ_i	Thermal conductivity of soil solids ($Wm^{-1\circ}\mathrm{C}^{-1}$)
λ_o	Thermal conductivity of pore medium ($Wm^{-1\circ}\mathrm{C}^{-1}$)
λ_{sat}	Thermal conductivity of saturated backfill ($Wm^{-1\circ}\mathrm{C}^{-1}$)
λ_w	Thermal conductivity of liquid water ($Wm^{-1\circ}\mathrm{C}^{-1}$)
λ_s	Sheath loss factor
ρ	Thermal Resistivity (Km/W)
ρ_d	Dry density (kgm^{-3})
ρ_o	Density of saturated water vapour (kgm^{-3})
ρ_w	Density of water (kgm^{-3})
Θ_A	Nodal temperature (K)
$\Theta_{i,j}$	Nodal temperature at slice i, radial location j (°C)
ζ	Proportion of cable surface in contact with air
σ	Stefan-Boltzmann Constant
σ	Surface tension of water (Jm^{-3})
υ	Mass flow factor
ϕ	Hydraulic Potential
ψ	Soil Suction (kPa)
ΔT	Timestep used in transient calculations (s)
Δx	Slice separation (m)
(∇T_a)	Temperature gradient in air filled pores

Acknowledgements

I would like to acknowledge the support of a number of people who have provided assistance in a wide variety of fields over the course of my PhD. Firstly I would like to acknowledge National Grid for funding the vast majority of the work contained within this thesis.

I am grateful to my colleagues here in the Tony Davies High Voltage Laboratory who have been a useful sounding board for ideas and a longstanding source of moral support and strong coffee. Particular mention should go to the laboratory technical team of Neil Palmer, Brian Rogers, Mike Smith and Melvyn Kelly, along with Richard Howell, for their assistance in carrying out practical work within the laboratory. I would also like to thank my supervisors Dr David Swaffield and Prof Paul Lewin for their support and guidance over the course of my studies and for inspiring me to finally sit down and write this thesis.

I would also like to express my gratitude to a number of engineers from outside of the University who have helped to ensure that this work has continuing relevance to industry, including David Payne and Francis Waite of National Grid, Steffen Larsen of Southampton Dielectric Consultants and Simon Sutton of Dow Chemical.

Finally I wish to acknowledge the support of Lucy Hartland throughout the good times, and the not-so-good times, over the course of my time at the University and for encouraging me to finally finish writing this thesis.

Chapter 1

Introduction

Electricity is the lifeblood of the modern digital economy, with much of our every day lives now reliant on it. Despite the huge levels of innovation in the devices which consume electricity, the manner in which that electricity is supplied has remained almost identical for the last 60 years.

1.1 Electricity Transmission in the UK

From the advent of formal power networks (c1900), there were large numbers of relatively small generating stations, each serving the needs of a local area. At the time this was the most economic model of operation, as distribution could be undertaken at medium voltages. This was a necessary step given the technological development of insulating materials at the time. Demand pressures soon began to mount, with the total system demand quadrupling in the 20 years after the power network was nationalised in 1948. This led to major changes in the economics of power generation. Larger, more efficient generation stations could be built, however these tended to be sited on coal fields (or coastal sites in the case of the new nuclear stations). Both were remote from the end users, with demand concentrated in South East England. The key development came when it became cheaper to transport the power than to transport the fuel [2].

Eventually the majority of the country was interconnected by a 132kV grid system. While this was a great success in reducing the per unit cost of electricity for the end user, it soon became apparent that a further voltage increase would also be necessary to transport bulk power over longer distances with minimal losses. This eventually led to the construction of the 275kV and finally the 400kV supergrid which is still in place today. The vast majority of the transmission network (almost 99% by distance) consists of overhead lines, stemming mainly from the fact that installation costs are almost a factor of ten lower than for the equivalent cable circuit [3]. This is exacerbated

by the fact that cables are strongly capacative meaning that cables of over 80km in length are not feasible without extensive power factor correction. However in some situations an underground cable circuit offers the only practical option, as evidenced by the 225km of high voltage cable circuits in operation on the network today. This figure is steadily increasing, with many urban network reinforcement projects being unsuitable for overhead line construction.

1.2 Development of Cables

During the early years of electrical transmission at the turn of the 20th century, the low voltages in use permitted engineers to make use of technology originally developed for telegraph cables. The innovation that really changed the way in which cables could be used was that of the oil filled cable system in 1920. These cables were constructed by winding paper tapes around a copper conductor, with the whole assembly then being immersed in oil to impregnate the paper. This massively increased the electrical breakdown strength of insulation from 4kV/mm to 40kV/mm, enabling the construction of cables at 132kV and above [4]. By housing the cable in a reinforced lead or aluminium sheath, covered in a protective polymeric oversheath it was possible to build a reliable cable system. During the original construction of the supergrid in the late 1960's and early 1970's, the technology was developed further with the construction of 400kV oil filled cables [5].

While this technology was reliable, with many circuits still operating today more than 40 years after their installation, it did present a number of drawbacks. Jointing the cables was a complex task, with joints prone to failure. The need to maintain oil pressure in the cable system across its potential range of operating temperatures required additional ancillary equipment and oil tanks, while the oil itself could pose a problem if the cable began to leak. During the late 1970's, advances in polymer science yielded cross-linked polyethylene (XLPE) as a potential replacement material for cable insulation [6]. While XLPE was mainly used at lower voltages initially, as confidence in the technology grew it eventually began to displace oil impregnated paper to become the insulation system of choice at transmission voltages. At the present time there is very little production of oil filled cable remaining in Europe, with most new installations on the National Grid network in the past decade using XLPE cable systems. Few major drawbacks have been found to the use of XLPE, however it is not a particularly sustainable material as it can not be melted for the purpose of recycling.

1.3 Rating of Cables

The limiting factor on the amount of power that can be transferred through a high voltage cable is typically determined by the maximum operating temperature of the cable. This limit arises partly due to the impacts of thermo-mechanical forces on the cable system, but most commonly due to the temperature limit on the dielectric. In the case of XLPE systems the limit commonly imposed is 90°C as a host of degradation processes begin to occur faster above this point. Defining the current rating hence requires the solution of a thermal problem, as the current rating itself is dependent on the temperature of the dielectric. The cable system will always operate at a higher temperature than the local ambient, owing to the presence of electrical losses in the conductor, dielectric and sheath. As the cable begins to heat up, thermal energy is transferred to the local environment. The rating calculation must therefore evaluate this balance between heat generation in the the cable and the transfer of this heat to the local environment away from the cable in order to find the critical point at which the temperature limit on the cable might be exceeded.

For the operation of the transmission network, a number of different rating specifications may exist for a cable circuit. Perhaps the most straightforward is the continuous rating, which is defined as the maximum continuous ac load current which can be carried through the cable circuit without exceeding the specified conductor temperature limit. At the medium voltage distribution levels, the continuous rating is likely to be the only one which is specified for a circuit. At transmission level, cable is typically purchased based on its continuous rating.

In reality, a cable circuit in the transmission network will never operate at its maximum rated continuous current all of the time. This is a consequence of the network design principles used, as the supergrid must operate with sufficient spare capacity to cope with unexpected failures and limited circuit outages for maintenance reasons. This gives rise to the concept of an emergency rating, defined as the maximum load current which can be transferred for a stated period of time (for instance six hours) without exceeding the conductor temperature limit, but based on previous operation at a defined continuous preload. Operationally these ratings have great significance as they allow power flows to be diverted, for instance where a circuit must be taken out of service to effect a repair. For certain cases a cyclic rating may also be specified, but at transmission voltage levels this is normally restricted to circuits which have unusual load profiles such as those attached to hydroelectric generating stations [7]. The use of cyclic ratings is more common at distribution voltage levels.

1.4 Cable Installations

As was noted in section 1.3, the thermal environment in which a cable is installed can have a substantial impact on the rating of the circuit. Perhaps the most straightforward installation scenario is that of direct burial, where cables are placed in a trench through the native soil. The trench can then be backfilled with either the original soil or an imported backfill of higher thermal performance. Where cables are to be installed in rural areas this is the preferred method as it offers the lowest installation cost.

Where circuits are required to meet higher loading requirements than a standard burial arrangement might permit, a common technique in the UK is to install water cooling pipes around the cables. This is frequently a requirement where short sections of cable sit in between long lengths of overhead line, as the continuous rating of the overhead line is generally much higher than that achievable from non-forced cooled cable circuits. Typically the pipes are arranged such that water is input into two pipes between the phases (pipes 2 and 3 in Figure 1.1), and then returned to a cooling station via the two outer pipes. Systems of this kind were first installed on the 275kV network in the London area, prompted by a previous cable failure which occurred due to the soil around the cable drying excessively [8].

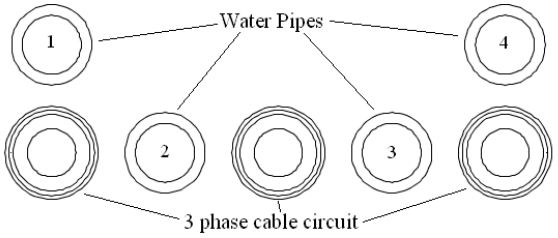

FIGURE 1.1: Water pipe locations for forced cooled cable circuit

A common installation method for shorter lengths of cable is that of surface troughing. For the most part, these installations are used for short runs of cable in substations and do not contain a backfill. The trough itself is manufactured from pre-cast concrete sections which are buried into a shallow trench such that the lids of the troughs are flush with the ground. Some longer installations do exist in London where troughs have been built into canal paths, however the practise is now largely superseded [8].

The final common installation method is that of the cable tunnel. These were relatively rare until the construction of the 400kV supergrid when they began to be used for river crossings where overhead lines were impractical, for instance at Southampton Water and under the Thames [9, 10]. In recent years the popularity of tunnel construction has increased in urban areas, where the level of disruption caused by large scale direct burial led to the higher capital cost of tunnels becoming more acceptable [11]. The longest cable tunnel in the UK was recently commissioned between Elstree and St Johns

FIGURE 1.2: 400kV XLPE cable installation in a tunnel

Wood [12], with several new transmission tunnels being planned at present. Significant amounts of the central London 132kV network have also been installed in tunnels [13].

1.5 Research Motivation

Of the presently existing cable technologies, both oil-paper and XLPE dielectrics are capable of operating to approximately the same temperature, typically a maximum of 90°C. Beyond this temperature, a number of problems are encountered. The rate of ageing due to depolymerisation in paper dielectrics has been found to double for every 6°C increase in temperature [14], with similar bulk degradation being observed in XLPE systems [15]. As understanding of the structure of polymeric dielectrics evolves still further, it may be possible to develop a material which lifts the temperature limit to over 100°C. For instance, recent work on polypropylene systems suggests that these materials may be a suitable candidate for replacing XLPE [16]. However, prior to developing new high temperature cables it is desirable to quantify how much of an improvement the new system might provide. In order to do this, it is necessary to evaluate the current ratings of such systems to allow a sensible discussion of where the benefits in the new technologies might lie. To be able to undertake this effectively, it is necessary to perform a critical analysis of present circuit rating methods. As the

existing calculation methodologies were designed for systems which would not operate beyond 90°C, they rely on simplifying assumptions which may not hold true under more extreme operational conditions.

1.6 Contributions of this Thesis

In answering the research motivation presented in Section 1.5, this thesis makes two significant contributions to the state of the art in the area of cable ratings. Firstly significant improvements in calculation methodology are presented which allow the calculation of ratings for existing cable circuits in situations where previously engineering judgment was relied upon over any standard calculation methodology. One such example is the case of partially ventilated cable trough installations. This has been achieved by applying modern computational techniques such as finite element analysis to bring improvements in both the precision and accuracy of rating calculations. The methods described within this thesis have already proven valuable when applied to operational transmission circuits and have been widely published at conferences and in leading international journals (the reader is referred to Appendix A for full details of publications derived from this thesis).

The second key contribution of this thesis is a comprehensive analysis of the potential offered by high conductor temperature (greater than 100°C) operation of transmission cable circuits. Through applying the new calculation methodologies developed, it has been possible to thoroughly investigate the possible benefits of such a technology and identify key application areas to which it would prove best suited. This analysis would prove extremely valuable both to cable manufacturers considering developing such technologies, and to electricity utilities assessing the operational benefits available to them from the installation of high conductor temperature cable circuits. Taken together, these two key contributions offer a significant step forward in the state of the art for cable rating calculations.

1.7 Thesis Structure

This chapter has outlined the general role of high voltage cables within the electrical transmission grid in the United Kingdom. The cable technology in present use has been described and observations made on the possible deployment scenarios for these cable circuits. Obtaining accurate current ratings for such cable circuits is vital in operating the grid in the most efficient manner practicable. If the current rating is specified too low, the cable may be under-utilised or in extreme cases network reinforcements may be constructed which are not truly necessary. On the other hand, an overly optimistic current rating has the potential to lead to excessive ageing of the cable asset and increase

the possibility of premature failure, leading to the early replacement of an expensive asset. Given the capital constrained environment in which today's privatised electricity network operates, neither of these scenarios is desirable. The remainder of this thesis intends to address these concerns such that the optimum balance between these two extremes can be found.

To provide both adequate background and inform the future direction of the work, a comprehensive review of the literature has been undertaken. Chapter 2 presents a summary of the key findings, including a critique of the existing cable rating methodology. Failings are highlighted and prioritised to allow improvements in performance to be made through the research effort which follows.

Chapter 3 introduces in-depth analysis of the reaction of soils to thermal gradients, starting from the common assumption of a uniform backfill medium before going on to examine in more depth the parameters affecting the movement of heat away from the cable system. A candidate backfill system has been identified for laboratory testing and a detailed characterisation undertaken to facilitate the derivation of backfill properties. From this work a more advanced backfill model has been developed to attempt to account for local variations in backfill thermal conductivity due to movement of soil moisture under temperature gradients. This has been compared to a number of laboratory experiments in order to verify the performance of the numerical model against a physical benchmark.

Having developed the more advanced backfill model, Chapter 4 presents a method by which the technique can be integrated into circuit rating models for buried cable circuits. These models have been used to obtain ratings for a standardised polymeric cable design at both conventional and enhanced conductor temperature limits. Comparisons are made between the results of these models and more simplistic treatments of the cable backfill and the sources of differences identified. This process highlights modes of cable circuit operation which stand to benefit from a lifting of the conductor temperature restriction.

Chapter 5 presents numerical methods for the analysis of cable joints, which can prove to be the limiting factor on the rating of a cable circuit in certain circumstances. The results obtained demonstrate that the jointing of high temperature cables could prove to be one of the main challenges in the design of such a system, owing to the disparity in the effectiveness of cooling systems between the joint and the parent cable.

In Chapter 6 the focus shifts to cooling of cables by forced air ventilation, with an appraisal of the potential offered by high temperature cable circuits operating in tunnels. To facilitate this a revised rating model has been developed to allow consideration of cable tunnels where multiple circuits are operating at different temperatures. Ratings of cables in air filled surface troughs are examined in Chapter 7 to conclude the study of different application areas. The final chapter summarises the deployment options for

high temperature cables which offer the greatest potential, and highlights the improved rating methodologies developed throughout the course of this work.

Chapter 2

Cable Rating Methodology

Soon after the development of the first high voltage cable systems, it became apparent that standard approaches to calculating the maximum current rating would need to be found, with some of the earliest work being undertaken by Kennelly in 1893 [17]. Since this time numerous researchers have examined thermal problems relating to cable systems, eventually leading to the development of a number of international standards. This chapter seeks to identify the key issues relating to the thermal performance of cable circuits, identifying the existing calculation methodologies and reviewing their potential applicability to cable circuits with elevated operating temperatures.

2.1 Heat Generation in Cable Systems

The main reason for the existence of cable rating calculations is the relatively large levels of heat generated by the electrical losses within the cable. Three main heat sources exist, two of which are dependent on the load current in the circuit, and one on its operating voltage. Perhaps the most significant of the electrical losses is the joule loss, W_c which occurs due to the electrical resistance of the conductor. This resistance R_{ac} leads to a reduction in electron energy as current, I, flows, with this energy being dissipated almost entirely as heat. The magnitude of the joule losses is easily defined using

$$W_c = I^2 R_{ac} \quad [W] \tag{2.1}$$

The conductor ac resistance is not a constant and is influenced by a number of parameters, including the conductor temperature, geometry (through the skin effect) and the proximity of other cables. Suitable calculation procedures are laid out in [18]. The second set of current dependant losses are the sheath losses, W_s, which occur through circulating currents being induced in the metallic cable sheath, and through eddy current losses owing to the skin and proximity effects. These losses are defined according

to

$$W_s = \lambda_s I^2 R_{ac} \ \ [W], \tag{2.2}$$

where λ_s is defined as the sheath loss multiplier. Thirdly, heat is generated by the dielectric loss, W_d, which is dependant upon the phase voltage, U, squared. These losses occur as the insulation is not perfect, hence allowing some currents to flow and charge to accumulate. Effectively, the dielectric acts as a capacitor, C_d, with an associated real power consumption [19]. The dielectric loss is defined as

$$W_d = 2\pi f C_d U^2 tan\delta \ \ [W], \tag{2.3}$$

where f represents the frequency of the voltage waveform in Hz, and $tan\delta$ represents the tangent of the dielectric loss angle.

Full discussion of the above relations can be found in [20]. The method of heat transfer by which heat from these sources is removed depends on the installation conditions. For buried cable circuits heat conduction is the dominating factor, whereas for installations in tunnels heat transfer modes of convection and radiation are much more significant than conduction, due to the low thermal conductivity of air [21]. The following Sections outline the rating methods presently used for transmission cable systems, including discussion of particular failings of each method and enhancements suggested by other authors.

2.2 Buried Cable Systems

A variety of different methods, both analytical and numerical, have been developed for the computation of ratings for buried cable systems. Traditionally analytical solutions have been preferred, partly because the problem can be well suited to such techniques if a number of simplifying assumptions are made. While the discussion of the early work in this field is not without merit, the majority of the applicable knowledge was drawn together in the review paper of Neher and McGrath [22]. This later acted as the basis for the IEC 60287 standard approach for calculating the continuous ratings of buried cable circuits [18]. Where water-cooled cable circuits are to be rated, numerical techniques are normally more advantageous, with the most common being that of Electra 66 [23]. The following Sections present a critique of these methods, drawing out the potential issues with their use for cables at elevated temperatures.

2.2.1 IEC 60287

IEC 60287 is an analytical method for the calculation of the continuous ratings of buried cables, although relations are also provided for cables installed in free air. The simplest

form of the equations used assumes that 3 single core cables are installed in a homogeneous medium (either a solid medium of constant thermal resistance or free air). IEC 60287 defines the phase current, I, as

$$I = \left[\frac{\Delta\theta - W_d[0.5T_1 + n(T_2 + T_3 + T_4)]}{RT_1 + nR(1 + \lambda_1)T_2 + nR(1 + \lambda_1 + \lambda_2)(T_3 + T_4)} \right]^{0.5} \tag{2.4}$$

where $\Delta\theta$ is the conductor temperature rise above ambient (°C), R is the conductor ac resistance at maximum operating temperature per unit length (Ω/m), W_d is the dielectric loss per unit length (W/m), T_1 is the thermal resistance between conductor and sheath per unit length (Km/W), T_2 is the thermal resistance of the bedding between sheath and armour per unit length (Km/W), T_3 is the thermal resistance of the serving per unit length (Km/W), T_4 is the thermal resistance between cable surface and the surrounding medium, n the number of load carrying conductors in the cable, λ_1 the ratio of losses in the metal sheath to total conductor loss and λ_2 is the ratio of losses in the armour to total conductor loss. For all of the work presented within this thesis it is assumed that the 400kV cables are cross bonded. Although the values of sheath loss have been calculated, recent work by Cigré suggests that they can be neglected for cables with a copper wire screen and aluminium foil sheath [24].

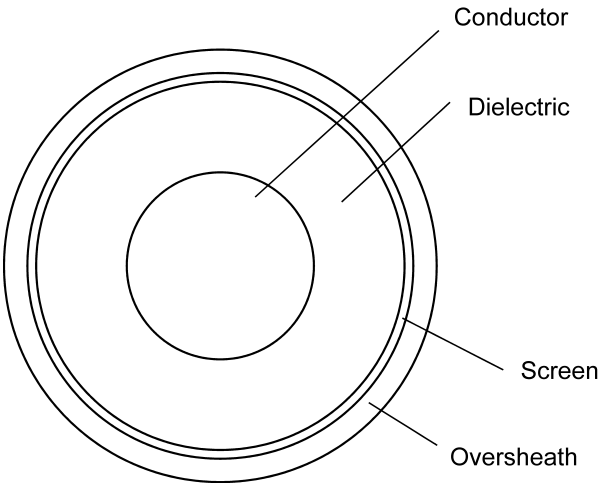

FIGURE 2.1: Schematic of typical non-armoured 400kV cable

The full procedure for the derivation of cable losses is largely similar to that of [22]. The ratios of losses λ_1 and λ_2 are determined according to the specific cable formation under consideration. Relations are given for single core cables in flat or trefoil formation, both with and without transposition. Through the same method it is possible to account for variations in spacing between sheath bonding points, differing types of armour and the presence of steel pipes. Load sharing amongst single core cables operating in parallel can be addressed through the examination of losses due to circulating currents [25].

Section 2.1 of the IEC 60287 standard outlines the calculation of the external thermal resistances, which are generally unique to each situation and allow the surrounding

environment to be defined [26]. The differing cable installation types are accounted for through reduction factors, defined for most common cases such as trefoil and flat formation installations. This also allows for the inclusion of effects such as proximity to a tunnel wall [27]. Some provision is made for the cases of cables which cross external heat sources, although this requires that the principle of superposition applies, which forces the introduction of a number of assumptions, for instance, that the area surrounding the cable has uniform thermal characteristics and that the ground surface is an isotherm. Some of these assumptions have begun to be challenged in later studies, for instance [28], which demonstrated that the use of a ground surface isotherm could over-rate a circuit by as much as 14% at shallow burial depths, although better results were seen at greater depths. As a result further increases in conductor temperatures are likely to be unsuited to this method. Although provision is made for the drying out of soil due to moisture migration, the treatment is relatively simplistic in that only two zones are considered, one which is assumed to be wet and the other which is fully dry.

2.2.2 IEC 60853

Transient and cyclic ratings for cables operating at voltages of 36kV or greater can be determined analytically using the method of IEC 60853-2 [29]. A number of methods are similar to those used within IEC 60287, for instance those determining the thermal resistances of system components, although much of the original work can be attributed to Goldenberg [30]. Lower voltage cables are not rated by this method as for the most part their thermal capacitance is negligible. The method relies on decoupling the thermal transient within the cable from the transient behaviour of the thermal environment in which the cable is located [31]. While this approach is justifiable, as the time constants involved in the two areas are very different, the method does pose a number of notable assumptions.

- Soil thermal resistivity and diffusivity are assumed constant.
- The ground surface is assumed to be isothermal.
- All cables are assumed to be subject to the same load cycle.

At present there does not appear to have been extensive verification of the IEC 60853 methodology and limited amounts of benchmarking have been undertaken against other techniques. The restriction that all cables present must be subject to the same load cycles prevents the application of the technique to more complex cable laying arrangements, and the requirement for an isothermal ground surface may prove an issue with higher conductor temperatures.

2.2.3 Cigré Electra 66

Published by Cigré committee 21-08, this method provides a guideline for obtaining the rating of a forced-cooled cable system via a numerical method [23]. In this case a forced-cooled system can be considered to be a buried cable circuit where additional cooling is provided, either by conductor cooling, surface cooling (for instance where the cable is enclosed within a water pipe) or external cooling (where coolant pipes run adjacent to the cables) [8]. There is no particular restriction on the range of Reynolds number, Re, with which the method will function, however not all quantities are well defined under transition flow ($1000 \leq Re \leq 3000$). Four key assumptions are applied to simplify the problem, the first being that the conductor, sheath and coolant pipe are assumed to be isothermal. Cable losses are assumed constant with length, with dielectric losses lumped at the conductor and sheath. It is also assumed that all material properties are independent of temperature. In reality the cable losses will increase slightly as the temperature of the water increases along the cable route.

The method implements a finite difference algorithm to determine the cable and coolant temperatures along the route, based on an initial estimate of the circuit loading. An iterative procedure is then used to arrive at the final value of permissible cable load, based on the specified maximum temperatures. At each point along the circuit route a slice of the geometry is taken, with a mesh then being applied to it. The number of nodes is defined by the cooling type being modelled. Heat transfer equations are then applied at each node to allow the calculation of temperatures throughout the 2D slice, based on the initial conditions (for instance water inlet temperature, initial cable loading). Thermal resistances other than those specifically linked to water cooling are as per IEC 60287 [26]. Slices are then axially linked along the route to allow the full circuit temperature profile to be obtained. Cable joints are not directly considered, although it is possible to extend the method to allow for this [32].

2.2.4 Cigré Electra 104

A number of different methods have been recommended for the calculation of cyclic and transient loads in forced-cooled systems; however the most commonly used is that published in Electra 104 by Cigré [33]. A more in-depth and accurate numerical method was published in [34], however the simpler method was found to be sufficient in most cases. For the case of interest to this project (external pipe cooling), two approaches are presented for use depending on the length of the transient under consideration.

For short duration overloads, it is considered that the increase in losses above the preload causes heating only in the cable and the soil immediately surrounding it. This simplifies the thermal transient to one which occurs in the radial direction only. Such an assumption allows the transient, calculated using [35], to be super-imposed on top of the

steady state preload solution obtained from Electra 66. Longer transients are dealt with by calculating the temperature rises for short transients and extrapolating the result to achieve either the maximum temperature or the desired overload duration. Similar procedures are used to determine temperatures under cyclic loading.

2.2.5 Finite Element Methods

Advances in computing hardware in recent years have made finite element methods much more accessible and suitable for everyday use, as the time required to build and solve a model has fallen substantially since the early works of researchers such as Flatabo [36]. One of the major uses of the technique has been the verification of existing, simpler methods. IEC 60287 has received much of this attention owing to its prevalence, with work from researchers including Swaffield et al [37], Walker [38] and Aras et al [39]. The agreement observed between the analytical method and more complex FEA methods was generally good at reasonable burial depths, however the work of Swaffield highlights one particular problem with the assumption of an isothermal ground surface. At shallow burial depths, forcing an isothermal solution at the ground surface leads to a significant impact on the thermal field around the cables. As a result the ratings calculated were optimistic in comparison to the assumption of a non-isothermal free or forced convective boundary condition.

Similar work has been undertaken on the Electra 66 model, however in this case the agreement between the standard model and a finite element solution was very good. This was attributed to the fact that the presence of the water pipes around the cable cools the ground sufficiently, such that an isothermal ground surface becomes a more reasonable assumption [40]. Other authors have made use of improved computational capabilities by trying to better represent the thermal behaviour of the backfill around the cable, for instance [41], which sought to couple the effects of moisture migration around the cable circuit with the temperature changes caused by the cable operation. Similar work was undertaken by Preece and Hitchcock [42]. While finite element methods may offer many benefits, it is also vital that the problem is not overcomplicated through the inclusion of unnecessary detail in the analysis.

2.2.6 Real Time Methods

In recent years researchers from both industry and academia have reported on the potential of real time thermal ratings (also termed dynamic ratings by some). Such techniques have been under research for several decades, with some of the earliest work carried out by the National Grid Company who made use of a cable system monitoring network to provide real time thermal ratings [43]. Another commercial real time monitoring system has been detailed by Anders, with computation still based on the Neher-McGrath and

IEC 60287 methods [44]. Through the use of temperature monitoring, cable hotspots can be found and a rating for the whole cable then based around these conditions. Benefits can be introduced through the knowledge of the cable loading history at any instant in time, although this would add severely to the complexity of the analysis for standard mechanistic models. Temperature data might not always be available, but methods do exist for inferring conductor temperatures from the known current data. Anders and Brakelmann have described a method by which the temperature dependence of losses is investigated to provide an improved loss factor which finds use in real time ratings assessments [45].

In order to calculate real time ratings with any level of accuracy, it is vital to know the cable temperature at any given time. This is most regularly achieved through the use of distributed temperature sensing (DTS), undertaken through fibre optic methods [46]. In order to determine the temperature at any point, a pulse of light is transmitted down an optical fibre which is attached to the cable. By analysing the wavelength of the "Anti-Stokes" Ramen band of scattered light as received back at the detector, it is possible to derive temperatures with a spatial resolution of 1-2m. Fibres may be attached to the outer sheath of a cable, or integrated into the cable construction, or even run separately in tunnels to measure ambient temperatures. Owing to the use of optical technology, DTS is not affected by electromagnetic interference which makes it especially suitable for power applications [47]. One particular method has been developed by Williams et al which uses the DTS measurement to directly obtain cable hot spot temperatures [48]. However the quality of the results obtained depends on there being a good contact between the DTS fibre and the cable itself. While this is generally the case for buried cable systems, the same is not always true for cable tunnels where a more rigorous attachment is needed.

2.2.7 Development Requirements

This review has highlighted a number of areas in which the traditional cable ratings methodology might fall short of being able to accurately rate next generation high temperature cable circuits. It is clear from the previous work on the IEC 60287 standard that an isothermal ground surface will be inappropriate for cable temperatures above 90°C as optimistic ratings will be produced. As the margins of error presented in [49] between the analytical and numerical methods at low burial depths are quite substantial, this would not lead to a fair assessment of the capabilities of the new technology. As this feature is common to the majority of transient methods, the new method must be capable of both continuous and transient calculations.

Perhaps an even more serious problem is that posed by moisture migration, as highlighted by [41]. Given that moisture migration is known to occur where conductor temperatures do not exceed 90°C, it is without doubt that some allowance must be

made for the phenomena above this temperature. As this problem lends itself to the finite element method far more so than any other kind of calculation, it would seem prudent to adopt this technique from the outset. In order to best characterise moisture migration, additional research will be required within the fields of soil mechanics and physics. This is discussed further within Chapter 3.

2.3 Tunnel Cable Systems

The normal rating method for tunnels where the cables are installed in air is that of Electra 143, although numerous others have been proposed. Some earlier work from researchers such as Weedy has been drawn into the Electra 143 method [50]. The main methods are outlined briefly in the following sections.

2.3.1 Electra 143

The numerical method of Electra 143 is still the most widely used method for calculating cable ratings in tunnel installations [50]. It allows the determination of both steady-state and transient ratings for shallow and deep tunnels (a deep tunnel being one where heat transfer between the tunnel and ground surface is negligible). Based on a lumped parameter thermal-electrical analogue approach, the method uses a one-dimensional thermal network to represent slices through the tunnel cross section. These slices are then linked axially in order to represent the full tunnel length. Using a modern computer results can be obtained in seconds, but at the expense of a number of key simplifying assumptions.

Some of the assumptions are relatively minor, for instance the requirement for a constant tunnel cross section, although this has effectively prevented the direct consideration of the tunnel riser shafts or enlargements at joint bays. Most significant is the assumption that all of the cables are of identical construction, voltage levels and carry equal current. In practice this is not true for all cable tunnel installations, therefore limiting the application of Electra 143 to these tunnel circuits. At present there is also no direct consideration of the effects of cable joints, which will be discussed further in later sections.

Heat transfer can occur by both convection and radiation, as per the model of Weedy and El Zayyat [51]. The cable itself is modelled by a 1D thermal resistance network with a radial mesh of 5 nodes, with a further 3 nodes to model the air within the tunnel and the tunnel walls. Soil and rock around the tunnel is modelled by dividing it into a set of annular rings. In order to create the representation of the full tunnel, meshes representing the tunnel cross-section (including the cable circuits and the tunnel

surroundings) are taken at intervals and linked together axially within the tunnel (axial heat transfer in the surrounding soil is not accounted for).

The majority of the reduction factors used (for instance for multiple cable installations) and the heat transfer coefficients employed are those from the previously reported work of Weedy and El Zayyat [51]. Some references are also made to the thermal resistance derivations published in IEC 60287 [26]. One notable assumption is that the air velocity within the tunnel is sufficiently high that turbulent flow occurs, restricting the use of the model to cases of forced convection. As a result alternative calculations must be used to evaluate the potential current rating were the forced ventilation system to fail, with a number of potential methods described in Section 2.3.2. As per all of the models discussed thus far, multiple circuits can only be considered if the cables are of identical construction and carrying identical load. Clearly for the vast majority of installations, this would be an unrealistic condition. In addition, if circuits of differing voltage levels are installed the rating obtained is likely to be conservative. Attempts were made in the original publication to validate the models, however this was only done against problems where an analytical solution could reasonably be computed, rather than against data obtained from a real installation.

2.3.2 Other Methods

A number of alternative methods are available for the solution of cable tunnel ratings. Some early works by authors such as Giaro and Kitagawa relied on the solution of analytical heat transfer equations [52, 53]. A review by Anders demonstrates the use of energy conservation equations to determine the heat transfer coefficients for cable groups in horizontal tunnels, while accounting for the effects of horizontal and vertical tunnel walls on the heat transfer of the system [54]. King also examines simple one-dimensional heat transfer, before going on to describe numerical methods including finite element analysis in both two and three dimensions as applied to cable tunnel installations [55]. However numerical methods are generally favoured for this type of calculation, with much of the experimental work conducted by Weedy and El Zayyat being used to inform early numerical models, along with the later Electra 143 [51, 56]. The complexity of these numerical models was severely limited by the availability and expense of computational power, hence the relative simplicity of the model.

IEC 60287 can in theory be applied to naturally ventilated tunnel installations, however the accuracy of such an approach will depend on the handling of T_4, the thermal resistance external to the cable [57]. Several formulae are suggested for this within the main standard depending on whether the cable circuit is exposed to solar radiation - as tunnel cables are rarely exposed to solar radiation the appropriate relation is

$$T_4 = \frac{1}{\pi D_e^* h \left(\Delta\theta_s\right)^{0.25}}, \tag{2.5}$$

where D_e^* is the external diameter of the cable (m), h is the heat dissipation coefficient ($W/m^2K^{5/4}$) and $\Delta\theta_s$ the excess of cable surface temperature above ambient temperature. Methods of determining h depending on the cable circuit formation are detailed within the publication, along with an iterative method of finding $\Delta\theta_s$. A key point to note here is that the IEC implementation includes both convective and radiative transfer within one value of h. Whilst these methods do in part consider the existence of a tunnel wall, they only hold for a straight wall. Forced air convection is not considered by this method, unless a calculation method for T_4 can be used which takes account of this in a satisfactory manner. Other works in this area have also sought to develop relations for the convective heat transfer coefficient of cable groups in air, for instance works by Slaninka and Morgan (who present relations for both free and forced convection) [58, 59]. Although programs such as the Subway Environment Simulator [60] have been used to examine air temperatures and assist in the design of cable systems, they are not directly used in the rating of the cable circuits themselves.

2.3.3 Development Requirements

Section 2.3.1 illustrated a number of failings in the ratings method currently used for forced ventilated cable tunnels. Perhaps the most significant problem is the requirement for all cables within the tunnel to be of identical construction and load cycle, something which does not apply to a modern tunnel with both transmission and distribution circuits co-located (such as that shown in Figure 2.2). As this assumption also places a requirement for the cables to be operating at the same temperature, the method is fundamentally unsuited to rating high temperature cables in conjunction with existing technology. However the existing method does obtain results quickly and is attractive in the level of detail it could potentially provide. It would appear that gains could be made through redesigning the thermal network on which the method operates to allow additional flexibility. Allowing simultaneous consideration of the riser shafts is also an important consideration.

More advanced modelling techniques also have a role to play in this work, for instance through improving the accuracy with which heat transfer coefficients can be calculated. This improves the precision of the calculation of the cable temperature profile, meaning that accurate transient ratings can be obtained for any given situation. Detailed consideration of cable joints is also thought to be essential at this stage, despite the fact that this area has been substantially overlooked in the past. Removing all of these limitations permits a comprehensive temperature profile to be obtained for a variety of different cable circuits, all installed within the same cable tunnel environment.

FIGURE 2.2: Cable tunnel with co-located 11kV and 132kV circuits

2.4 Cables in Troughs

The majority of instances where cables are installed in troughs tend to be at substations, with the troughs being flush with the ground surface. However in some circumstances troughing is used over much longer distances, for example in London where a number of National Grid circuits are installed in a trough along the side of a canal. Frequently substation trough installations are not backfilled hence the cable is cooled through the impact of natural convection in the air filling the trough. Accurate rating of the cable in this instance is largely dependent on the convective heat transfer coefficients used and it may be preferable to obtain them experimentally as in [61].

Calculating suitable circuit ratings for cable trough installations can be much more complex than for directly buried cables due to the proximity of the cables to the ground surface. This greatly increases the impact of environmental conditions on the rating of the circuits, as demonstrated by the work of Lewin et al [62]. A major consideration with backfilled surface troughs is that significant amounts of moisture may evaporate out of the troughs, leading to an increase in the thermal resistivity of the backfill, as described in [63]. Where the level of moisture migration might be considered minimal it is possible to rate a trough installation using IEC 60287 methods, providing that a suitable value for the equivalent resistance offered by the ground around the trough can be found [64]. Where this becomes difficult, it may be more helpful to adopt a finite element based approach similar to that used for cable ducts by Karlstrand and Henning [65].

2.4.1 Development Requirements

Although any length of high temperature cable installed in troughing is likely to be short, it may still form the limiting factor on the overall circuit. Due to the differing heat transfer processes at play, separate methods may well be required for air filled and backfilled troughs. Taking the case of air filled troughs, it is unlikely that adequate ratings would be available with natural convection alone. The literature search presented here did not identify any rating method directly suited to forced ventilated troughs, hence it will be necessary to develop one. Considering backfilled troughs, it is likely that an extension of the method developed for directly buried cables may be the most suitable. These issues are discussed further in Chapter 7.

2.5 Summary

This chapter has presented a broad overview of existing cable ratings standards as applicable to higher voltage (132kV and above) cable systems. Some of the inherent assumptions which might restrict the applicability of these methods to higher temperature cable systems have been highlighted. Key issues need to be addressed in the development of new or improved rating techniques for all of the deployment options considered in this Chapter. The next chapter introduces an in-depth analysis of heat transfer in soils, in order to develop an improved model for buried cables, which captures accurately the effects of moisture migration on circuit ratings. Improved methods for cables in tunnels are presented in Chapter 6, with cable troughs being addressed in Chapter 7.

Chapter 3

Dynamic Backfill Models

This chapter outlines the theory behind moisture migration, introducing the parameters involved and the necessary equations. The Philip and de Vries model [66] is perhaps the most widely used and is described in some detail prior to a more brief discussion of other theories. A synopsis of past methods used to account for moisture migration within cable ratings calculations is also presented. Important backfill parameters are identified and a candidate backfill system is characterised. The model is then benchmarked against laboratory tests, building on the work of [67].

3.1 Heat Transfer in Soils

Whilst heat transfer within soils occurs predominantly by conduction, effects due to other modes including convection, radiation and the changing of state of soil moisture must also be considered. Heat transfer by conduction is principally limited by three main factors; these being the soil particle thermal conductivity, the degree of contact between soil solids and the temperature gradient. Generally speaking, the higher the thermal conductivity of the particles and the better the contact between them, the more heat can be transferred by conduction. A good estimate of the degree of contact can be obtained by calculating the soil void ratio, defined as the volume of voids to the volume of soil solids [68].

Heat transfer by convection occurs in two stages in soils. For the case of moisture in close proximity to the solid soil particles, the moisture velocity is low and the heat is transferred by diffusion. Further away from the soil particles the movement of moisture is less inhibited and heat can be transferred by the flow of moisture along the temperature gradient. Convection is also an important consideration at the ground surface as it represents the dominant mechanism for the removal of heat from the ground to the atmosphere. In this case the magnitude of the convective heat transfer coefficient is dependent on the wind speed across the surface [69].

Whilst radiation transfer within the soil itself is negligible, it can represent a significant heat source at the ground surface. This mostly takes the form of short wave radiation from the sun. The extent to which daily and annual cycles propagate downwards through the ground is determined by the thermal diffusivity of the soil [70]. Daily cycles tend to be quickly attenuated and are only of significance very close to the surface, whereas longer duration cycles have a greater impact at typical cable burial depths.

Changes of state of soil moisture also play a part in the heat transfer around cable groups, with this effect being more pronounced at higher temperatures. Heat released from the cable group can cause evaporation of the moisture in soil pores (the spaces between solid soil particles). Once the moisture has become a vapour it is driven to regions of lower vapour pressure, hence transferring the latent heat away from the cable group until the point where the vapour condenses.

3.2 Moisture Migration Theories

This Section introduces the physical processes behind moisture migration under a thermal gradient along with pertinent theories on how it occurs, including that of Philip and de Vries [66] which is perhaps the most widely known and applied.

3.2.1 Basic Concepts of Moisture Migration

A difference in concentration aside, the main cause of moisture migration within a soil is a temperature gradient. Fourier's Law of heat conduction shows that an increase in temperature gradient causes a greater rate of heat transfer by conduction, with similar effects being seen on the rate of moisture migration. The physical process is time variant when applied to cable circuits as the temperature and heat flux at any point will vary with time.

As water in the soil pores becomes warmer, the surface tension of the water decreases. This acts to reduce the forces which are retaining the water in its position in a higher temperature region, allowing it to move to an adjacent lower temperature region [71]. The rate at which this may happen is controlled by the hydraulic gradient (which is a function of the temperature gradient) and the soil permeability (determined by the physical properties of the soil in question). As more moisture is transferred to the cooler region the hydraulic pressure in this region exceeds that of the warmer region, meaning that the hydraulic gradient limits the rate of moisture migration by causing the cooled moisture to move back in opposition to the temperature gradient.

As such, it is possible for the effects of the temperature and hydraulic gradients to equal each other limiting the possibility for moisture migration. However, this will depend

on the magnitude of the soil vapour permittivity to its liquid permittivity. Where the liquid permittivity is too low, it is possible that the system can become unstable as the return of moisture along the hydraulic gradient is slower than its removal by the temperature gradient [72]. Where this occurs the moisture migration process continues until the higher temperature area has dried out. This causes an effective increase in the thermal resistivity of the soil, thus reducing the transfer of heat away from the power cable. Such "thermal runaway" behaviour was first encountered as a problem in the summer of 1962 in the London area [73], it has also been suggested as one possible cause of the major system failures in Auckland in 1998 [74].

3.2.2 Philip and de Vries Equations

Of the various models proposed for quantifying moisture migration, perhaps the most widely used has been that of Philip and de Vries [66]. The method can be applied to porous materials such as soil or sand and, with the application of a numerical method, can obtain approximate solutions to the problem of coupled moisture and temperature gradients. The movement of vapour and moisture are treated separately through the use of Fick's Law and Darcy's Law respectively.

Fick's Law describes the passive movement of molecules due to a concentration gradient and states that where no such concentration gradient exists, diffusion of vapour is not possible. The Law states that j, the diffusion of vapour flux ($kg.m^{-2}s^{-1}$), is determined by the diffusion coefficient D of the vapour (m^2s^{-1}) and c, the concentration gradient of the vapour flux ($kg.m^{-3}$) such that

$$j = -D\nabla c \tag{3.1}$$

Darcy's Law was derived through experiments on water flow, from which Darcy concluded that the rate of fluid flow through a porous medium was proportional to the potential energy gradient within that fluid [75]. The Law states that the moisture flux v (ms^{-1}) is equal to the hydraulic conductivity K_c, multiplied by the difference in the hydraulic potential $\nabla\phi$, i.e.

$$\nu = -K_c\nabla\phi \tag{3.2}$$

To improve the applicability of the model to porous materials, an extended version of Fick's Law was used to describe the vapour transfer, based on work by Carman [76]. An improved treatment of vapour transport was implemented, owing to its dependence on physical adsorption and capillary condensation. Carman found that for low values of relative humidity the physical adsorption was the dominant factor, with capillary condensation becoming dominant at higher values. Adsorption can be considered as the degree of attachment to a surface (for instance of liquid water molecules to a solid soil particle), and it occurs due to the differential forces of attraction and repulsion between

molecules. Physical adsorption mainly involves van der Waals forces and consequently has a relatively low energy associated with it.

Having obtained an extended version of Fick's Law, it is possible to separate the vapour flux into components related to the moisture gradient and the temperature gradient. As the hydraulic potential ϕ already consists of components due to pressure and gravitational components, the total liquid flux can be separated into components due to temperature gradient, moisture gradient and gravity, allowing the liquid flux density to be stated as

$$\frac{q_L}{\rho_w} = -D_{TL}\nabla T - D_{\theta L}\nabla\theta - k_{unsat}i, \tag{3.3}$$

where q_L is the liquid flux density ($kgm^{-2}s^{-1}$); ρ_w is the density of liquid water (kgm^{-3}); D_{TL} is the thermal liquid diffusivity ($m^2s^{-1}{}^{\circ}\mathrm{C}^{-1}$); $D_{\theta L}$ is the isothermal liquid diffusivity (m^2s^{-1}); k_{unsat} is the unsaturated hydraulic conductivity (ms^{-1}); T is temperature ($^{\circ}$C); θ is volumetric moisture content and i is the unit vector in the vertical direction.

For vapour flux density, the appropriate relation is:

$$\frac{q_v}{\rho_w} = -D_{TV}\nabla T - D_{\theta V}\nabla\theta, \tag{3.4}$$

where q_v is the vapour flux density ($kgm^{-2}s^{-1}$); D_{TV} is thermal vapour diffusivity ($m^2s^{-1}{}^{\circ}\mathrm{C}^{-1}$) and $D_{\theta V}$ is the isothermal vapour diffusivity (m^2s^{-1}).

Combining the relationship between liquid flux density (3.3) and vapour flux density (3.4), the total moisture flux density may be obtained in the form

$$\frac{q_m}{\rho_w} = -D_T\nabla T - D_\theta\nabla\theta - k_{unsat}i, \tag{3.5}$$

where the thermal diffusivity D_T is the sum of the thermal vapour diffusivity and the thermal liquid diffusivity, and the isothermal diffusivity D_θ is the sum of the isothermal liquid diffusivity and the isothermal vapour diffusivity.

Using this information it is possible to write the differential equation for moisture transfer, i.e.

$$\frac{\partial\theta}{\partial t} = \nabla.(D_T\nabla T) + \nabla.(D_\theta\nabla\theta) + \frac{\partial k_{unsat}}{\partial z} \tag{3.6}$$

The isothermal vapour diffusivity obtained from the moisture gradient component of the vapour flux density is used in the heat distribution equation to account for the transfer of latent heat such that

$$C\frac{\partial T}{\partial t} = \nabla.(\lambda\nabla T) + L\rho_w\nabla.(D_{\theta v}\nabla\theta), \tag{3.7}$$

where C is the volumetric heat capacity of the soil ($kJm^{-3}{}^{\circ}\mathrm{C}^{-1}$); λ is soil thermal conductivity ($Wm^{-1}K^{-1}$) and L is volumetric latent heat of vaporisation (Jm^{-3}).

Experimental observations have verified that for low moisture contents the vapour diffusivities (both isothermal and non-isothermal) become dominant, whereas liquid diffusivities dominate at higher moisture contents [77]. In a further study, Rose showed that the liquid conductivity decreased slowly from saturation to the dry state, whilst vapour conductivity rises from zero in the saturated case, to a maximum just before complete drying of the medium, prior to decreasing back to zero [78].

Although the Philip and de Vries model is commonly used for describing moisture transport in soils under a temperature gradient, it does have limitations. One of the most significant is that it only uses a single variable, θ, to describe the volumetric moisture content. This means that the volume fractions of liquid water and water vapour are not modelled explicitly. Instead the model attempts to account for them through the use of the split liquid and vapour diffusivities. A more realistic approach would be to describe the overall moisture flux, q_m, in the form

$$q_m = \Psi_L q_L + \Psi_v q_v \tag{3.8}$$

where Ψ_L and Ψ_v represent the volume fractions of the liquid and vapour phases respectively. This would be particularly important if soil wetting (in addition to drying) was to be modelled. However as a starting point it was considered that the Philip and de Vries theory was an adequate basis for the modelling required for buried cable circuits.

3.2.3 Alternative Theories

Several theories exist regarding the simultaneous transfer of heat and moisture in soils, although a number are linked to the Philip and de Vries Equations. Taylor and Cary proposed an approach based on irreversible thermodynamics [79]. The treatment of the soil water diffusivity is largely common with [66]. This approach has the potential benefit of reducing the number of assumptions about the actual mechanisms of the moisture transport, however, this might not offer the best understanding of the true phenomena [80].

Slightly later work by Cassel and Nielsen demonstrated that net moisture flux could be under-predicted by Fick's Law [81]. However, the use of the Taylor and Cary approach was found to double this under-prediction, with the only acceptable agreement being with the work of Philip and de Vries.

Dakshanamurthy and Fredlund proposed a model relying on Fick's Law and Darcy's Law which would allow for compressible media [82]. The model also takes account of the effect of pore air and water pressures under both hydraulic and temperature gradients. Most other models assume that the soil is an incompressible media as this greatly reduces the computational effort in solving the equations.

Milly [83] and Sophocleous [84] made independent generalisations of the Philip and de Vries theories in an attempt to account for the presence of hysteresis and inhomogeneity of the media. This required a conversion of the original theory such that it operated on matric head (an expression of the soil suction as an equivalent height of water) rather than moisture content. The theory by Milly is perhaps more complete as Sophocleous made extra simplifications to the temperature dependence of relative humidity and the liquid thermal diffusivity. Milly's model is based around the finite element method and additionally accounts for advection (the transport of a substance or property by a moving fluid).

Hartley and Black [85] developed a model specifically aimed at applications such as moisture migration around power cables due to the consideration of cylindrical heat sources. The model is, however, somewhat simplified as it has both radial and axial symmetry, meaning that the effects of gravity, the water table and changes at the ground surface are all neglected. The main aim of the work was to examine thermal stability in such regions by attempting to define the critical moisture content beyond which the movement of moisture increases rapidly. With a critical moisture content well defined it was also possible to predict the critical heat source, although the value of the critical moisture content was found to be almost independent of the magnitude of the heat source.

3.3 Existing Rating Adjustments

The majority of standard cable rating methods are solved on the assumption of a uniform thermal conductivity throughout the soil, hence neglecting entirely the possibility of moisture migration. Some methods, for instance that of IEC 60287, have the ability to consider the burial environment in two zones - one where the soil is fully dry, and one where the soil is in its normal uniform state. The work of Arman, Cherry and Gosland was also based on this method [73]. Such techniques are of course heavily approximate, hence the desire to model the moisture migration explicitly.

Another attempt was made to solve this problem through the consideration of soil suction to identify drying [86]. The soil suction at cable depth is estimated through the use of a hydraulic conductivity model, a vegetation factor model, and a water balance model. A critical value of soil suction is found such that where soil suction is below the critical value, drying out will occur. However, using this approach was found to lead to an underestimate of the soil suction which led to the cable surface temperature being overestimated.

Later works began to make use of the heightened availability of computational power to employ methods such as finite element analysis (FEA). Work by Radhakrishna and Anders [41] has demonstrated the possibilities of solving the Philip and de Vries equations

when applied to moisture migration around power cables. The FEA technique is well suited to this problem as the material properties are strongly nonlinear. Models produced were validated against field installations and experimental studies, and reasonable agreement was observed.

An alternative method has been demonstrated by Freitas et al, who make use of the finite volume method to solve the moisture migration problem for a variety of cable load cycles [87]. Generalised versions of both Fick's Law and Darcy's Law are employed, meaning that the method is essentially similar to that of Philip and de Vries. While the method does account for the nonlinear dependence on temperature and moisture content of the various soil properties, the method is not fully dynamic, hence it introduces some errors. Preece and Hitchcock have also shown that using constant soil properties could lead to changes in moisture content which are not physically valid [42].

3.4 Backfill Characterisation

Examination of the moisture transport equations shows that a number of properties must be accurately defined in order to obtain an accurate result in any moisture migration model. Whilst properties such as the density of water can be easily defined where the temperature is known, properties such as diffusivity depend not just on temperature and moisture contents but also on the physical properties of the backfill. Major properties of significance are identified here and the implications they have on the overall moisture migration phenomenon are discussed. The properties of soil depend on its size, shape, size distribution, and also interactions between phases (solid particles, liquid and gas). As a result the analysis is quite complex, with many interdependencies between properties. The initial work has been undertaken with a sand backfill, as buried transmission cables are generally laid in sand rather than the local soil alone. This can take the form of either a "selected sand" (which will typically be high in quartz and designed to have a minimal void ratio), or a cement bound sand.

3.4.1 Particle Size

Basic classification of soils is normally achieved using particle size distributions, which can be undertaken easily using a set of graduated sieves as specified by BS 1377. This allows a curve to be drawn showing the fractions of the sample which correspond to each different particle size. Soils are normally classified using their effective diameter, which is the diameter of a hypothetical sphere that is assumed to act in the same way as the soil particle [88]. The particle size distribution of a soil will impact almost all other properties of interest in this work, both thermal and hydraulic. The distribution obtained for the sand under test is that shown in Figure 3.1 below. It can be seen that

the sand has a very small gravel content, with over 98% of the particles in each sample being smaller than 2mm in diameter. A range of particle sizes are seen in the region between 0.1mm and 1mm, which is typical of a well graded sand. This is beneficial from the thermal point of view as the quantity of voids within the sample will be lower than for backfills where all of the particles are of similar sizes. For the backfill shown in Figure 3.1, the clay content is extremely low (as evidenced by the small percentage of particles in the micron scale). The vast majority of particles present are classified as quartz.

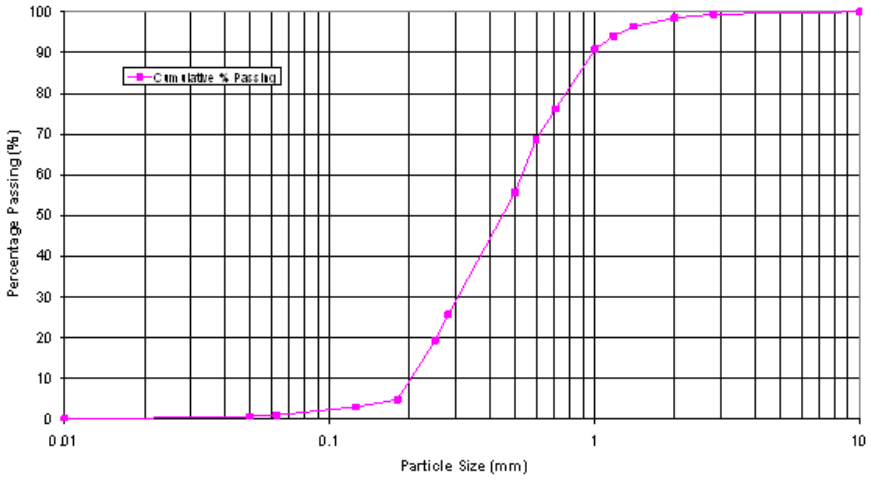

FIGURE 3.1: Backfill Particle Size Distribution of sand used for testing purposes

3.4.2 Porosity

The porosity of a soil is determined by the volume of air voids within the solid medium. This will be affected by the particle size distribution, the compaction of the soil and the bonds between the individual particles [75]. Porosity is defined by:

$$\epsilon = (V_l + V_g)/V_t \tag{3.9}$$

where ϵ represents the porosity, V_l the volume of liquid (m^3), V_g the volume of gas (m^3) and V_t the total volume. The porosity of a soil will have an impact on both hydraulic conductivity and vapour diffusion, meaning that it is a vital parameter in the magnitude and rate of moisture migration. The porosity of the backfill under test here is found to be approximately 0.38.

3.4.3 Matric Suction

The water within the soil can be broadly classified into three groups: ground water, capillary water and hydroscopic water [89]. Ground water is subjected to no force other

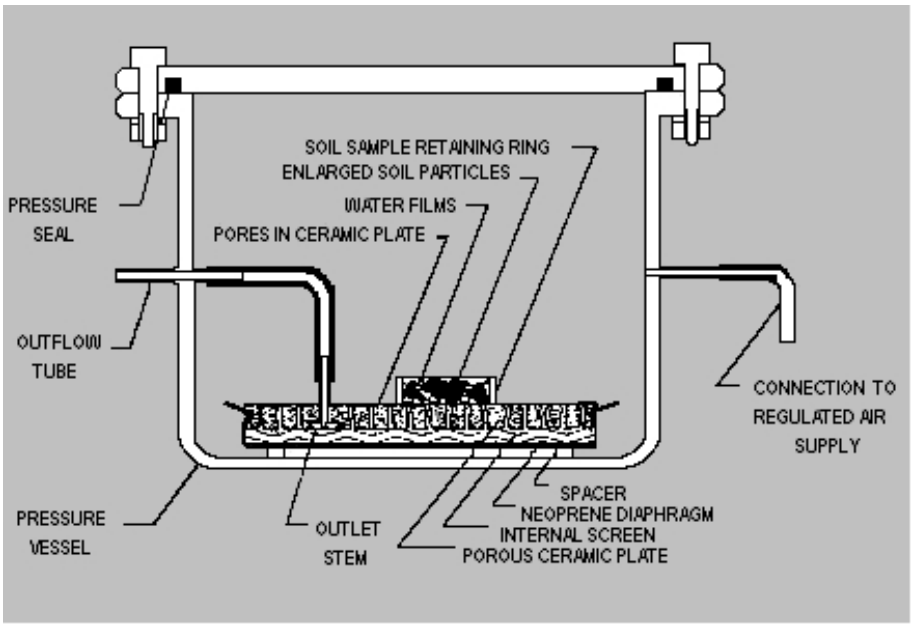

FIGURE 3.2: Cross section view of pressure plate extractor [1]

than gravity and is hence the first to be removed under a temperature gradient. This is because the ground water is subject to the lowest suction force (represented by the first horizontal section of Figure 3.3, prior to the rapid gradient change occurring at the air entry value). Capillary water is held into voids by surface tension and is hence slower to move under a temperature gradient. Finally the hydroscopic water is that held on the soil particle surface, for instance by adsorption. This water is generally the last to be removed from the void under a temperature gradient. When only hydroscopic water remains inside the pore the matric suction is high, representing the right hand side of the curve in Figure 3.3. Limited amounts of structural water may also exist inside the soil particle, but this water is very hard to remove from the soil.

The water-holding characteristics of a backfill can be found experimentally through undertaking a study of soil suction using a pressure plate extractor, a schematic of which is shown in Figure 3.2. A saturated sand sample is placed on the porous ceramic plate, with the regulated air supply being adjusted to change the pressure within the vessel. Each sample is held under pressure for a minimum period of 24 hours to allow the movement of moisture to reach steady state. The sample can then be oven dried to determine its moisture content, allowing a graph of moisture content versus soil suction to be plotted (as the applied pressure will be equal to the soil suction).

The shape of the soil suction curve (often referred to as the Soil Water Characteristic Curve or SWCC) is strongly dependent on the particle size distribution of the material under test. Materials containing high fractions of sand display a very swift transition from saturated to almost dry over a small suction range. With very fine materials such as clay, the transition is much more gradual and requires significantly higher levels of

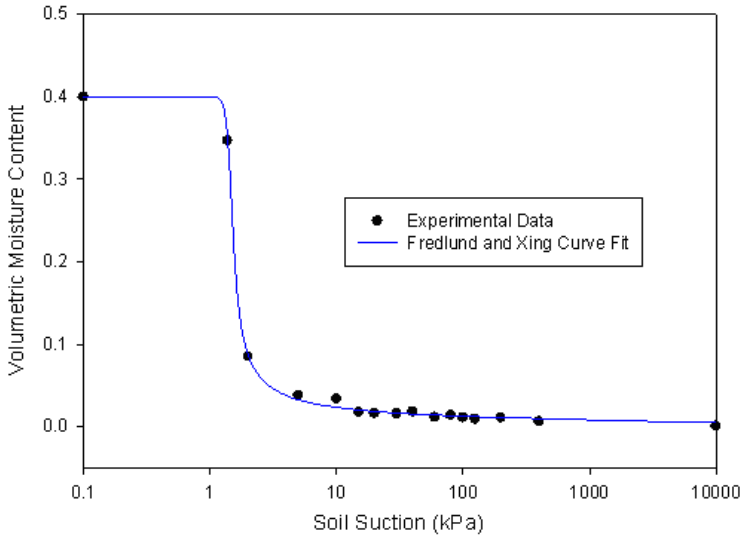

FIGURE 3.3: Experimentally derived soil water characteristic curve

suction to achieve a completely dry material. Examining the data points plotted in Figure 3.3, it is apparent that the backfill material behaves very much like a sand. In order to provide a continuous function of soil suction for use in numerical backfill models, a function developed by Fredlund and Xing,

$$\theta_v = \theta_s \left[1 - \frac{ln(1 + \frac{\psi}{h_r})}{ln(1 + \frac{10^6}{h_r})}\right] \left[\frac{1}{(ln(e^1 + (\frac{\psi}{a})^n))^m}\right] \tag{3.10}$$

has been fitted to the data [90]. Here ψ represents the soil suction (kPa), θ_s the saturated volumetric moisture content (equal to the porosity of the backfill) and h_r the suction at residual water content. The parameters a, n and m are essentially curve fitting parameters however they are also a function of physical processes; a is related to the soil suction at which air enters the soil (air entry value), n is a function of the rate of moisture extraction and m is a function of the residual water content. The coefficients used in Figure 3.3 are shown in Table 3.1.

Coefficient	Value
θ_s	0.38
h_r	1000
a	1.4088
n	21.8037
m	0.7526

TABLE 3.1: SWCC Coefficients

A final adjustment must be made to these values during the solution of the backfill model, as the value of suction is not independent of temperature. This is because the soil suction is linked to the surface tension of water, $\sigma(Jm^{-3})$, which is temperature dependent [91]. As a result the soil suction curve $\Psi(\theta, T)$ is calculated from data in [92]

using expressions;

$$\Psi(\theta, T) = \frac{\sigma_{ref}}{\sigma_T}\psi(\theta)_{ref} \tag{3.11}$$

$$\sigma(T) = 0.122 - 0.0002(T + 273.15) \tag{3.12}$$

3.4.4 Hydraulic Permeability

The hydraulic permeability of a soil defines the speed at which moisture can move through the medium. There are two components, the saturated hydraulic permeability (which can easily be derived experimentally) and the unsaturated hydraulic permeability (which is much more difficult to derive experimentally). The saturated hydraulic permeability can be determined in a laboratory test using a constant head permeameter as described in [93]. To ensure that a good average result was obtained, the test was repeated 3 times for 5 backfill samples, yielding an average value of $2.297x10^{-4}\ ms^{-1}$.

Numerous authors have published methods both theoretical and empirically derived which allow the calculation of unsaturated hydraulic permeability. However the method demonstrating the best fit for this backfill type has been found previously [67] to be that by Fredlund and Xing [94], which calculates a relative permeability through reference to the SWCC using

$$k_r(\Psi) = \frac{\int_{ln(\psi)}^{b} \frac{\theta(e^y)-\theta(\psi)}{e^y}\theta'(e^y)dy}{\int_{ln(\psi_{aev})}^{b} \frac{\theta(e^y)-\theta_s}{e^y}\theta'(e^y)dy} \tag{3.13}$$

where, θ represents moisture content, b equals ln(1000000) and y represents a dummy variable of integration for the logarithm of suction. The subscript aev denotes the value of the air entry value. Multiplying the relative permeability by the saturated permeability gives the unsaturated permeability, shown in Figure 3.4.

As with soil suction, there is an additional consideration regarding the dependence of permeability on temperature. The unsaturated permeability $k_{unsat}(\theta, T)$ can be found to be inversely proportional to the dynamic viscosity of water. As a result, a correction for temperature can be achieved using,

$$k_{unsat}(\theta, T) = \frac{\eta_{ref}}{\eta_T}k_{unsat(\theta)ref} \tag{3.14}$$

$$\eta(T) = 0.0014e^{-0.0177T} \tag{3.15}$$

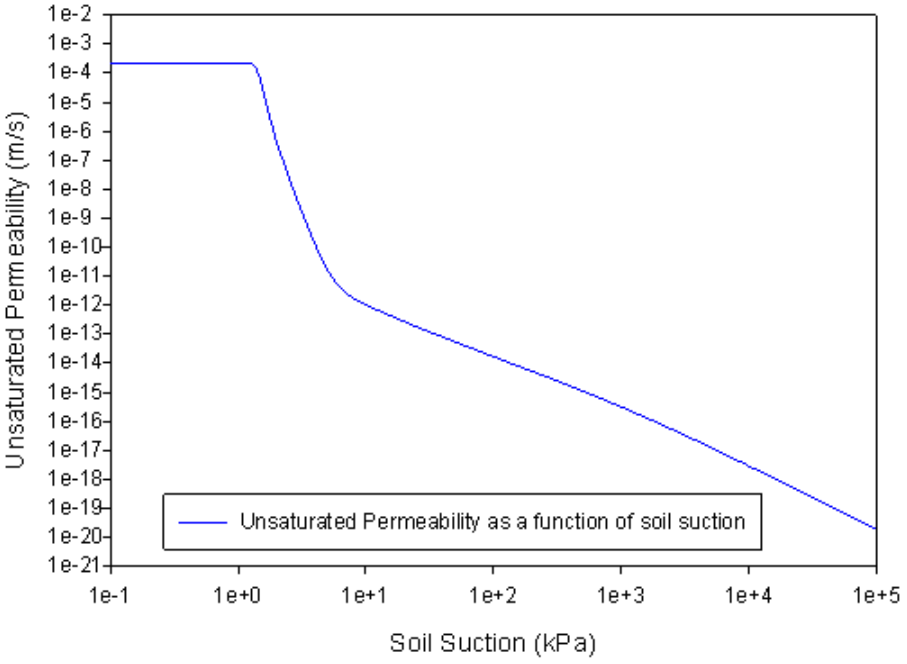

FIGURE 3.4: Unsaturated Permeability as a function of soil suction

3.4.5 Liquid Diffusivity

Accurate experimental measurement of liquid diffusivities is known to be an in-depth process which is beyond the scope of this thesis. However Philip and de Vries suggest a method for obtaining the liquid diffusivities from the equation for the liquid water velocity, **U**, and Darcy's Law. It is possible to arrange the liquid water velocity equation into a form yielding terms for both the temperature and moisture gradients, i.e.

$$\mathbf{U} = -k_{unsat}(\theta, T)\gamma\psi\frac{d\psi}{d\theta}\nabla\theta \tag{3.16}$$

As a result it is possible to determine the two liquid diffusivity values, D_{TL} with units of $m^2 s^{-1} {}^{\circ}\mathrm{C}^{-1}$,

$$D_{TL}(\theta, T) = k_{unsat}(\theta, T)\gamma\psi(\theta, T) \tag{3.17}$$

and $D_{\theta L}$ with units of $m^2 s^{-1}$,

$$D_{\theta L} = k_{unsat}(\theta, T)\frac{d\psi}{d\theta} \tag{3.18}$$

where γ is determined by

$$\gamma = \frac{1}{\sigma_T}\frac{d\sigma_T}{dT} \tag{3.19}$$

As a result it is necessary to calculate the values of the diffusion coefficients with respect to both temperature and moisture, as both suction and unsaturated permeability are functions of these values. These functions are plotted in Figures 3.5 and 3.6 below at a number of temperatures pertinent to high voltage cables.

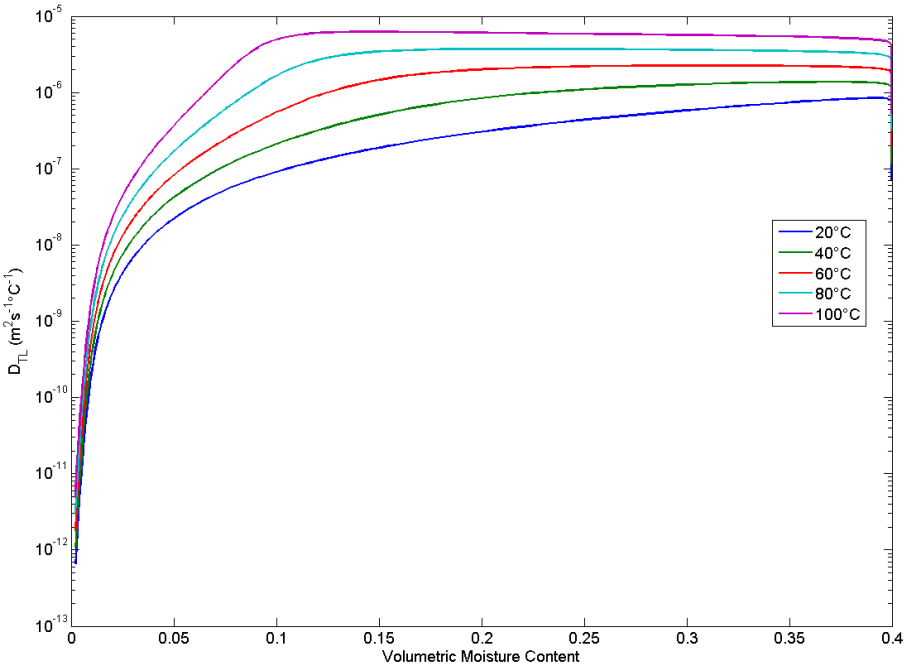

FIGURE 3.5: Thermal Liquid Diffusivity (D_{TL})

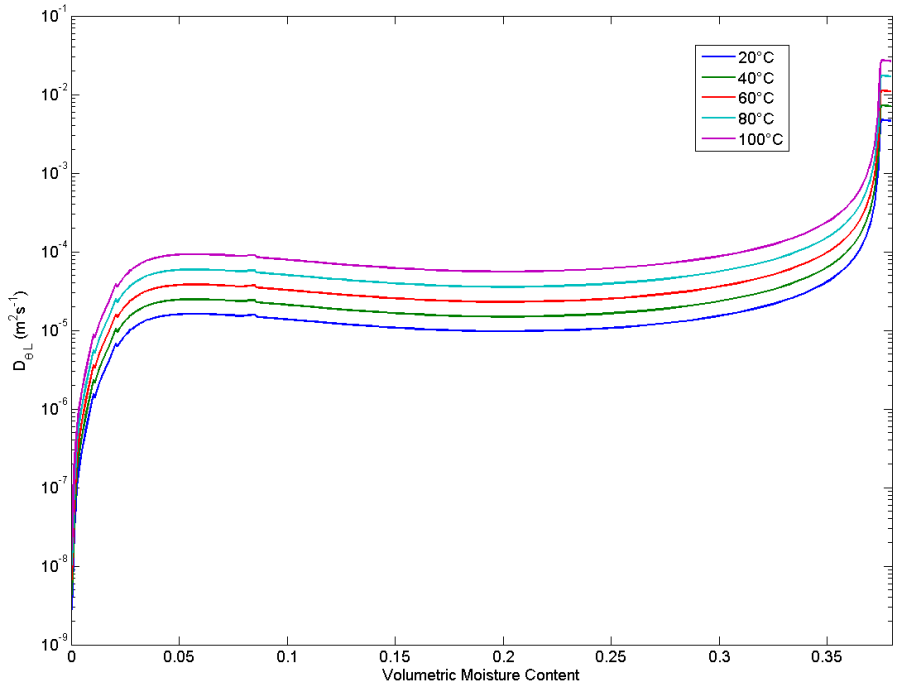

FIGURE 3.6: Isothermal Liquid Diffusivity ($D_{\theta L}$)

3.4.6 Vapour Diffusivity

Vapour diffusivities are defined as per the work of [66], with a contribution to the overall vapour velocity, $\mathbf{V}$ (ms^{-1}), due to the thermal gradient and the moisture gradient. The vapour velocity equation is defined as

$$\mathbf{V} = -D_{TV}\nabla T - D_{\theta V}\nabla\theta \tag{3.20}$$

The calculation of the diffusion coefficients is more complex than for the liquid terms, with the thermal vapour diffusivity D_{TV} $(m^2s^{-1}{}^{\circ}\mathrm{C}^{-1})$ as plotted in Figure 3.7 being given by

$$D_{TV} = D_{atm}\upsilon\Lambda\frac{\frac{(\nabla T)_a}{\nabla T}}{T}(T + 273.15)h\frac{\frac{\delta\rho_0}{\delta T}}{\rho_{ref}} \tag{3.21}$$

Here D_{atm} is the molecular diffusivity of water vapour in air (m^2s^{-1}), h the relative humidity, ρ_o the saturated water vapour density (kgm^{-3}), ρ_{ref} the density of water at room temperature (kgm^{-3}), R is the ideal gas constant at 461.5 $Jkg^{-1}K^{-1}$ and υ is the mass flow factor defined as

$$\upsilon = \frac{P}{(P-p)} \tag{3.22}$$

where P is the air pressure, taken as a constant at 101325Pa and p is the partial pressure of water vapour (kPa). Λ represents the equivalent flow area calculated by

$$\Lambda = 0.3 + 1.32(0.4 - \theta) \tag{3.23}$$

and $\frac{\nabla T_a}{\nabla T}$ is the ratio of the average temperature gradient in air-filled pores to the overall temperature gradient which is defined according to work by Preece and Hitchcock [95] as

$$\frac{(\nabla T)_a}{\nabla T} = \frac{1}{3}\left(\frac{2}{1 + (1 - \frac{\lambda_i}{\lambda_o})G_a} + \frac{1}{1 + (1 - \frac{\lambda_i}{\lambda_o})(1 - 2G_a)}\right) \tag{3.24}$$

Here λ_i is the thermal conductivity $(Wm^{-1}{}^{\circ}\mathrm{C}^{-1})$ of the individual constituent of the backfill, λ_0 is the thermal conductivity of pore medium in the soil $(Wm^{-1}{}^{\circ}\mathrm{C}^{-1})$ and G_a is the air shape factor. The air shape factor is calculated by a method similar to that used by Kimball [96].

The isothermal vapour diffusivity $D_{\theta V}(m^2s^{-1})$ as plotted in Figure 3.8 is defined by

$$D_{\theta V} = D_{atm}\upsilon\frac{\Lambda}{RT}\rho_v\frac{\frac{\delta\psi}{\delta\theta}}{\rho_{ref}} \tag{3.25}$$

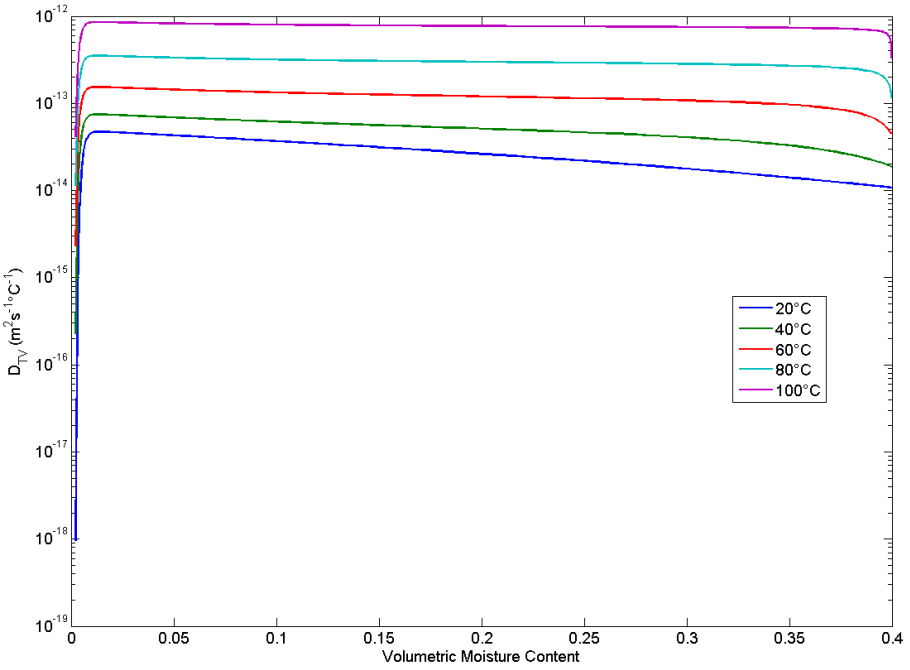

FIGURE 3.7: Thermal Vapour Diffusivity (D_{TV})

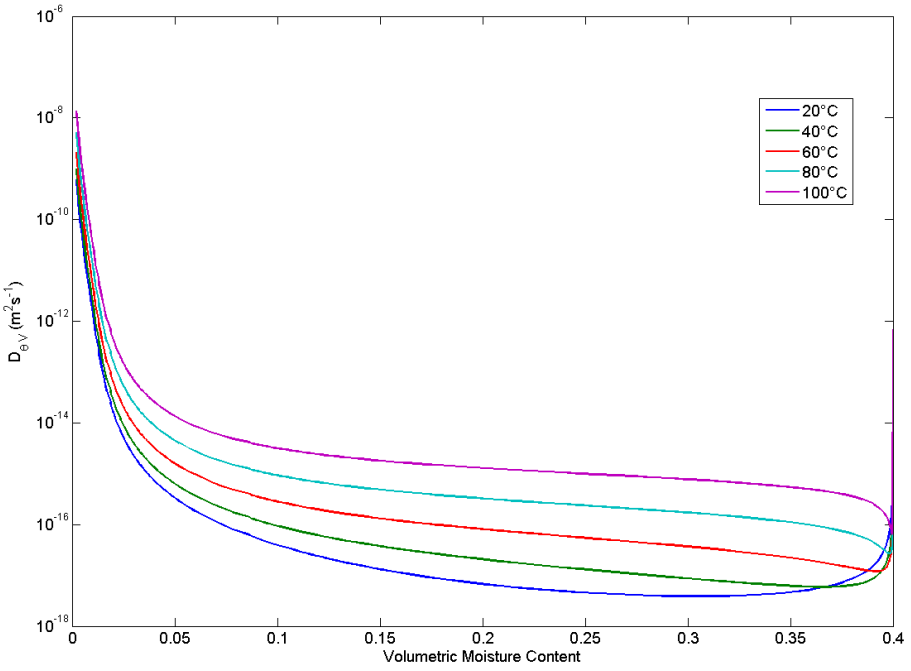

FIGURE 3.8: Isothermal Vapour Diffusivity ($D_{\theta V}$)

3.4.7 Thermal Conductivity

Thermal conductivity of a backfill can easily be measured using the thermal probe technique outlined in IEEE Std 442-1981 [97]. To undertake the tests at a range of moisture contents the backfill is oven dried at 105°C for a minimum of 24 hours. It is then allowed to cool and the desired volume of water is added to make up the sample. A total of five samples were tested for each moisture content to offset against changes due to small variations in packing density for each test. The experimental data obtained is shown in Figure 3.9, with the fitted curve corresponding to,

$$k = 0.3906 + 1.6248(1 - e^{(-16.6292\theta)}) \tag{3.26}$$

In order to express the thermal conductivity information inside the finite element model and to allow for the dry density of the backfill model to be changed, a technique similar to that employed by Johansen is employed [98]. This allows an expression for the dry thermal conductivity of the backfill to be derived

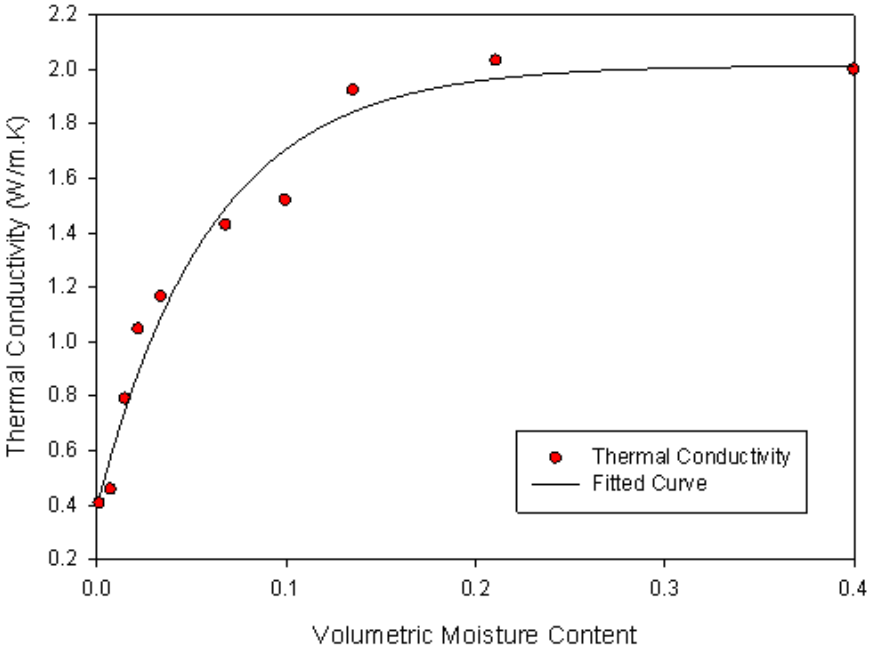

FIGURE 3.9: Experimentally derived thermal conductivity function

$$\lambda_{dry} = 0.232\left(1 + 1.29(\frac{\rho_d}{1000} - 1.575)\right) \tag{3.27}$$

where ρ_d is the dry density of the backfill (kgm^{-3}), and also for the saturated state, whose thermal conductivity can be defined as [67]

$$\lambda_{sat} = \lambda_w^{Por}\lambda_s^{(1-Por)} \tag{3.28}$$

Here Por is equal to the porosity of the backfill, λ_w is the thermal conductivity of water as a function of temperature given by

$$\lambda_w = 0.5599 - 10^{-5}T^2 - 0.0021T \tag{3.29}$$

and λ_s is the thermal conductivity of the solid fraction of the backfill (modelled in this case as 60% quartz and 40% mineral content). Any thermal transport by conduction or convection in the pore air is neglected.

A dimensionless quantity known as the Kersten number, Ke, is used to characterise the slope of the curve relating moisture content to thermal conductivity. This can be defined from experimental data as

$$Ke = \frac{\lambda - \lambda_{dry}}{\lambda_{sat} - \lambda_{dry}} \tag{3.30}$$

It is also possible to express the Kersten number through the methodology adopted by Fredlund as:

$$Ke = \left(1 - \frac{ln(1 + \frac{\psi}{h_r})}{ln(1 + \frac{1000}{h_r})}\right)\left(1/ln(e^1 + \frac{\psi}{a})^n\right)^m \tag{3.31}$$

This method of predicting the Kersten number has been shown to be acceptable for a degree of saturation greater than 10%, however other researchers have shown that the best procedure below 10% is to apply a linear interpolation [99]. As a result, the thermal conductivity function implemented in the backfill model is

$$\lambda = \lambda_{dry} + Ke(\lambda_{sat} - \lambda_{dry}) \tag{3.32}$$

3.4.8 Specific Heat Capacity

The volumetric specific heat capacity of a backfill may be obtained by calculating the sum of the volumetric heat capacities of its individual constituent's, weighted by their volume fractions [100]. For the purposes of the backfill models developed here, a function is defined as

$$C_s = c_{qs}\rho_d(1 - Por) + c_w\rho_w\theta \tag{3.33}$$

where c_{qs} is the specific heat for a quartz sand, taken to be $295 Jkg^{-1}{}^{\circ}\mathrm{C}^{-1}$. Using this method leads to an overestimate of the thermal capacitance of the candidate backfill used within this thesis. A correction factor is hence employed to reduce the magnitude of the soil thermal capacitance by a factor of 4 in line with the behaviour seen in the verification experiments.

3.5 Experimental Verification

As the backfill models developed within this project are highly nonlinear, it is considered vital that any numerical modelling is benchmarked against experimental data. This Section presents a comparison of the performance of the backfill model against two experiments. The first represents the simplest possible one dimensional heating arrangement, whilst the second utilizes a cable trough geometry to allow comparison with a more typical installation arrangement.

3.5.1 Moisture Migration Cylinder

The moisture migration cylinder is a piece of apparatus which allows a simple one dimensional moisture migration process to be observed. A sample of backfill of known moisture content is placed between two metal plates, the lower of which is heated and the upper of which is maintained at a constant temperature. This allows a temperature gradient to be induced across the medium, hence initiating the process of moisture migration. The outer jacket of the cylinder is insulated to reduce the impact of the ambient temperature on the temperature distribution inside the experiment. Figure 3.10 shows a cross-sectional view of the equipment.

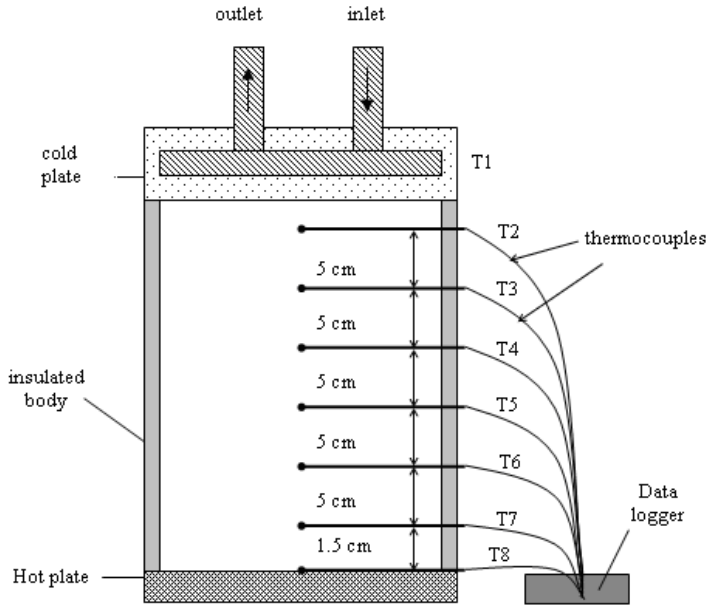

FIGURE 3.10: Moisture Migration Cylinder

A series of experiments have been conducted at a range of initial moisture contents between 1% and 10% (by volume) to allow comparison across the ranges of conditions which might be seen in the field. On each occasion the backfill is oven dried and then allowed to cool, prior to a known volume of water being added to the sample. The backfill is compacted into the cylinder in layers to ensure the most uniform density possible and

to prevent the thermocouple position being disturbed. In each case the heating load is applied for a minimum of 48 hours, which is considered to be the maximum transient period for power cable applications.

3.5.1.1 Initial Results

A finite element representation of the experiment shown in Figure 3.10 has been constructed using the nonlinear coefficients obtained for the candidate backfill system. The results are presented in Figures 3.11 and 3.12 below for initial volumetric moisture contents of 1%, and 3% respectively. It can be seen that the predicted temperatures from the model are much lower than those observed from the experiment. Analysis of Figures 3.13 and 3.14 shows that very little moisture migration is calculated by the modelling, which contrasts with clear experimental evidence of moisture migration.

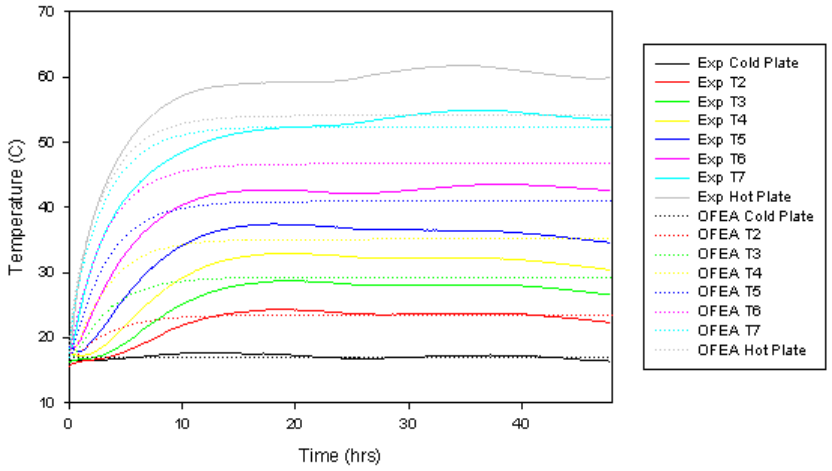

FIGURE 3.11: FEA model with original coefficients, 1% initial moisture content

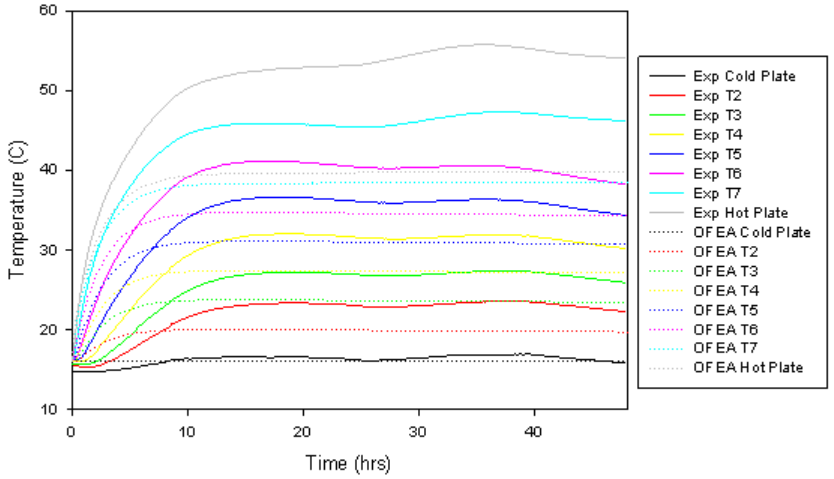

FIGURE 3.12: FEA model with original coefficients, 3% initial moisture content

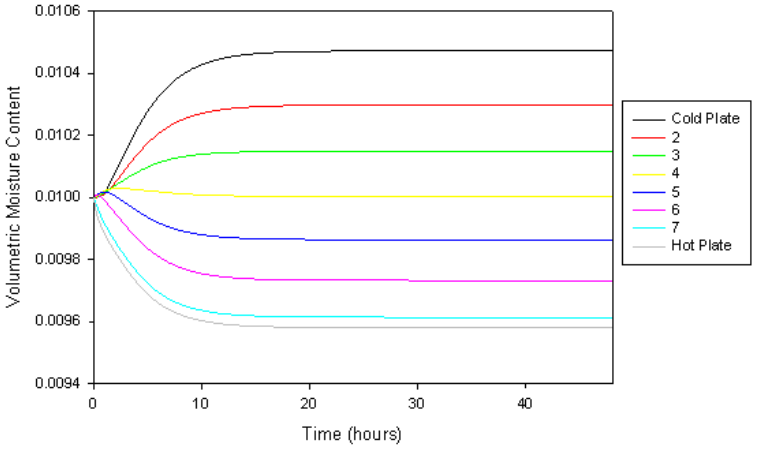

FIGURE 3.13: Moisture profile for original FEA model at 1% initial moisture content

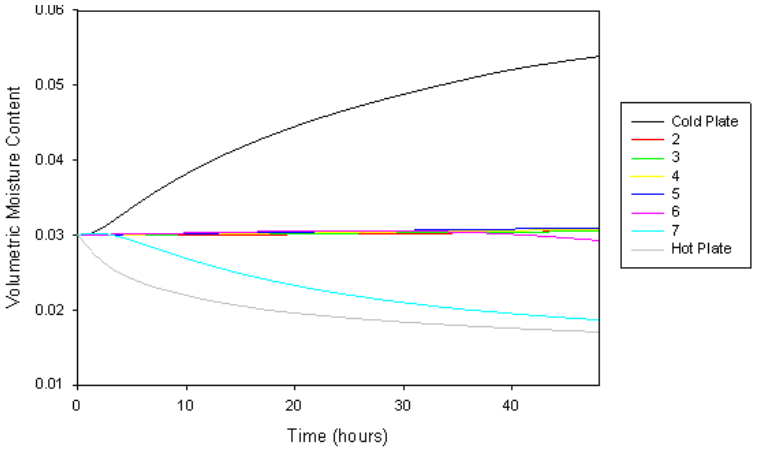

FIGURE 3.14: Moisture profile for original FEA model at 3% initial moisture content

Analysis of the coefficients obtained from solving the FEA models presented above shows that the level of isothermal diffusion has been overestimated considerably by the relations used to determine its magnitude. This is particularly true for the isothermal vapour diffusion term, which should be small at the temperatures under consideration due to the very small amounts of vapour being produced. Other researchers have reported similar experimental results [67]. As a result, in order to obtain a closer agreement with obtained experimental results, a correction factor is applied to the isothermal diffusion terms to reduce the vapour diffusion coefficient by 2 orders of magnitude.

3.5.1.2 Modified MMA Results

By applying the correction factor discussed above, the results shown in figure 3.15 and 3.16 are obtained for an initial moisture content of 1%. On removing the backfill from the experimental apparatus after heating had been completed, it was observed that the backfill in the lower 15cm of the apparatus was almost completely dry. This was verified by oven drying, indicating that the hypothesis that there was insufficient moisture mi-

gration (due to the unrealistically high isothermal diffusion term) in the original FEA model was correct. Figure 3.16 demonstrates moisture migration behaviour much more similar to that of the experiment.

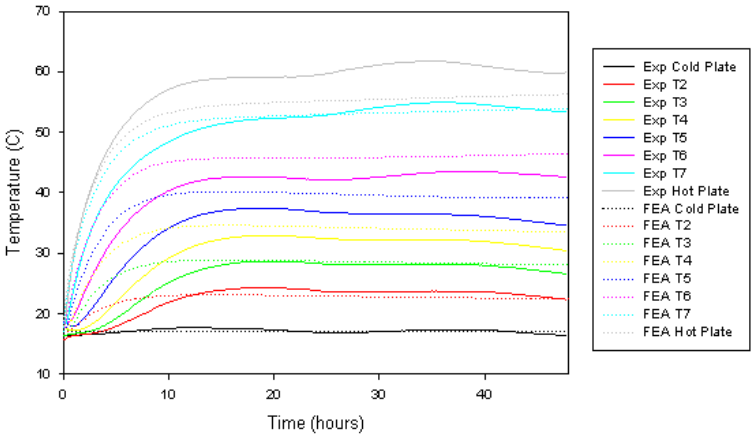

FIGURE 3.15: Temperature profile for modified FEA model, 1% initial moisture content

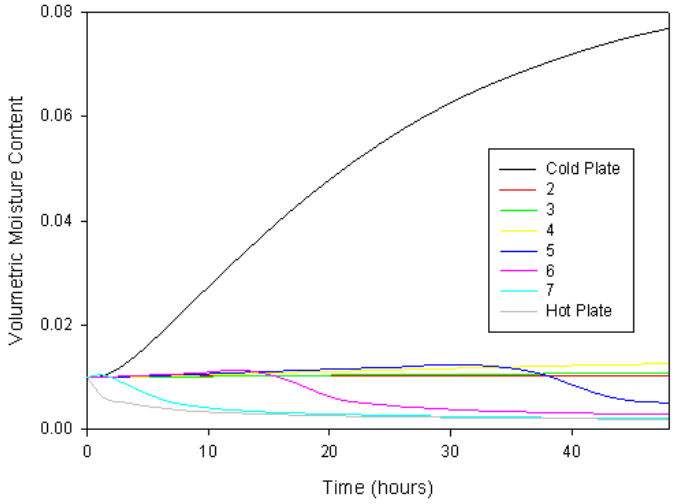

FIGURE 3.16: Moisture Profile for modified FEA model, 1% initial moisture content

The average thermal conductivity between two temperature measurement points can be calculated from the experimental data and compared with simulation results from the model. The results of this analysis are presented in Figure 3.17 and show that they are in general agreement. However the thermal conductivity between locations 7 and 8 (the 1.5cm band of backfill above the hot plate) demonstrates a thermal conductivity significantly below the theoretical minimum value of $0.232 W/m^2K$. This provides an explanation for the larger temperature difference between points 7 and 8 in the experimental data than in the model. It is possible that this effect arises due to the temperature dependence of the thermal conductivity of quartz or from inconsistent packing density within the experiment. However, the interface between the dry and moist zones of backfill appears in approximately the same location as in the FEA model, hence validating

the reduction in the isothermal diffusion coefficients. In order to improve the performance of the model in very dry regions, a correction factor is applied to the soil thermal conductivity equation which permits the thermal conductivity to decrease to 60% of the theoretical value, inline with the minima seen from the experimental data.

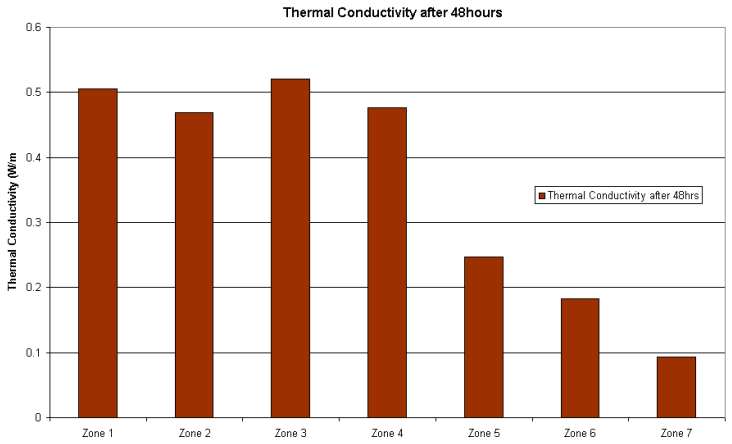

FIGURE 3.17: Experimentally derived thermal conductivity, 1% initial moisture content, 40W heating power

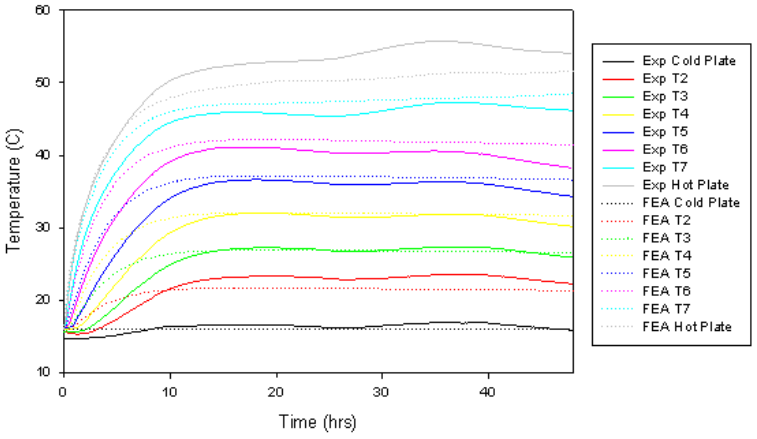

FIGURE 3.18: Comparison of modelled and experimental results for 3% initial moisture content at a heating power of 40W

Having tuned the parameters of the model, it is possible to contrast the results obtained for the full range of models. Figures 3.18 and 3.19 demonstrate the temperature profiles obtained when a 40W heating power is used for the case of an initial volumetric moisture content of 3% and 5%. Examining these plots it is possible to see the moisture migration process through the gradual changes in gradient of the temperature curves. Figures 3.20 and 3.21 show the respective thermal conductivity profiles. However the experimental data is also influenced by the diurnal variation of laboratory temperature.

In order to ensure that the model works acceptably for slightly higher heating rates, as would be expected in the case of application to high temperature cable circuits, the

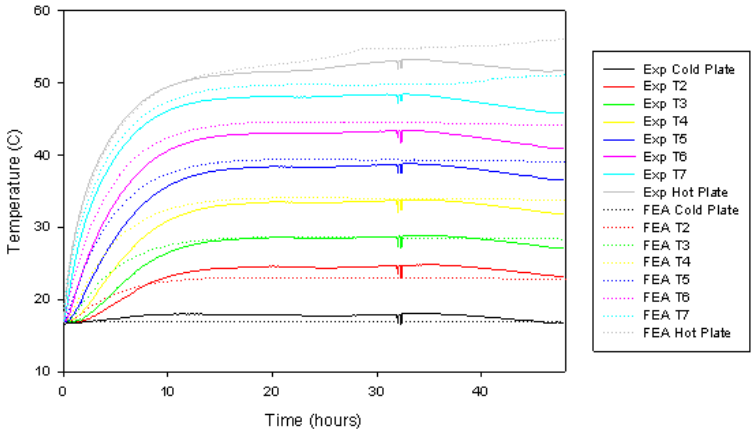

FIGURE 3.19: Comparison of modelled and experimental results for 5% initial moisture content at a heating power of 40W

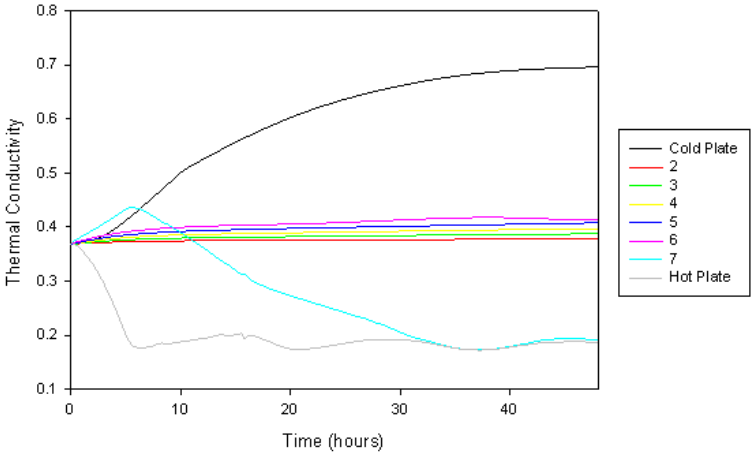

FIGURE 3.20: Thermal conductivity profile for 3% initial moisture content, 40W heating

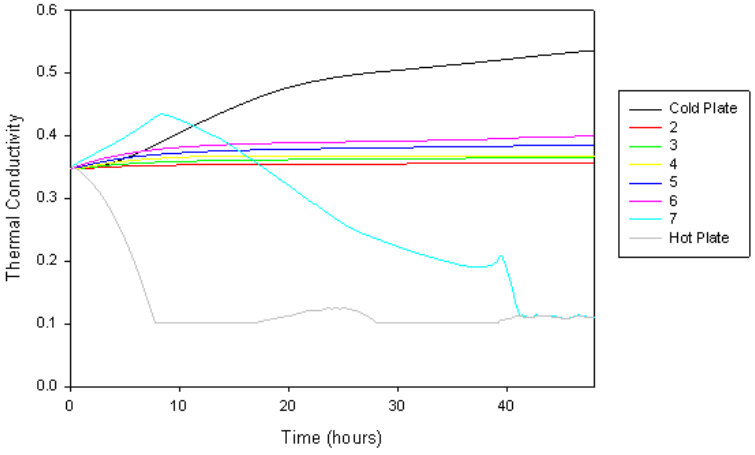

FIGURE 3.21: Thermal conductivity profile for 5% initial moisture content, 40W heating

experiment and simulation were repeated for an initial moisture content of 3% and a heating power of 80W. Acceptable prediction of hot plate temperature was achieved, as demonstrated by Figure 3.22, despite poorer correlation at points T5 and T6. Evidence of moisture migration is apparent from the thermal conductivity plot in Figure 3.23. The oscillations on the low moisture content curves occur due to numerical error in the solver as the moisture content tends to zero. The behaviour seen from the model is similar to the two zone behaviour predicted by the IEC 60287 model, as can be seen from the sharp transitions in the thermal conductivity curves in Figure 3.23.

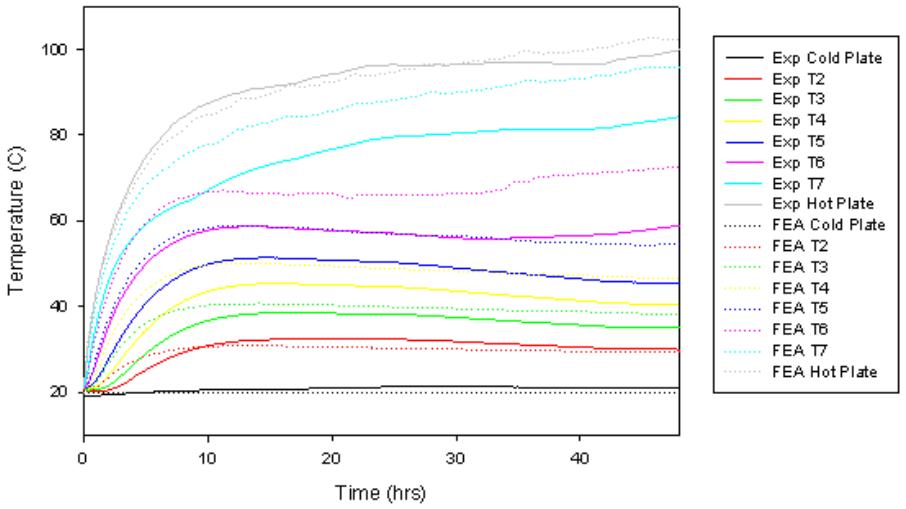

FIGURE 3.22: Comparison of results for 3% moisture, 80W heating

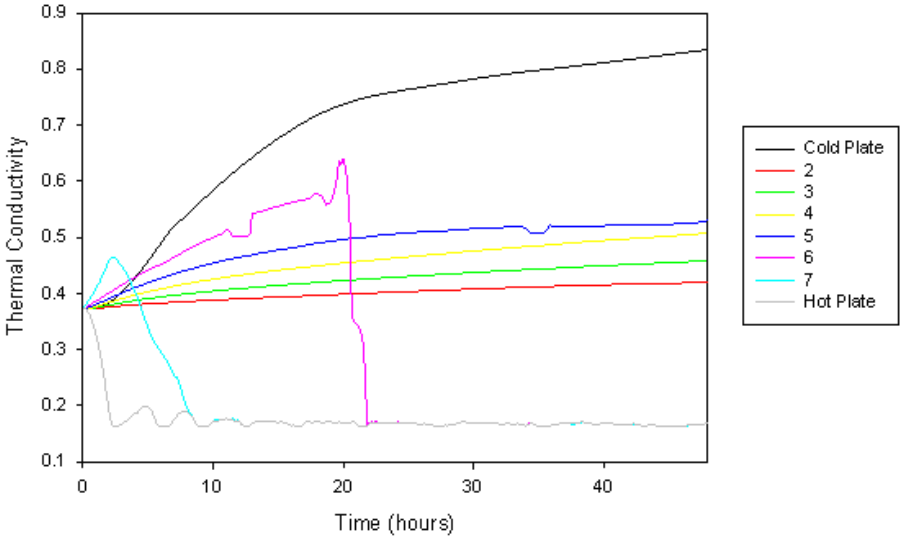

FIGURE 3.23: Thermal Conductivity profile for 3% moisture, 80W heating

3.5.2 Cable Trough

In order to further validate the moisture migration based backfill model prior to its use on buried cable scenarios, an experimental cable trough installation, constructed for a previous project, was used. A 2m length of concrete surface trough has been fitted with a 10cm diameter simulated cable and a dense network of thermocouples for temperature measurement. Heating tapes on the outside of the simulated cable provide a uniform heat output, with current supplied from a variable ac transformer. The trough is filled with a uniformly moist backfill (5% initial moisture content by volume), with additional thermal insulation provided around the trough by means of polystyrene sheets. A schematic of the test trough is shown in Figure 3.24, with the location of the thermcouple arrays summarised in Table 3.2.

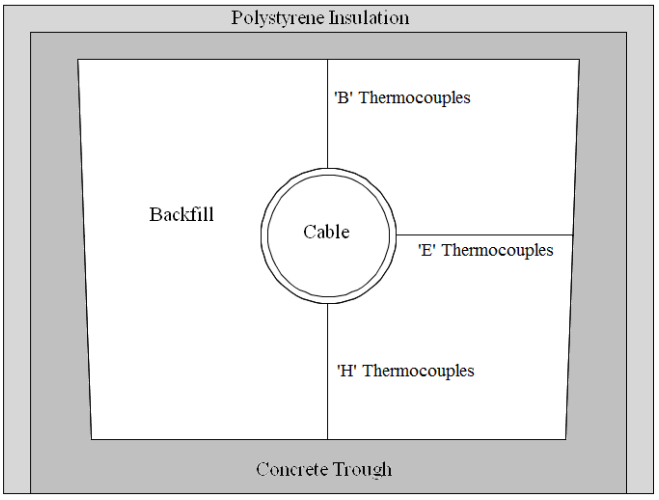

FIGURE 3.24: Schematic of single phase experimental cable trough

Location	Array B	Array E	Array H
1	1.0cm	1.5cm	1.5cm
2	2.5cm	3.0cm	2.5cm
3	4.5cm	5.5cm	3.5cm
4	5.5cm	7.5cm	5.0cm
5	7.0cm	9.5cm	7.0cm
6	8.0cm	11.5cm	9.0cm

TABLE 3.2: Thermocouple Locations in Experimental Trough (all distances are measured from the cable surface)

3.5.2.1 Model Construction

In order to generate a 2D model of the cable trough system, it is assumed that heat generation is uniformly distributed along the 2m cable length and that any end effects are negligible. This assumption allows a fair comparison with the temperature measure-

ments obtained from the central section of the experimental trough rig. It is assumed that the backfill was placed into the trough at a uniform density and a homogenous moisture distribution of 5% by volume. As the cross section of the cable trough geometry is symmetrical both geometrically and physically (in terms of the heat and moisture transport), it is only necessary to model half of the cross section. This provides benefits in terms of computational time required to solve the problem.

The finite element representation of the problem consists of four subdomains, these are the dummy cable, backfill region, the concrete cable trough and the polystyrene insulation around the outside. The backfill region is modelled as discussed in Section 3.4, whilst the other two regions are assigned constant properties. The concrete trough is presumed to be impermeable to moisture (hence neither liquid nor vapour may escape the trough), and possesses a thermal conductivity of $1 W m^{-1} K^{-1}$ and a thermal capacitance of $2 M J m^{-3} {}^{\circ}\mathrm{C}^{-1}$. The expanded polystyrene insulation is specified to have a thermal conductivity of $0.08 W m^{-1} K^{-1}$ and a $32.5 M J m^{-3} {}^{\circ}\mathrm{C}^{-1}$ thermal capacitance.

Simple thermal boundary conditions can be applied to the problem. A heat source is introduced along the cable boundary equal to the per metre length heating power used in the experiment. The top and side of the polystyrene insulation are assigned a convective heat transfer coefficient of $2 W m^{-2} K^{-1}$ as in reality they do not behave as perfect thermal insulation. The base of the trough is assigned a thermal insulation boundary as it the trough sits on additional insulating material. The mesh used in solving the model is shown in Figure 3.25.

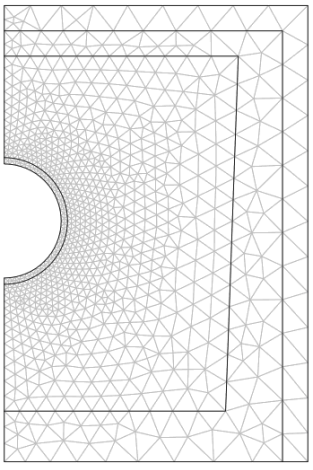

FIGURE 3.25: Finite element mesh representation of cable trough geometry

3.5.2.2 Results Comparison

The obtained results illustrate the temperature profiles obtained when a heating power of 50W/m is applied to the cable for a duration of one week. Figure 3.26 displays the temperature profile obtained throughout the cable trough region at the end of the one

week heating period, while Figure 3.27 illustrates the effect of the moisture migration phenomenon on the thermal conductivity of the backfill.

It is clear from Figures 3.26 and 3.27 that a dry band of backfill is predicted to form around the outside of the cable, causing a decrease in thermal conductivity close to the cable circuit. Figure 3.28 shows a comparison between the measured values of temperature and those obtained from the model for the thermocouple networks to the side of the cable (Thermocouple Array E).

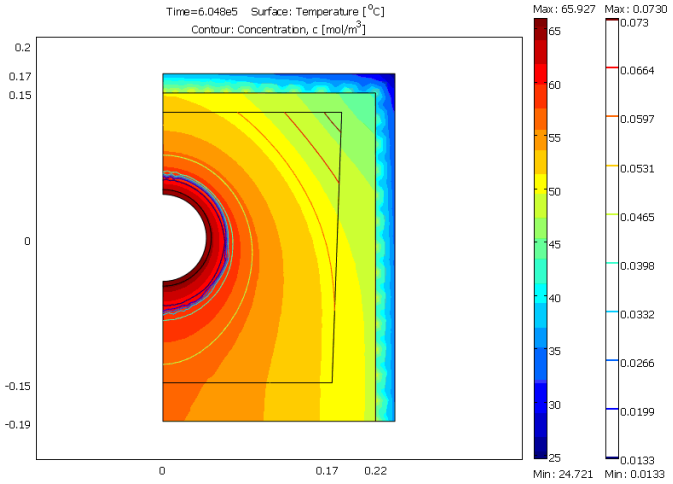

FIGURE 3.26: Trough temperature profile with contours of volumetric moisture content

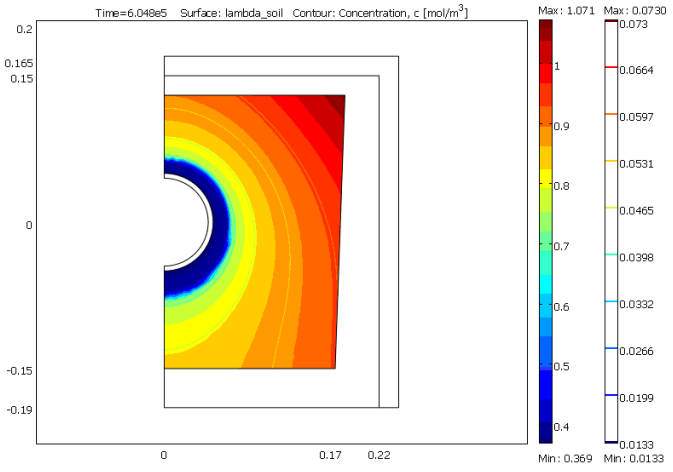

FIGURE 3.27: Trough thermal conductivity profile with contours of volumetric moisture content

The heating load on the simulated cable is then increased to 80W/m for a further week. The resultant temperature profile between the side of the cable and the trough wall is shown in Figure 3.29, with cross-sectional temperature and thermal conductivity plots from the numerical model shown in Figures 3.30 and 3.31.

It can be seen from the thermal conductivity profiles that the dry band around the cable

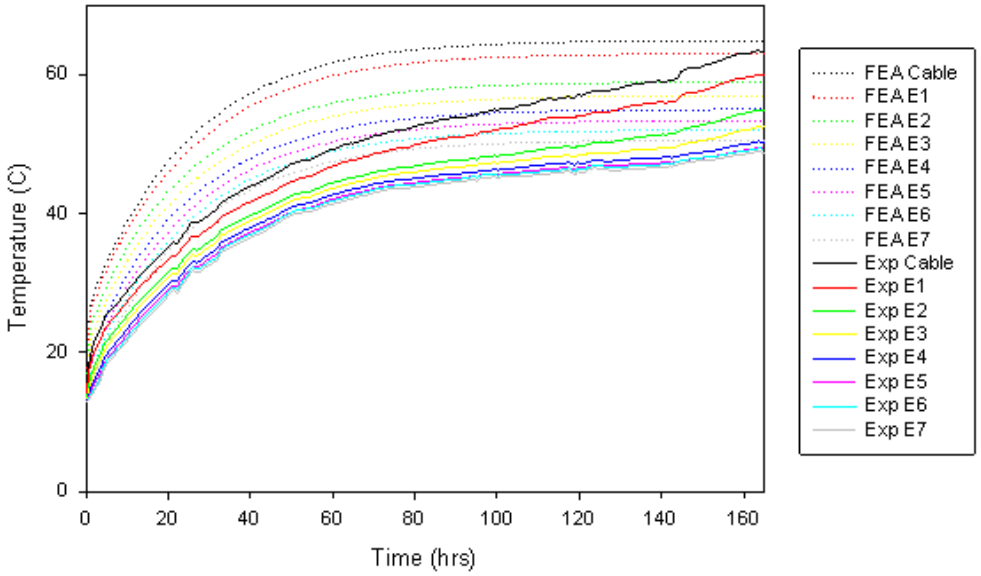

FIGURE 3.28: Temperature Comparison (side of cable)

has increased slightly in magnitude. Examination of the steady state temperatures in 3.29 shows a reasonable agreement between the model and the experiment at the cable surface, with a difference of around 1°C. In this case it can be seen that the numerical model overestimates the temperatures around the trough walls, however it is possible that this arises from the assumptions regarding the convective heat transfer from the polystyrene insulation.

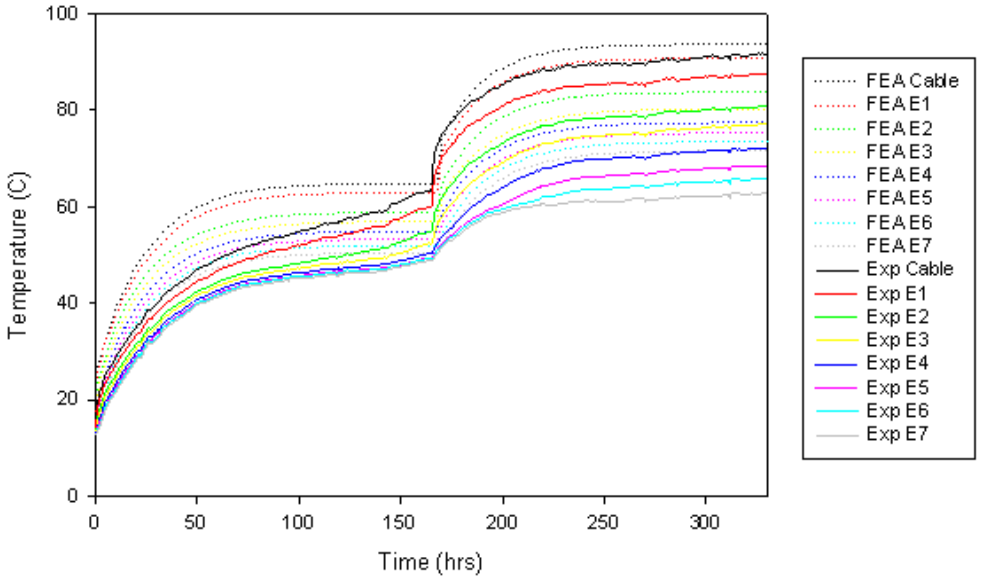

FIGURE 3.29: Temperature Comparison after two weeks operation

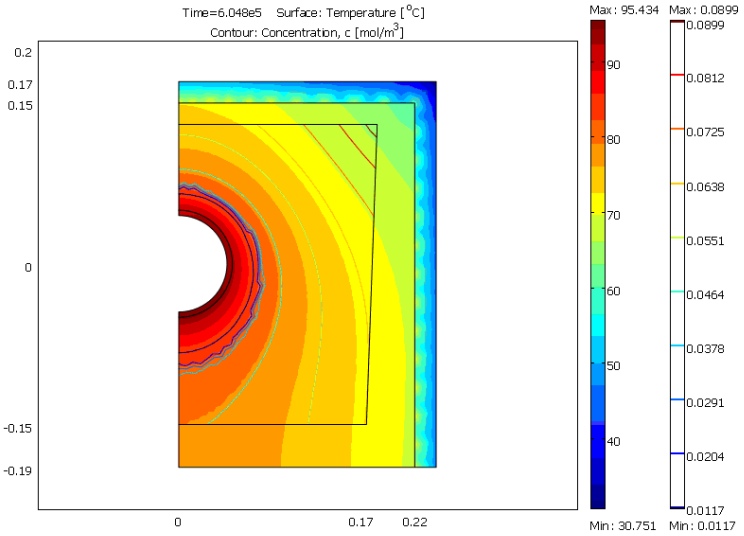

FIGURE 3.30: Trough thermal profile with contours of volumetric moisture content (after two weeks operation)

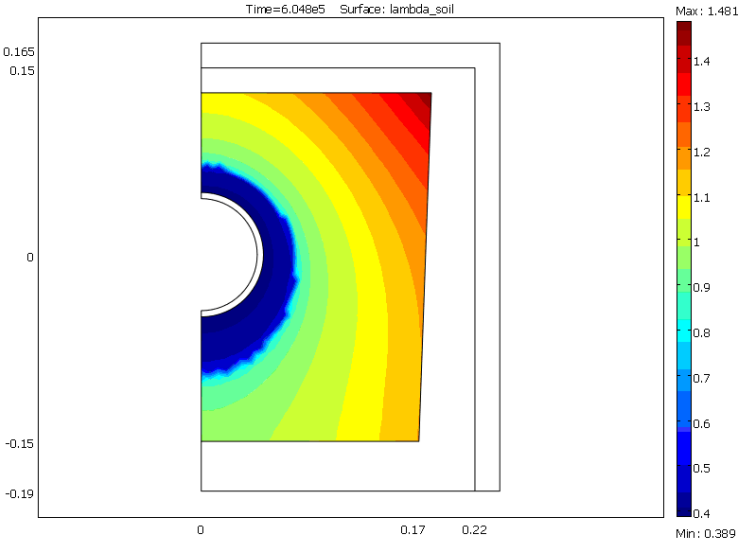

FIGURE 3.31: Trough thermal conductivity profile with contours of volumetric moisture content (after two weeks operation)

3.6 Summary

This chapter represents an essential step towards developing rating models for high temperature cable circuits. By combining a dynamic backfill model with finite element based rating models such as those described in [49] it is possible to examine the effect of moisture migration on realistic cable circuit geometries. Initially the study focuses on directly buried cable circuits, contrasting the rating potential of higher temperature cables against traditional XLPE designs. Having shown the ability to solve the problem of directly buried cable circuits, the backfill model has been integrated into rating models

for water cooled cable circuits. It can be shown that the use of water cooling may extend the available transient duration by reducing moisture migration.

Chapter 4

Rating Buried Cable Circuits

The previous Chapter detailed the development and validation of a dynamic backfill model for buried high voltage cable systems. Having successfully benchmarked the model against laboratory experiments, it is possible to model directly the process of moisture migration around directly buried cable systems. The main type of installation considered is where cables are directly buried in the ground without any additional cooling. It is also possible to install water cooling pipes around the cables to further increase the circuit rating, a technique which has been used by National Grid in a number of cases. However this approach does generate a significant maintenance overhead and also introduces a risk to the system availability, as the full design rating will not be achieved should the water cooling fail. For this reason the potential ratings available from high temperature cables without water cooling have been compared to those from a conventional XLPE cable which is water cooled.

4.1 Modelling Strategy

The calculation of ratings for the buried cable circuits can be achieved by modelling 2D slices through the cable route, subject to the following assumptions:

- The burial depth remains constant
- The backfill material remains the same along the cable route
- There are no external heat sources which might affect the thermal profile of the cable

The modelling process for water cooled cable circuits is slightly different to that of directly buried cable circuits, as the temperature of the water increases with distance from the coolant inlet point. This means that even where the burial depth of the cable

circuits remains constant, the conductor temperature of the cable circuit will change depending on the axial location under consideration. As a result, a pseudo 3D model is created to represent the circuit. This involves modelling a slice through the cable circuit at regular intervals, with these slices being connected by calculating the increase in water temperature between each slice. The following section outlines the modelling parameters and the processes involved.

4.1.1 Installation Arrangement

This Section details the installation arrangements of the cable circuit and outlines modelling conditions utilised for this study. The cable design used is common to all models presented within this thesis and is based on a design presently in use on the National Grid 400kV transmission network. The cable has a copper conductor which is surrounded by a polymeric dielectric - the dielectric thickness is the same regardless of whether the dielectric material is conventional XLPE or a high temperature dielectric. As the properties of high temperature dielectrics are not yet known in full, it is necessary to make some assumptions regarding the appropriate thermal and electrical properties. The approach taken here is to assign the same thermal and electrical properties to the HT cables as the XLPE cables, meaning that any rating gain is purely related to the additional thermal headroom rather than potential improvement in material properties. Both cables are considered to have a copper wire screen and a polyethylene oversheath. A summary of the applicable properties is detailed in Table 4.1.

The installation arrangement considered for the directly buried (naturally cooled) case is that of a modern XLPE cable circuit, shown in Figure 4.1 below. The core-core conductor spacing is 385mm, with all cables buried at a depth of 1050mm. Throughout the modelling it is assumed that the sheaths are cross-bonded, yielding the lowest possible sheath losses.

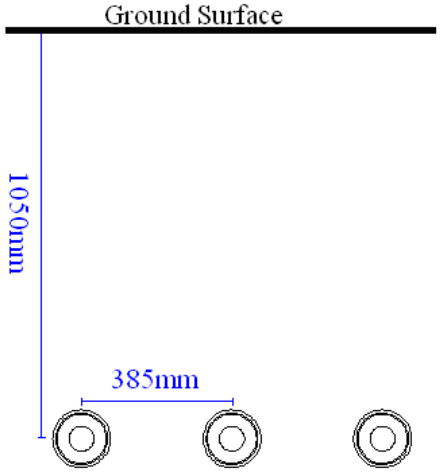

FIGURE 4.1: Cable installation arrangement for naturally cooled circuit

Geometric Parameters	**400kV cable**
Conductor Cross Sectional Area (mm^2)	2500
Conductor Diameter (mm)	64
Dielectric Thickness (mm)	31
Outer Spaced Copper Wire Screen Diameter (mm)	132
External Diameter (mm)	148
Phase Separation (mm)	385
Thermal Parameters	
Dielectric Thermal Resistivity (Km/W)	3.5
Serving Thermal Resistivity (Km/W)	3.5
Volumetric Specific Heat Capacity of Conductor (J/m^3K)	$3.45x10^6$
Volumetric Specific Heat Capacity of Dielectric (J/m^3K)	$2.4x10^6$
Volumetric Specific Heat Capacity of Spaced Copper Wire Screen (J/m^3K)	$3.45x10^6$
Volumetric Specific Heat Capacity of Serving (J/m^3K)	$2.4x10^6$
Cable Surface Emissivity	0.9
Conductor Temperature Limit (°C)	90/120/150
Electrical Parameters	
Resistivity of conductor Ωm	$1.7241x10^{-8}$
Conductor temperature coefficient of resistance ($°C^{-1}$)	0.00393
ks coefficient	0.62
kp coefficient	0.8
Screen Loss Factor (left, centre, right)	0.0111/0.0433/0.0105
Dielectric relative permittivity	2.4
System Frequency (Hz)	50
Phase to Earth Voltage (V)	230940
Tangent of dielectric loss angle	0.001

Table 4.1: Cable Specifications

For the water cooled system the geometry is slightly different, as shown in Figure 4.2. In this case, the cooling system "go" pipes (i.e. those connected to the inlet) are numbers 2 and 3, such that the coolest water is running past the centre phase. The water is then returned to the cooling station via pipes 1 and 4. The cables and water pipes are installed in a small region of CBS (1m in width by 30cm in depth), with the cable centres 10cm from the base of the CBS region. The phase to phase spacing of the cables is 385mm. The water pipes themselves are polymeric in construction, with an internal diameter of 66mm and an external diameter of 90mm. The overall length of the cooling circuit (from inlet to turnaround point) is 2.7km, the coolant flow rate 1 litre per second per pipe and the coolant inlet temperature assumed constant at 15°C.

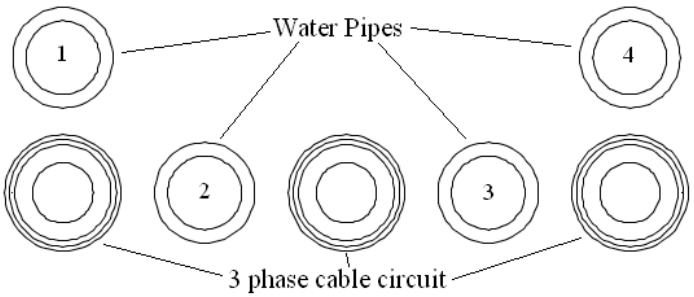

FIGURE 4.2: Geometry of forced-water cooled circuit

4.1.2 Modelling Assumptions

In order to allow clear comparison between different cable design options, the majority of model properties remain the same across all of the cable variations studied. Full details on cable construction are provided in Table 4.1 The most important are highlighted below:

Assumptions relating to the cable:

- Joule losses are assigned to the outer boundary of the conductor, which is modelled as a solid piece of copper.
- Dielectric losses are distributed across the dielectric region using the voltage dependent function described in [49].
- Sheath losses are assigned to the inner boundary of the sheath region (i.e. the interface between the dielectric and the sheath).
- Conductor ac resistance is considered to be fully variable with temperature. The calculation implemented is that presented in [18].

Assumptions relating to the thermal environment:

- The remote ground temperature is assigned to be 12°C, as suggested by [62].
- The air temperature is fixed at 15°C, with the ground surface modelled as a still air convection boundary with a heat transfer coefficient of 6 $Wm^{-2}K^{-1}$. This is essential as assuming an isothermal ground surface condition with high temperature cables would be too optimistic based on the work reported in [49].
- At the start of a steady state calculation, the moisture distribution within the backfill is uniform with the initial temperature being 12°C.
- Dry density of the backfill is assumed to be $1575kgm^{-3}$.

- All external boundaries are considered to be insulating to moisture. This does mean that there is no moisture input to the backfill (for instance due to rainfall).

A number of assumptions must also be made regarding the operation of the water cooling system in the cooled models. The heat transfer coefficient, h, is determined from

$$h = \frac{q}{T_s - T_b} = \frac{Nu_D k}{D} \tag{4.1}$$

where T_s and T_b are the inner pipe wall and bulk coolant temperatures in K, k is the thermal conductivity of water (taken as $0.5991 W.m^{-1}.K^{-1}$ at 20°C) and D is the characteristic diameter of the flow. The Nusselt number, Nu_D, is determined using the Gnielinski relation [101],

$$Nu_D = \frac{(f/8)\,(Re_D - 1000)\,Pr}{1 + \left[12.7\,(f/8)^{0.5}\left(Pr^{2/3} - 1\right)\right]} \tag{4.2}$$

where Re_D is the dimensionless Reynolds number, Nu_D the Nusselt number for the coolant flow, and Pr is the Prandtl number of water (taken as 7.14 at 20°C). As the pipe wall is assumed to be smooth, the Blasius resistance formula is used to find the friction factor, f [92],

$$f = 0.3164 {Re_D}^{-0.25} \tag{4.3}$$

In order to calculate the increase in the water temperature between slices, it is necessary to integrate the heat flux crossing each of the water pipe boundaries. This is then used within

$$T_{b,out} = T_{b,in} + \frac{q\pi DL}{mC_p} \tag{4.4}$$

to obtain the temperature rise between the two slices, where $T_{b,in}$ is the water temperature in a particular pipe at the current slice, q is the heat flux (Wm^{-2}) entering the pipe, D is the pipe diameter (m), L is the length of pipe between slices (m), m is the mass flow rate ($kg.s^{-1}$) and C_p is the specific heat capacity of water ($kJkg^{-1}K^{-1}$).

4.2 Continuous Ratings for Uncooled Circuits

As stated previously, continuous ratings are to be obtained for both the standard XLPE cable and high temperature cables capable of conductor temperatures of 120°C and 150°C. All continuous ratings are calculated by solving the full transient calculation over a period of 40 years, at which point steady state conditions have been reached. As a further comparison, the rating is also calculated using an FEA model with the same assumptions as the partial drying algorithm provided within IEC 60287 [18].

4.2.1 Results with Dynamic Backfill Model

The performance of the high temperature cable designs is to be benchmarked against that offered by the existing capability of standard XLPE cables. The continuous rating for this system is derived using the same dynamic backfill model as that used for the high temperature cables to ensure a true comparison. Ratings are obtained by iteratively solving the model for higher levels of current, until the maximum conductor temperature criterion is reached.

To obtain a steady state solution, a transient model is solved for a forty year period that represents the design lifetime of the cable. A variable timestep is specified such that the solution takes smaller steps initially (when the change in temperatures and movement of moisture is relatively large), but does not excessively extend the computational time required towards the end of the time period. The results obtained are summarised in Figure 4.3 and Table 4.2 below.

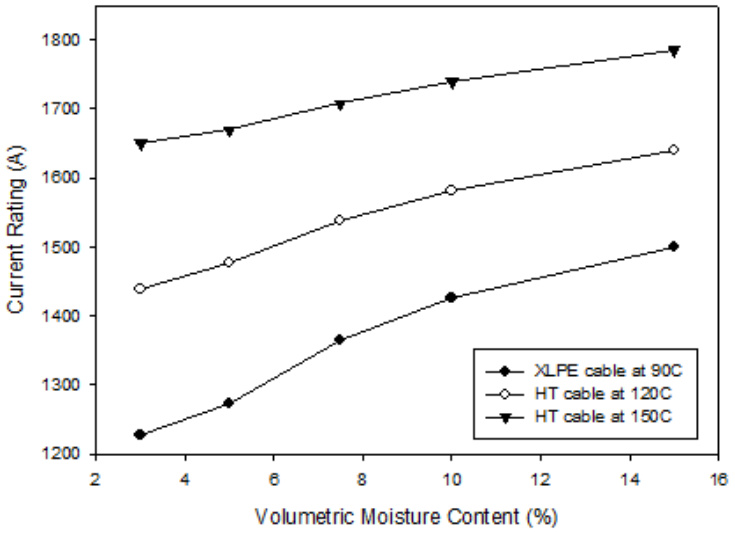

FIGURE 4.3: Variation of continuous rating with conductor temperature and volumetric moisture content

θ	90°C	120°C	150°C
3%	1228A	1439A	1650A
5%	1274A	1476A	1670A
7.5%	1365A	1538A	1708A
10%	1426A	1582A	1739A
15%	1500A	1641A	1785A

TABLE 4.2: Continuous Ratings from Dynamic Backfill Model

As would be expected, the circuit rating increases with increasing volumetric moisture content due to the rise in thermal conductivity of the backfill. The extent of the dry zone around the cable circuit depends largely on the initial volumetric moisture content. The steady state moisture distribution for two initial moisture contents are shown in

Figures 4.4 and 4.5. Examining Figure 4.4 for the resulting moisture distribution with a 3% initial condition, it is apparent that the whole of the area around the cable is almost completely dry, with the moisture front being located in the region of the 20°C isotherm. For the case of the 10% initial condition shown in Figure 4.5, the dry zone appears much smaller, with the interface between dry and moist soil occurring at around the point of the 35°C isotherm. The much smaller dry region, combined with the higher thermal conductivity of the remote soil, explains why the rating obtained in this case is much higher than for the 3% case.

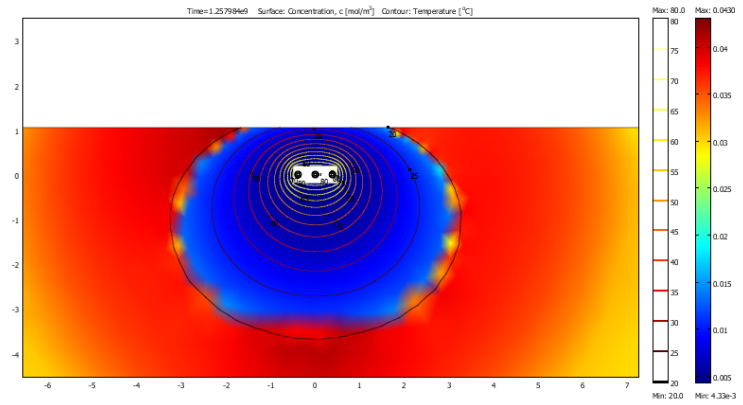

FIGURE 4.4: Steady State Moisture Distribution (Conventional Cable, initial θ=3%)

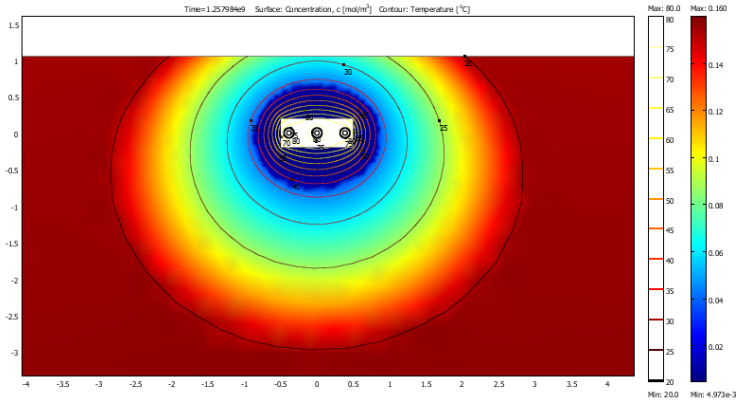

FIGURE 4.5: Steady State Moisture Distribution (Conventional Cable, initial θ=15%)

Although the utilisation of higher conductor temperatures does lead to some rating gains, they are on the whole modest. For 150°C operation the highest percentage increase is 34%, which is found for the 3% moisture condition, but the percentage increase is only 19% at 15% initial moisture content. However, were such high conductor temperatures to be used on a continuous basis the temperature rise at the ground surface would be substantial, as shown in Figure 4.6.

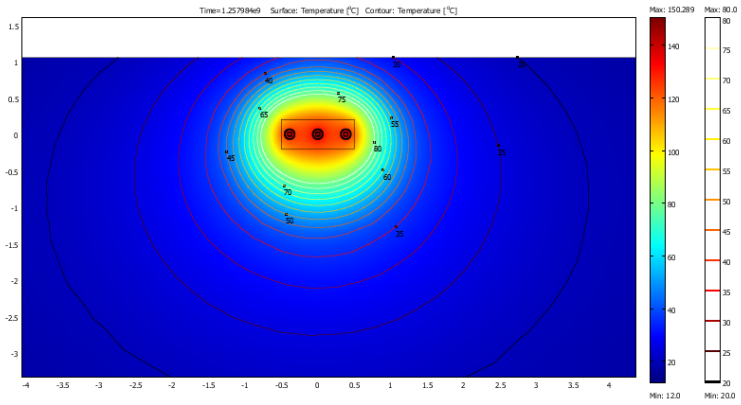

FIGURE 4.6: Temperature profile for continuous operation at 150°C, 10% moisture content

4.2.2 Comparison to Two Zone Methodology

To allow comparison between the results obtained above and standard methods, a finite element version of the IEC 60287 partial drying calculation was implemented. This additional model has been created with a temperature dependent backfill thermal conductivity, where the difference between moist and dry material is defined by the location of either the 20°C or 50°C isotherm. At temperatures greater than the stated limits the thermal resistance was set to $3.45 K m W^{-1}$ (the maximum found in the full dynamic backfill model), while below the same temperature the thermal resistance of the backfill matches the initial condition from the dynamic backfill FEA model. Three sets of steady state results were obtained:

- Simplified two zone FEA model with dry interface at 20°C
- Simplified two zone FEA model with dry interface at 50°C
- Full dynamic backfill model

Assessing the data summarised in Tables 4.3 and 4.4 below, a number of trends are apparent. When compared to the results from the full dynamic backfill model, the 2 zone model with wet/dry interface at 20°C appears pessimistic by between 2.6% and 12.3% (expressed as a percentage of the dynamic backfill model ratings), with the greatest range across the moisture contents being for the standard XLPE cable system. For the 90°C cable at least, the discrepancy with the full backfill model appears to increase with moisture content. It was noted in Section 4.2.1 that the temperature at which the dry zone occurred appeared to increase with moisture content, most likely due to a corresponding decrease in soil suction. This could explain the reasoning behind the differences in results, as placing the wet/dry interface at 20°C would be pessimistic for an initial moisture content of 15%.

θ	90°C	% Change	120°C	% Change	150°C	% Change
3%	1195	2.6%	1398	2.8%	1560	5.5%
5%	1228	3.6%	1430	3.1%	1594	4.5%
7.5%	1262	7.5%	1467	4.6%	1627	4.7%
10%	1298	8.9%	1503	5.0%	1662	4.4%
15%	1316	12.3%	1520	4.4%	1680	5.9%

TABLE 4.3: Continuous Ratings from 2 zone FEA model (convective ground surface, dry zone at 20°C)

θ	90°C	% Change	120°C	% Change	150°C	% Change
3%	1434	16.8%	1582	9.9%	1707	2.7%
5%	1584	24.3%	1711	15.9%	1822	9.1%
7.5%	1712	26.2%	1824	18.6%	1921	12.5%
10%	1825	28.0%	1926	21.7%	2021	16.2%
15%	2004	33.6%	2114	28.8%	2190	22.7%

TABLE 4.4: Continuous Ratings from 2 zone FEA model (convective ground surface, dry zone at 50°C)

The data in Table 4.4 demonstrates the importance of selecting the most appropriate temperature for the interface isotherm. By placing the isotherm at 50°C, the vast majority of the soil/backfill region is outside of the dry zone, meaning that the calculation is showing almost no moisture migration for a conductor temperature of 90°C. This explains the very high rating differences (up to 33.6%) observed between this model and the full dynamic backfill model, with the 2 zone model being optimistic. Again, the difference between the two ratings increases as the initial moisture content increases.

The key conclusion that can be drawn from the data presented in this Section concerns the validity of assuming that the wet/dry interface will occur at a set temperature. While the results seen in Chapter 3 support the existence of a fairly well defined boundary between the two regions, it was clear in Section 4.3.1 that increasing the initial moisture content from 3% to 15% changed the location of the wet/dry interface in the dynamic backfill model from 20°C to 35°C. This means that the bulk moisture content of the material may need to be considered, as well as the dry properties of the material. However, it is beyond the scope of this thesis to determine the most appropriate method as it would require a wide range of soil types to be tested using the methodologies described in Chapter 3.

4.3 Calculation of Continuous Ratings for Water-Cooled Circuits

In order to benchmark the performance improvement available from the HT cable circuits, ratings have been calculated for a water-cooled conventional XLPE cable circuit.

The use of water cooling greatly increases the continuous rating of the cable circuit by removing heat from the backfill medium which surrounds the cable circuit. As a result, the conductor temperature of the cable will be significantly lower for any given load, even where the coolant flow rate is reasonably small.

4.3.1 Full dynamic backfill model

Steady state temperature distributions have been obtained for a range of moisture contents with a loading of 2564A, which gives the 90°C rating with the lowest moisture content of 3% (Figure 4.7). The solution time required for the model varies as a function of circuit loading. The reason for this is that where the level of moisture migration is low and the speed of the moisture front is sufficiently slow, the FEA solver may take relatively large time steps without a reduction in the accuracy of the solution. As a result, it is possible to obtain the solution to the model for a loading of 1500A within one hour. The solution time appears to increase exponentially with circuit loading, as the time necessary at the 90°C rating of 2564A (3% moisture) is around 12 hours.

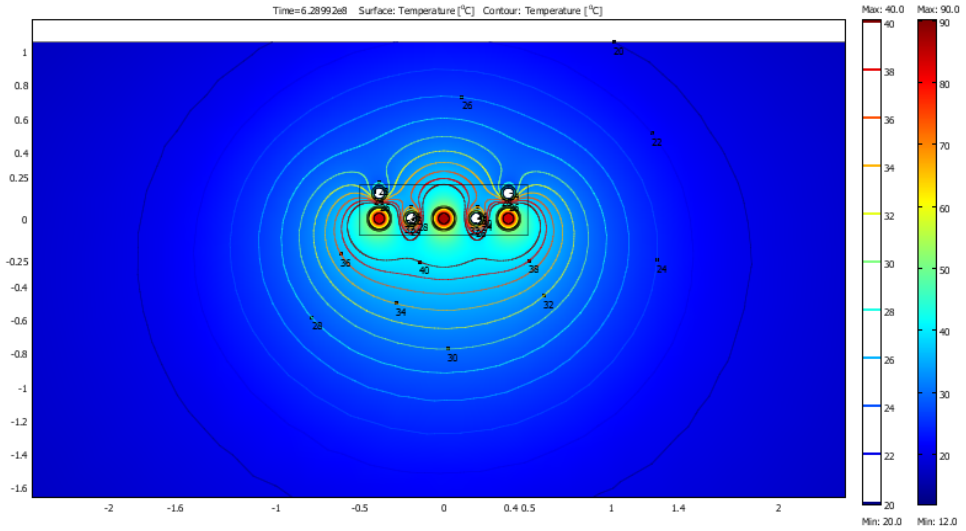

FIGURE 4.7: Contours of temperature at 2564A, initial moisture content 3%

When compared with the ratings of the equivalent directly buried circuits, it is apparent that the use of water cooling brings significant gains in steady state rating. Where the cables were directly buried, the continuous rating at 90°C is only 1228A, compared to the 2564A available when water cooling is used, a gain of 109%. The available rating from the water-cooled XLPE circuit is significantly higher than the rating for the 150°C un-cooled circuit (1650A). Even where the initial moisture content for the buried model is 15%, the water-cooled XLPE circuit still offers a rating 43.6% higher than the 150°C buried cable circuit. This reinforces the notion that the true benefits of high temperature operation of buried cables are likely to be under emergency rating conditions, as the water-cooled system will still offer a better continuous rating.

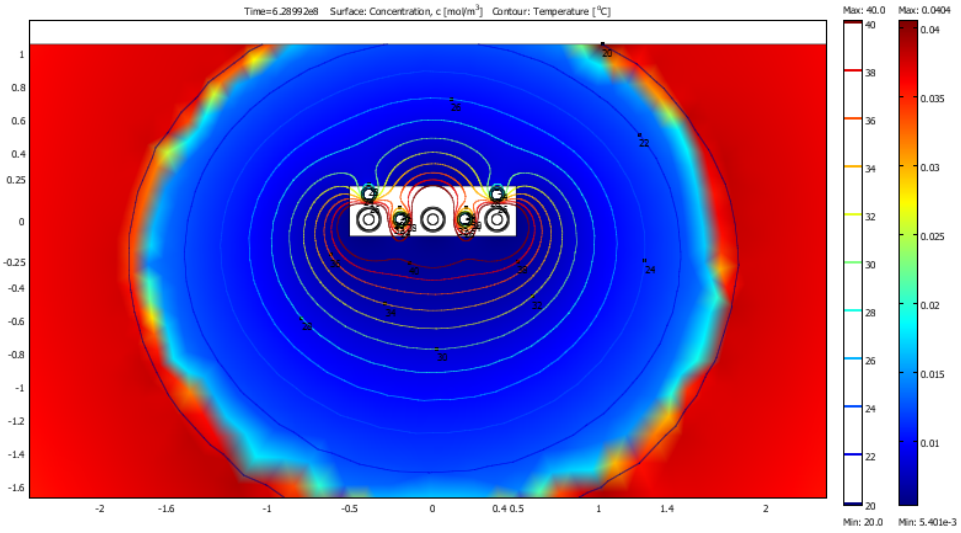

FIGURE 4.8: Contour plot of moisture content at 2564A, initial moisture content 3%

Figure 4.8 also demonstrates the effect of the water cooling pipes on reducing the level of moisture migration around the cable groups when compared to the equivalent directly buried case (Figure 4.5). While moisture migration does still occur, the overall size of the dry zone is significantly smaller than was seen in the directly buried case. Hence it is clear that a significant part of the rating gain from the water cooling appears not just from the cooling of the cables by the water pipes, but also the reduction in the ground thermal resistance outside of the CBS region.

As the coolant temperature increases as it passes along the cable route, the conductor temperature profile is not uniform. Figure 4.9 demonstrates the cable temperature profile for the 90°C rating case, with the centre conductor rising in temperature from 83.9°C at the coolant inlet to 90°C at the turn around point. The outer phases show

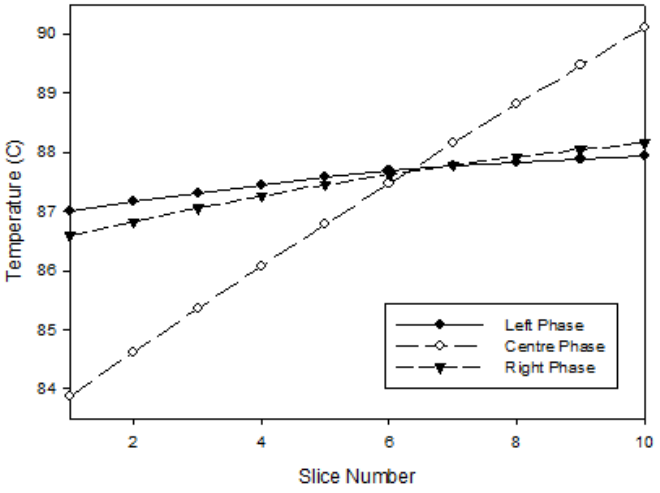

FIGURE 4.9: Conductor temperature variation at steady state rating (2564A, 3% moisture content)

less of an increase in temperature along the route due to the water in the return pipes at the inlet end (slice 1) being at its maximum temperature. The corresponding change in coolant temperature is shown in Figure 4.10, with the water in the "go" pipes increasing from 15°C to 23.5°C at the turnaround point. As less heat is transferred to the water whilst in the return pipe (due to the position of these pipes further away from the cable groups), the coolant temperature increase on the return leg is lower with a water temperature at the outlet of 28.6°C.

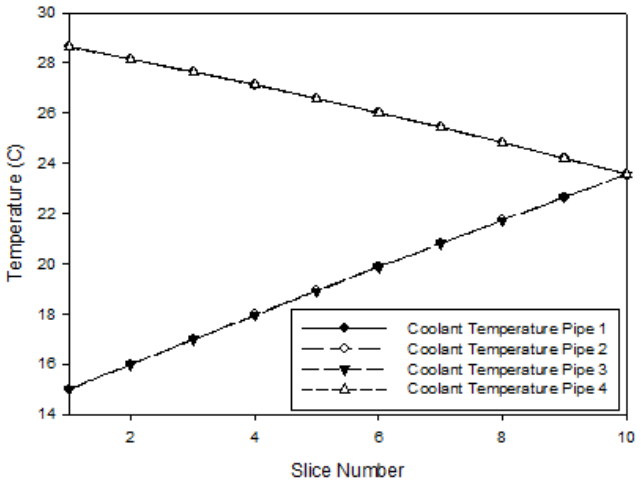

FIGURE 4.10: Variation in water temperature along route

4.3.2 Two zone FEA model

During the study of directly buried cable ratings, a comparison was undertaken between the dry zone implementation of IEC 60287, a similar two zone FEA model and the full dynamic backfill model. It was observed that where the simple two zone FEA model was specified as having a free air convection boundary condition, it would underestimate the true rating of the cable circuit (partly as this model does not consider the transfer of latent heat in water vapour as it migrates away from the cable and partly due to specification of the wet/dry interface). However, this model offers a significant advantage in that it can be solved in a much shorter time frame.

In order to investigate whether the outcome would be similar for water cooled circuits, the thermal properties of the backfill model have been simplified to allow a two level temperature dependent thermal resistivity. At temperatures greater than 20°C, the thermal resistance is $3.45 K m W^{-1}$ (the maximum found in the full dynamic backfill model), while below 20°C the thermal resistance of the backfill is matched to the initial condition of the dynamic backfill model. The CBS region remains at its maximum thermal resistivity of $1.2 K m W^{-1}$ throughout. A comparison is formed by solving both water-cooled models for the same value of current (2564A giving 90°C at 3% moisture content). The maximum conductor temperatures are as indicated in Figure 4.11. It can

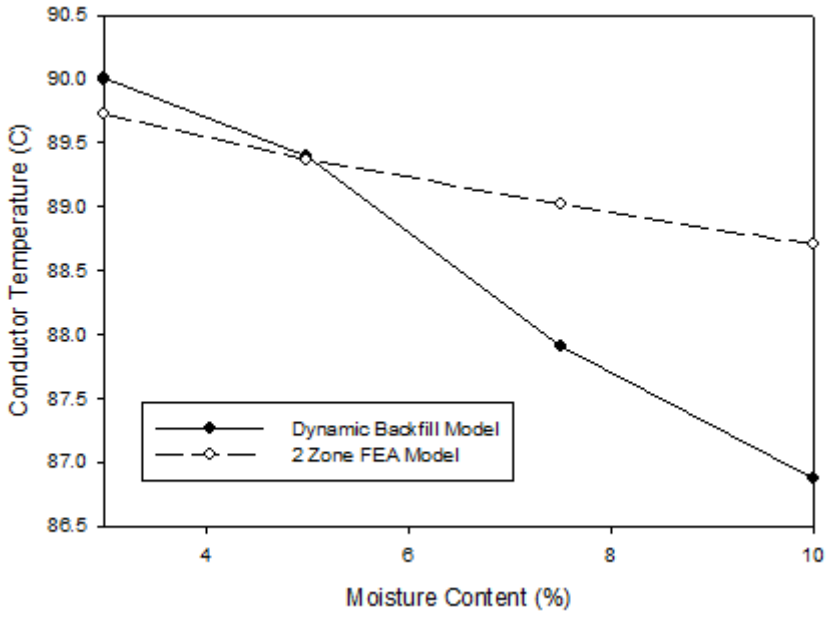

FIGURE 4.11: Comparison of conductor temperatures at 2564A for water cooled models

be seen that at 3% the agreement between the two models is very good, with the two zone model giving a lower conductor temperature by 0.3°C. At a moisture content of 10% the 2 zone model over-predicts the conductor temperature by around 1.8°C. This demonstrates that where the level of moisture migration is limited, taking a two zone approximation may be valid.

4.4 Emergency Ratings for Uncooled Circuits

Having obtained the continuous ratings of the cable circuits under investigation, it is possible to conduct a more detailed examination of the emergency rating capability. The first set of emergency ratings discussed here are for a post-fault period of 6 hours, as this is the most commonly used emergency rating specification within National Grid. The possibilities of extending the duration of the post-fault rating are explored in Section 4.4.2. The pre-fault loading is specified as either 60% or 75% of the continuous current rating for the circuit, unless otherwise stated. Given the observations made on the agreement between the simple 2 zone model, the results are compared to those results from the two zone model where the wet/dry interface falls at 20°C.

4.4.1 Results for the 6hr Rating

In order to calculate the 6hr rating, the dynamic backfill model is solved for the preload current flowing for a duration of 40 years to obtain a steady state solution. This steady

state solution is then set as the initial condition for the transient solution. The same variable timestep approach is used to solve the emergency rating models to ensure that the start of the transient is calculated accurately. The results obtained for a 60% preload are shown in Figure 4.12 and for a 75% preload in Figure 4.13.

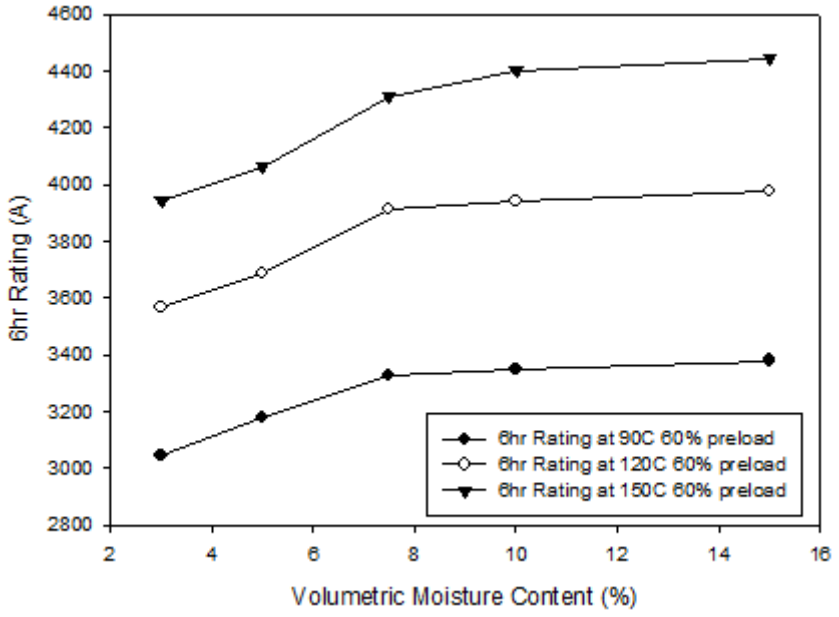

FIGURE 4.12: 6hr Ratings with 60% preload

Examining the data in Figures 4.12 and 4.13 it is immediately apparent that for all conductor temperatures studied the emergency rating does not greatly increase once the initial moisture content exceeds 7.5%. Such behaviour is observed due to the initial conductor temperatures (at the start of the transient) being very similar. Indeed for each maximum conductor temperature considered there is a maximum increase of only 11% to the emergency rating between the initial moisture contents of 3% and 15%. The reason for this behaviour is that the time constant of the cable is of a similar order of magnitude to the length of the transient being modelled. Therefore the thermal impact of the cable on the surrounding soil is quite limited.

Although the variation in emergency rating for constant maximum conductor temperature across a range of soil water contents is small, substantial differences are observed where the water content is constant and the 6hr ratings at 90°C and 150°C are considered. Examining the data for a 60% preload and a 3% initial moisture content, the 6hr rating increase is almost 30%. From an operational standpoint such an increase could prove extremely valuable in lifting network constraints and may in fact prove more utilizable than the increases in continuous rating.

Although the IEC 60287 methodology is not designed for transient analysis, it is possible to compare a transient version of the 2 zone FEA model to the results from the full dynamic backfill model. The results for a 60% preload are shown in Figure 4.14, with

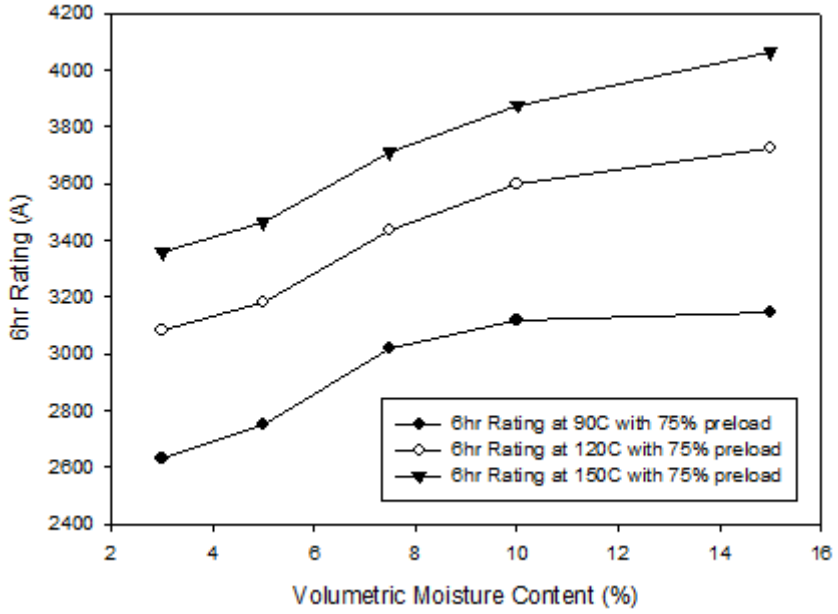

FIGURE 4.13: 6hr Ratings with a 75% preload

similar trends visible to those seen in the steady state analysis. The agreement between the two models is better at low initial moisture contents, with the two zone model becoming pessimistic once the moisture content exceeds 5%. Again this occurs as the moisture migration model allows a gradual transition to the fully dry zone at lower moisture contents, while the 2 zone model forces an immediate transition at the 20°C isotherm.

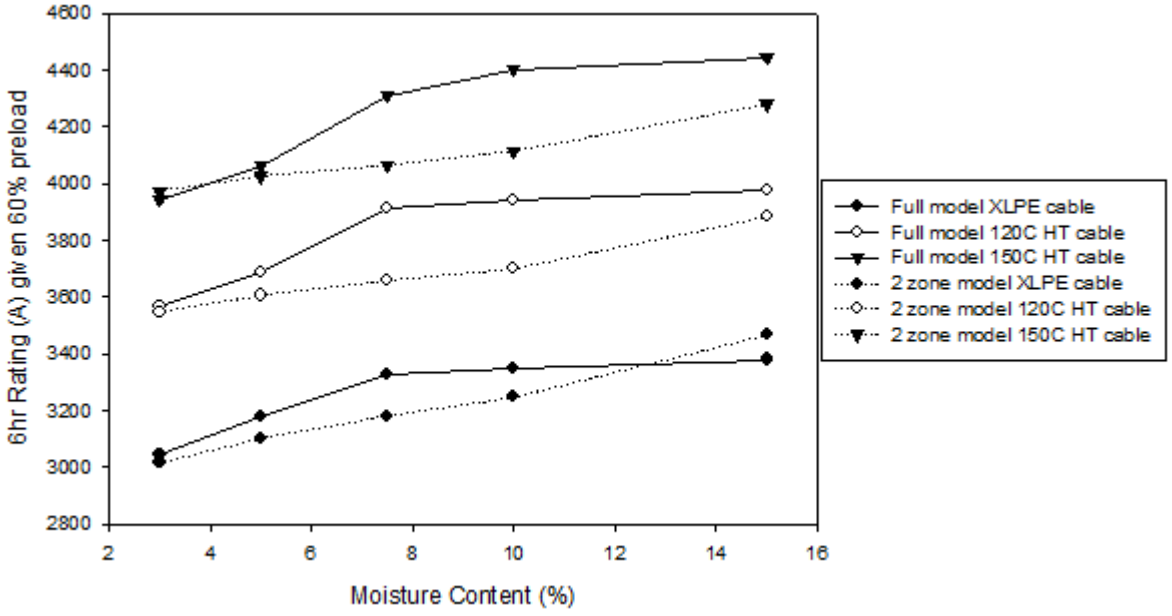

FIGURE 4.14: Comparison of 6hr ratings between moisture migration and 2 zone FEA models

Given that high temperature operation may prove more beneficial under the emergency rating conditions than in steady state, it might prove advantageous to operate the high temperature cable as if it were a standard XLPE cable except where the 6hr rating is brought into use. This then provides the maximum possible conductor temperature headroom as the initial conductor temperature could be as much as 100°C below the maximum limit. Figure 4.15 illustrates the available 6hr ratings in this case, with the curves showing that the rating available could be as much as 600A higher than when the full continuous rating is used. Such a mode of application would allow like for like replacement of existing life expired 400kV cable, with an emergency rating still being available even if the system had been operating at or near to its continuous rating.

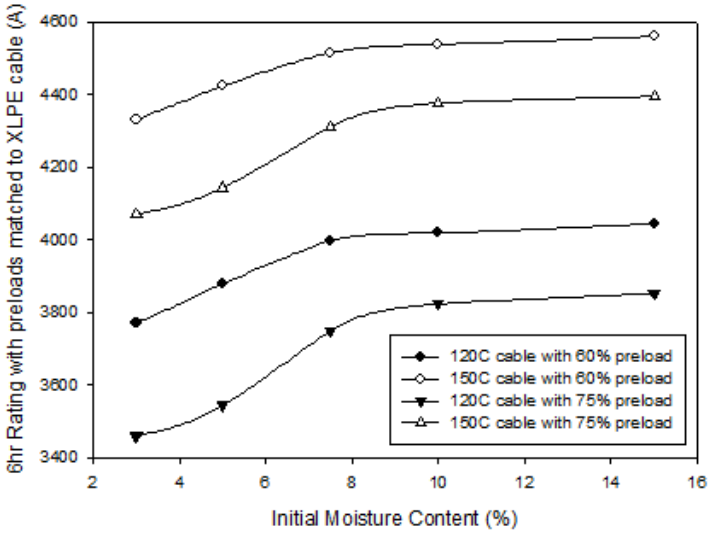

FIGURE 4.15: 6hr Ratings where continuous is constrained to 90°C

4.4.2 Results for the 24hr Rating

It was demonstrated in Section 4.4.1 that the high temperature cables may be able to lift some network constraints through their higher 6hr rating. However in some cases a constraint may arise not just from the maximum value of load current available, but also the duration for which it can be applied. The additional flexibility available from the high temperature cables might be able to extend the 6hr rating period significantly, perhaps as far as 24 hours. Were this to be technically feasible, it would greatly extend the time frames available for both fault repair and scheduled maintenance. To explore this possibility further, the calculations undertaken for the 6hr rating are repeated but for a maximum duration of 24 hours.

Figures 4.16 and 4.17 compare the 6hr and 24hr ratings available for preloads of 60% and 75% respectively. As would be expected the 24hr ratings are lower than the 6hr ratings, however one key conclusion can be drawn from these plots. In both cases when

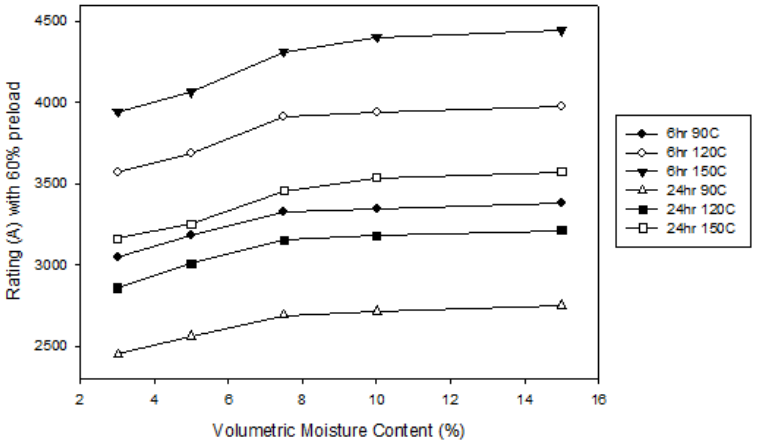

FIGURE 4.16: Comparison of 6hr and 24hr ratings with a 60% preload

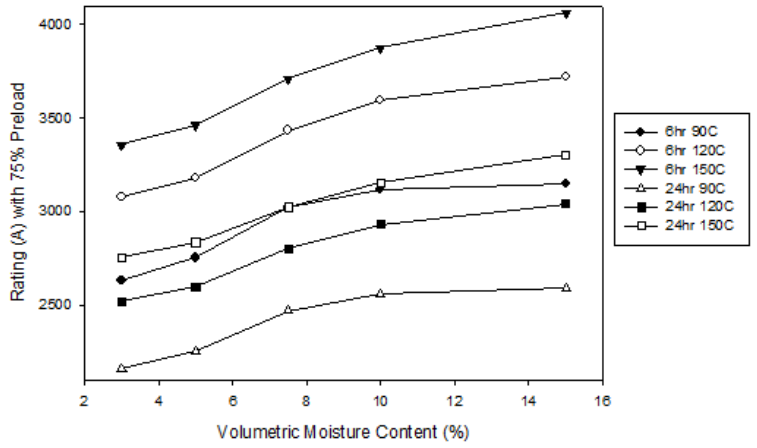

FIGURE 4.17: Comparison of 6hr and 24hr ratings with 75% preload

comparing the 6hr rating at 90°C and the 24hr rating at 150°C it can be seen that the latter slightly exceeds the former. Therefore it would seem feasible that the introduction of 24hr ratings could allow the 6hr rating of a buried XLPE cable to be available for 4 times the current emergency rating duration.

When comparing the data from the full model and the 2 zone model, the trends seen are very similar to the 6hr rating, as evidenced by Figure 4.18. Agreement is best at the lowest moisture contents, with the 2 zone model becoming slightly optimistic at 15% moisture content. However for the majority of combinations tested the difference is less than 3%. This further validates the modelling techniques used within the full dynamic backfill model, as it demonstrates that the ratings being calculated are within the expected ranges from more conventional techniques.

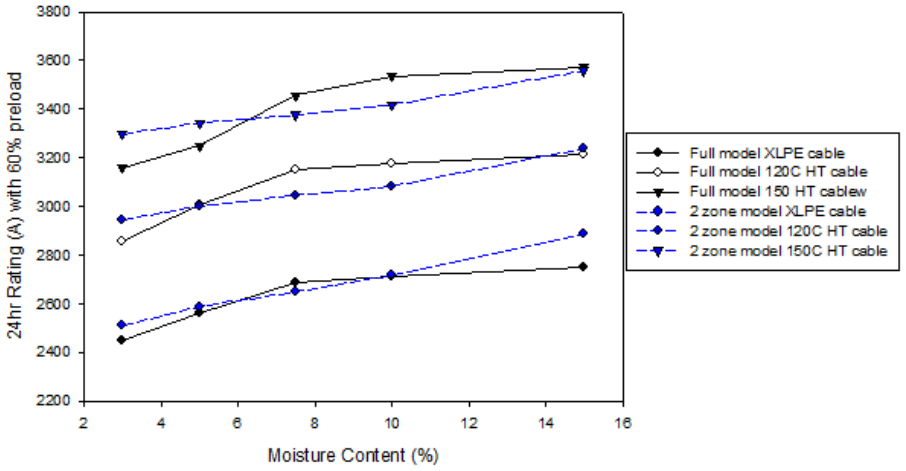

FIGURE 4.18: Comparison of 24hr ratings from full and 2 zone models

4.5 Emergency Ratings for Water-Cooled Circuits

Having obtained the continuous ratings of the cable circuits under investigation, it is possible to conduct a more detailed examination of the emergency rating capability of water-cooled circuits. The first set of emergency ratings discussed here are for a post-fault period of 6 hours, as this is the most commonly used emergency rating specification within National Grid. For comparison, the appropriate 24 hour ratings have also been calculated and are presented in the following Section. Comparisons are made to the performance of the directly buried high temperature cables to further inform the final discussion on the merits of the new technology.

4.5.1 Results for the 6hr Rating

The preload settings specified for this analysis is 60% of the continuous rating of the water cooled XLPE circuit. The results obtained are detailed in Table 4.5. As at present the rating would be restricted to 4000A by other components (such as circuit breakers) in most cases, the ratings for operation at 90°C are already sufficiently high that the cable would no longer be the limiting factor in the 6hr rating of the overall circuit. The performance at 120°C and 150°C is sufficiently high that it is likely to exceed the available rating of an overhead line.

Conductor Temperature	Preload (A)	6hr Rating (A)	6hr Rating of buried cable
90°C	1538A	3811A	3044A
120°C	1538A	4391A	3566A
150°C	1538A	4855A	3943A

TABLE 4.5: 6 Hour Ratings with a 60% preload at 3% initial moisuture content

To allow further comparison between the full backfill model and the reduced two zone

approach, the reduced approach has also been used to calculate the six hour emergency ratings on the assumption of a 60% preload and the results are shown in Table 4.6. The agreement between the two models is surprisingly good, with the variation being less than 1.5% in all cases. The reason for this accuracy is that the positioning of the water cooling pipes within the CBS region reduces the relative impact of the remainder of the backfill on the conductor temperatures. This provides an explanation for the closer agreement between the models than that found for the directly buried cables.

Conductor Temperature	Preload (A)	6hr Rating (A)	6hr Rating (2 zone)
90°C	1538A	3811A	3850A (1.0%)
120°C	1538A	4391A	4433A (0.95%)
150°C	1538A	4855A	4927A (1.5%)

TABLE 4.6: 6 Hour Ratings with a 60% preload at 3% initial moisture content, 2 zone model

4.5.2 Results for the 24hr Rating

During the analysis of the directly buried cable circuits, it was noted that the 24 hour ratings available from the high temperature cables could match and in some cases exceed the 6 hour ratings available from XLPE circuits. As a result, additional modelling for water-cooled circuits has been carried out to establish how this behaviour compares to a water-cooled cable circuit. In order to allow direct comparison between the 6hr and 24hr ratings, the same preloads of 60% of continuous has been specified for both. From the results in Table 4.7 it is immediately clear that the 24hr rating of a water-cooled high temperature circuit would exceed the 6hr rating of the same circuit in its uncooled form. The agreement seen between the simple model and the full dynamic backfill model is poorer than was the case for 6 hours - the reason for this is linked to the time constant of the cable. Due to the thermal capacitance of the cable, the effect of the sudden increase in load does not have a significant effect on either the coolant water temperatures or those of the soil outside of the CBS region. As a result the thermal environment is much less significant than the initial cable temperature over 6 hours. However, quadrupling the duration of the emergency rating to 24hrs means that thermal effects of the ground become much more influential on the magnitude of the rating.

Conductor Temperature	Preload (A)	24hr Rating (full)	6hr Rating (2 zone)
90°C	1538A	2950A	3281A (11.2%)
120°C	1538A	3406A	3762A (10.4%)
150°C	1538A	3763A	4145A (10.1%)

TABLE 4.7: Comparison of 24hr Ratings with a 60% preload at 3% initial moisuture content

Even though the ratings from the two models differ by around 10%, it is clear that water cooling of conventional cables will still lead to 24hr ratings comparable to the

6hr ratings available from uncooled XLPE cables. Overall, the performance of the high temperature cables over 24 hour ratings (both with and without cooling) clearly exceeds what is available from XLPE cables today and may allow Transmission System Operators (TSO's) such as National Grid considerably more flexibility in the operation of their networks through extending the standard post fault rating period to 24 hours.

4.6 Summary of Buried Ratings

This Chapter has presented a method by which the dynamic backfill model developed in Chapter 3 can be successfully applied to the case of buried cable circuits. Although the computational requirements for these models are reasonably high, they are well within the capability of high specification personal computers. Throughout the results presented, comparisons have been made with a simpler model based on the two zone concept introduced in IEC 60287. This has permitted the benchmarking of the full dynamic backfill models against what is effectively a conventional rating technique. In the majority of cases the results obtained from the two zone model are within 10% of the rating of the more complex dynamic backfill model.

The continuous ratings obtained for the high temperature cables in the direct burial case are up to 30% greater than the continuous ratings calculated for the XLPE cables, however, the analysis of water cooled cables has shown that conventional external pipe water cooling technology will always give a higher continuous rating than the uncooled high temperature cable. Given the substantial increase in losses associated with higher conductor temperatures, it is therefore likely that operating buried cables at 150°C continuously would not prove economic especially if the utility in question needs to account for transmission losses financially.

Where the real benefits from the high temperature cables become available is the scenario of emergency ratings. Two main benefits were noted - the first benefit being the increase in available emergency rating over the 6hr period, which might allow better matching of cable post-fault ratings to those of overhead lines. Secondly, it would appear possible to stretch an existing 6hr rating from an XLPE cable to a duration of 24hrs when a 150°C cable is deployed. Both of these benefits could have a significant impact upon the constraint costs experienced by utilities when one or more circuits are unavailable either due to a fault or scheduled maintenance.

However in most 400kV cable circuits the route length required cannot be achieved with a single length of cable, bringing about the need for high voltage cable joints. Chapter 5 will build on the results detailed here to determine the possible thermal impact of high temperature operation on cable joints through the use of three dimensional finite element modelling.

Chapter 5

Analysis of Buried Cable Joints

Work presented in Chapter 4 has illustrated the value of using finite element analysis techniques for performing circuit rating calculations for both directly buried and buried forced cooled cable circuits. In determining the ratings of these circuits, no consideration was given to the joint bay itself. While some authors feel that the joint is intrinsically similar to the cable circuit (hence behaving in a similar way thermally), this is unlikely to be the case where high temperature circuits are concerned. Previously published research by the author has also proved that this is not the case where external pipe water cooling is employed [102]. This chapter presents a reliable method by which the thermal implications of joint bays can be analysed, allowing the criterion under which they might prove to be the limiting factor on the circuit thermal rating to be identified. Methods are presented for both directly buried and buried forced cooled joint bays, with future design considerations for high temperature jointing systems identified.

5.1 Background

Traditionally most uncooled circuit ratings are derived by calculation of the rating of the cables alone, assuming that any cable accessories operate at an equivalent or lower temperature owing to the increased core-core spacing at the joint position relative to the remainder of the cable route. Within the UK transmission network, for forced-cooled joint bays, an allowance is made for an increase in temperature across the joint bay through the use of a de-rating factor. Consequently, this Chapter aims to examine the implications of different joint bay types on the steady state circuit rating and identify where direct consideration of the effect of a joint bay may be necessary. This is to be achieved through the creation of 3D FEA models, allowing the conductor temperature profiles through the joint bay to be examined.

Early methods for the calculation of temperatures within high voltage cable joints largely relied on the use of electrical analogues, with simple admittance and capacitance net-

works designed to represent the thermal properties of the joint [103]. These systems can be solved mathematically, or alternatively the equivalent circuit can be constructed and physical measurements made to derive the required results, as in [104]. This technique can also be used to estimate thermal conditions quickly when applied to temperature monitoring systems [105]. Whilst in some cases this may be a useful technique, there are practical limits on the level of geometric detail which can be modelled.

Other researchers have developed numerical methods based on the lumped parameter approach, for instance [106, 107] where 2D slices of a joint bay geometry are linked axially between materials of high thermal conductivity. Methods of this type offer an improvement in solution quality over the simpler analogue approach, however, the number of mesh nodes used was restricted by the available computational power. Modern FEA tools now allow for automatic mesh generation and have improved post-processing capabilities, reducing the complexity of building a model when compared with [106]. Such tools have been used by many authors to examine problems related to cable ratings, as outlined in Section 2.2.5. Recent improvements in the cost and availability of computational resources now allow more complex models for situations such as joint bays to be built and solved.

5.2 Naturally Cooled Installations

The first type of installation considered here is that of directly buried cable circuits without additional cooling, for which the cable only ratings were presented in 4.2.

5.2.1 Modelling Approach

Large scale 3D FEA models have the potential to become inefficient in terms of the computational time and effort required to obtain a solution. To ensure that the level of detail within the 3D joint bay models developed here is sufficient but not excessive, initial studies were performed on single joints under the assumption of axial symmetry. Such models can be built and solved at a much greater speed, allowing a sensitivity analysis of the model parameters to be undertaken to identify the relative importance of individual components of the cable joint to the overall solution. Employing this method allows unnecessary detail to be removed from the 3D joint bay models, while simultaneously providing qualification results.

5.2.2 Installation Properties

The joint design used within this analysis is based on a 400kV XLPE joint design to match the cable dimensions under study. The two sections of conductor are joined using

a copper ferrule, enclosed within polymeric insulation. The electrical components of the joint are enclosed within a copper case, with the whole joint then enclosed within a glass fibre enclosure. An outline image of the joint is shown in Figure 5.1. Details of the joint construction and material properties are given in Table 5.1

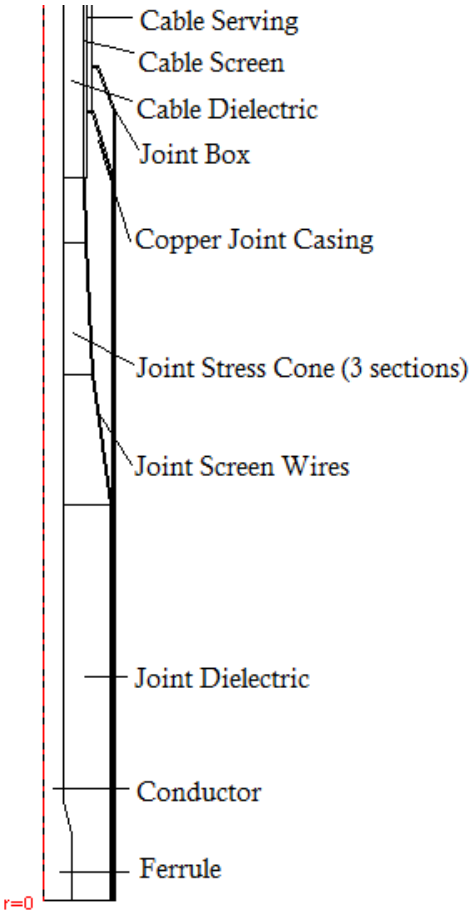

FIGURE 5.1: Construction of 400kV joint

Component	Outer Diameter (mm)	Material	Thermal Conductivity ($W.m^{-1}K^{-1}$)
Joint Screen Wires	2	Copper	120
Cable Conductor	64	Copper	385
Joint Ferrule	90	Copper	385
Cable Dielectric	126	XLPE/HT	0.286
Cable Sheath	132	Copper wire	298
Cable Serving	148	PE	0.286
Joint Dielectric	206	XLPE/HT	0.286
Joint Case	215	Copper	385
Joint Box	220	Glass Fibre	0.167

TABLE 5.1: Joint Construction Data and Material Properties

5.2.3 Axially Symmetric Model

The majority of the models discussed in Section 5.1 are reliant upon the assumption of axial symmetry. This is a reasonable assumption for a joint in air, where the air temperature around the circumference is approximately constant, but may be less acceptable in a buried system. However it represents the first step of model development in this Chapter.

In order to model under the conditions of axial symmetry, a number of assumptions regarding the model geometry must be made. The box surrounding the joint has been considered to be cylindrical, neglecting the turrets found on the top where the earth bonds would be attached. The copper screen wires wound around the joint have been modelled as a solid and continuous region, but with a reduced thermal conductivity value of $120 W m^{-1} K^{-1}$. Derivation of this value was through a simple FEA model where a small section of the screen wire is placed between two isothermal surfaces. The regions between the wires and the interface are modelled as the polymeric dielectric, as would be the case in the joint itself, with Fouriers Law being applied to determine the equivalent thermal conductivity of the region from the heat flux across it. All small geometric details, such as bolts, are removed from the model geometry due to the negligible effect they represent to the overall heat-transfer problem.

The modelling of the heat sources is achieved via the same methods used in Chapter 4 for the buried cable modelling. The joule losses are calculated using the full IEC 60287 equations as presented in [18], with the heat source applied to the outer boundary of the conductor. The sheath losses are calculated in a similar manner but with the heat source applied to the inner boundary of the sheath. The heat flux from the dielectric losses is distributed throughout the dielectric regions according to the expression of [49]. It is not possible to directly represent a ground surface within the axially symmetric model. Instead, the remote environment boundary condition is specified as an isotherm of 12°C, located a set distance, D_{ext}, from the radial centre of the joint. This value was selected to represent the thermal resistance equivalent to the 1.05m burial depth used in Chapter 4 for the cable modelling, where the thermal resistance, T_{ext}, is defined as:

$$T_{ext} = \frac{1}{2\pi}\rho_s ln\left(\frac{2L}{D_e} + \sqrt{\left(\frac{2L}{D_e}\right)^2 - 1}\right) \tag{5.1}$$

where ρ_s is the thermal resistivity of the soil ($K m W^{-1}$), L is the burial depth (m) and D_e is the external diameter of the cable (m). This allows the position of the external boundary in the axially symmetric model to be located at a distance D_{ext} from the cable, calculated by

$$D_{ext} = D_e\left(exp\left[T_{ext}\frac{2\pi}{\rho_s}\right]\right) \tag{5.2}$$

A zero heat flux boundary is specified 10 m along the conductor from the joint centre.

This distance was verified as being large enough such that the conductor axial heat flux distribution was not artificially constrained.

As was noted previously, the 2D axially symmetric joint model is best suited to the case where the joint is installed in air and hence this step in the model development process is extremely useful for the case of joints installed in forced ventilated tunnels, as presented in Chapter 6. For the buried case, the model can still provide temperature profiles for the case of a single cable and joint assembly in thermal isolation (i.e. with no mutual heating effects from other joints). An example result for the 10% moisture content case is shown in Figure 5.2. From the plot it is clear that the temperature in the joint centre is around 7°C higher than the remote cable temperature. This clearly demonstrates the potential for the joint ferrule temperature to exceed the conductor temperature in a buried three phase system unless additional core-core spacing is provided in the joint bay. This issue will be studied further in Section 5.2.4.

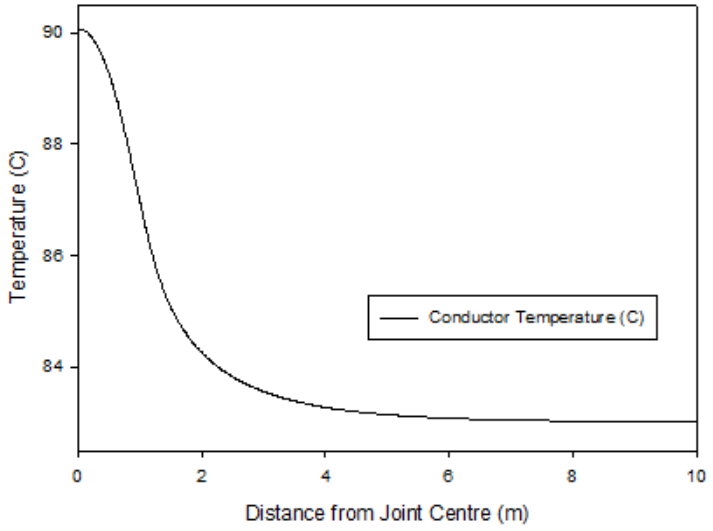

FIGURE 5.2: Example Joint Temperatures for Axially Symmetric Model

Prior to extending the modelling into 3D space, it is essential that the number of mesh elements required for the problem are minimised as far as possible. However this must not be at the expense of the quality of the solution. Work published in [102] demonstrated the use of a sensitivity analysis technique for oil-paper cable joints which identified that a number of geometric features could be removed or combined with minimal impact on the solution. Some of the simplifications described are not applicable here (for instance the removal of the oil duct, which is not present in a polymeric cable system); some, however, merit further consideration.

The 90°C rating of the model shown in Figure 5.2.3 is 2368A with all geometric details modelled. Several of the minor geometric details can be removed without making a large impact on the overall joint rating. The copper screen wires along the joint stress cone can be included into the adjacent dielectric region at a cost of a rating decrease

of only 13A. The decrease occurs for two reasons, firstly the minor increase in radial thermal resistance, and secondly a reduction in the amount of axial heat transfer. Another simplification which can be made without material decrease in accuracy is the merging of the cable screen and oversheath. As there are no heat sources between these components they can be simply represented with an equivalent thermal conductivity of $0.295 W.m^{-1}K^{-1}$, leading to a rating decrease of only 1A. Combining these two simplifications with the combination of the joint copper case into the adjacent joint box gives an overall rating decrease for the axially symmetric model of 1.73%. Although this reduction does mean that the overall accuracy of the model is reduced, the number of mesh elements required for the 3D model is reduced significantly. This is a key requirement for the very large 3D models to be produced within this Chapter.

5.2.4 3D Models

Although 2D axially symmetric models can be built and solved quickly, they do not offer the ability to evaluate more than one joint at a time. For the technique to be of practical use, 3D models are required to allow effects such as mutual heating and force cooling to be examined. Taking the knowledge gained from the axially symmetric modelling process, 3D models of two commonly deployed directly buried joint bays have been constructed to allow examination of the conductor temperature profiles through the bay.

5.2.4.1 Parallel Spaced Joint Bay

A parallel spaced joint bay represents the simplest installation case, with three joints side by side in flat formation, providing two lines of symmetry. The first is a vertical plane through the axial centreline of the centre joint, as the burial conditions are assumed to be uniform (at a depth of 1.05m), with the second line of symmetry being another vertical plane cutting through the centres of the joints. Along the cable route the core-core spacing is 38.5cm, increasing to 1m within the joint bay. A straight section of cable models the transition between these two spacings, which occurs between 2m and 5m away from the joint centre (see Figure 5.3). The joint bay is encased in cement bound sand with constant thermal properties as per the buried cable models developed in Chapter 4. All boundary conditions and heat generation terms match those used for the cable only models. The length of the model is increased to 15m (measured from the joint ferrule) to ensure that the exterior boundary condition of thermal insulation at the end of the cable does not adversely affect the joint bay temperature profile.

Due to the size and complexity of the 3D joint bay model, it is not computationally viable to model moisture migration using the full dynamic backfill model. Instead the two zone approximation tested in Chapter 4 is applied to account for the possibility

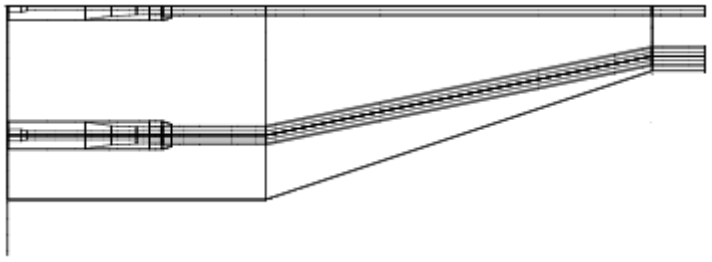

FIGURE 5.3: Geometry of Parallel Joint Bay

of moisture migration and allow comparison with the ratings generated for the cables without joints. Figure 5.4 demonstrates the conductor temperature profile through the joint bay for a remote conductor temperature of 90°C with an initial moisture content of 10%. It is evident that the increase in conductor spacing significantly decreases the conductor temperature within the joint. This is assisted in this model by the increase in the width of the CBS region to 3m (centred around the centre phase cable), which is assigned a constant thermal resistivity of $1.2K.m/W$, which is a lower thermal resistivity than the surrounding soil in which moisture migration is assumed to have taken place.

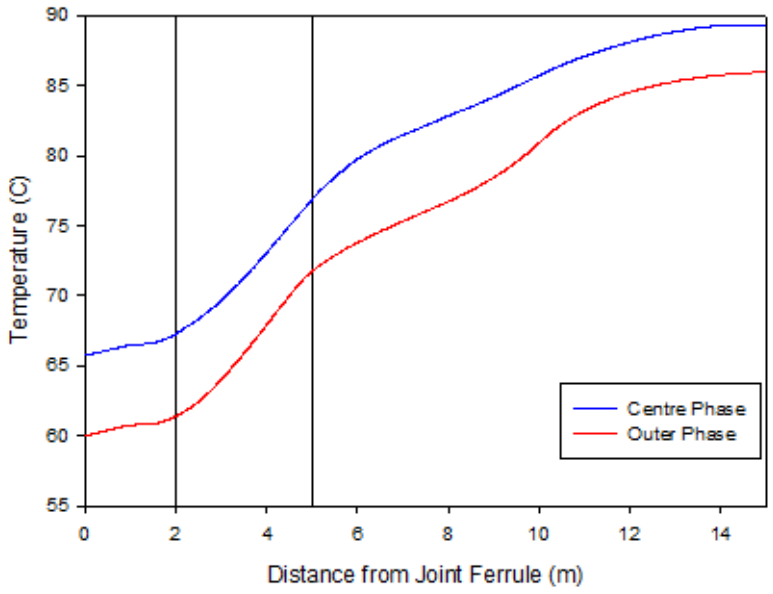

FIGURE 5.4: Conductor Temperature Profiles for Parallel Spaced Joint Bay, XLPE Cable at 10% initial moisture content

This trend continues for the 150°C HT cable as shown in Figure 5.5, indicating that the joint does not prove limiting on the circuit continuous rating where the core-core spacing is increased sufficiently. This would prove to be an important design step for any future high temperature cable installation. Figure 5.5 also shows a plot for the case of the 150°C HT cable where the backfill thermal properties are assumed to remain constant (i.e. there is not moisture migration). Despite the much larger load in this case (2321A against 1662A from the standard 2 zone case) the joint ferrule temperature

remains below that of the remote cable. This finding is in agreement with a previous study on conventional oil filled cable joints [102].

Cable	Remote Conductor Temperature (°C)	Joint Ferrule Temperature (°C)
XLPE	88.61	66.51
120°C HT	119.21	88.52
150°C HT	147.02	107.17

TABLE 5.2: Comparison of Joint and Cable Temperatures (Parallel Spaced Joint Bay)

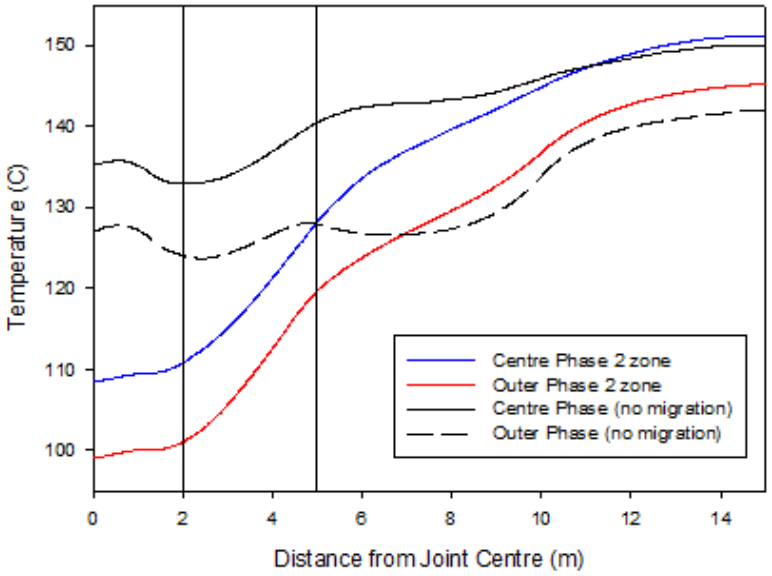

FIGURE 5.5: Conductor Temperature Profiles for Parallel Spaced Joint Bay, 150°C HT Cable at 10% initial moisture content

Although the parallel spaced joint bay does not prove to be a limit on the continuous rating for the example cable circuit, it is also important to consider its impact on the emergency rating of the cable circuit. This is achieved by solving the 3D model for a steady state preload equal to 60% of the continuous rating and setting the solution obtained as the initial condition of a transient solution of either 6hr or 24hr duration. For all the results studied here the emergency rating value assigned is that found in Chapter 4 for the buried cable circuit, hence the remote conductor temperature would be expected to attain its maximum value at the end of the emergency rating period.

Figure 5.6 illustrates the rise in both remote conductor and joint temperature over the course of a 6hr emergency rating for the 120°C HT cable. As would be expected from the steady state solutions discussed here, the initial conductor temperature at the joint ferrule is lower than that of the cable, in this case by 11.4°C. At the end of the 6hr period, the joint ferrule temperature remains 9.1°C below that of the remote cable conductor, despite the larger radial thermal resistance of the joint. Figure 5.7 demonstrates the conductor temperature profile across the joint bay. Unlike in Figure 5.4, the elevated level of current means that the joint itself attains a higher temperature

than the cable immediately adjacent to it - however this remains 8°C cooler than the remote conductor temperature. This trend continues across the 3 different cable types tested, as summarised in Table 5.3. It can be noted that the difference in the remote conductor temperature and joint temperature has decreased by the end of the 6hr rating period, however, the joint temperature remains considerably lower than that of the cable.

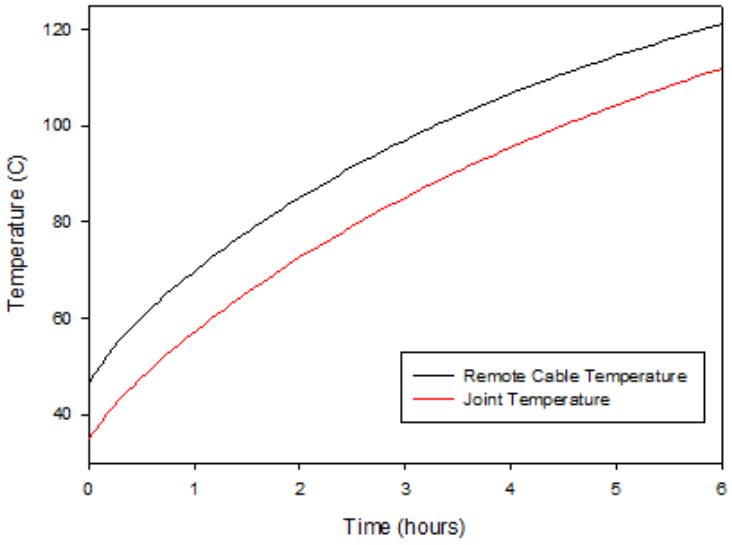

FIGURE 5.6: Temperature profile at 6hr rating (120°C)

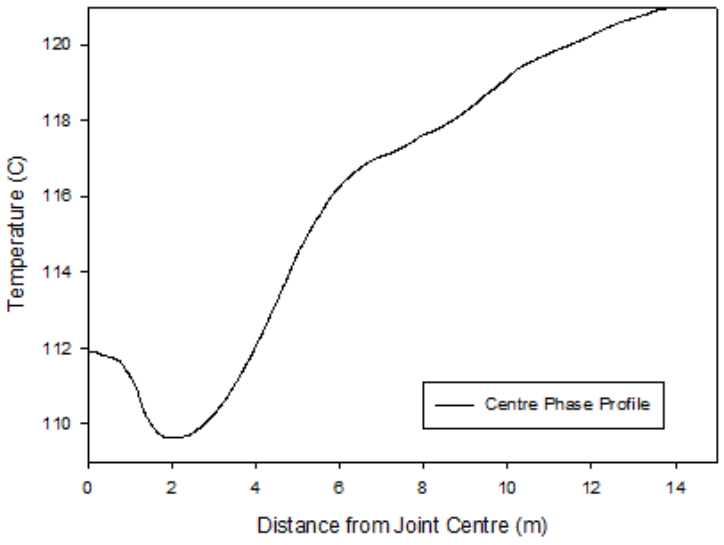

FIGURE 5.7: Conductor Temperature Profile at end of 6hr rating period

Cable	ΔT (t=0) (°C)	ΔT (t=6hrs) (°C)
XLPE	7.83	7.27
120°C HT	11.42	9.09
150°C HT	13.88	11.34

TABLE 5.3: Comparison of Joint and Remote Cable Temperatures at the start and end of 6hr rating period

The trends seen for the 24 hour emergency ratings differ slightly from those at six hours. Although the joint remains cooler than the remote cable temperature for all models solved, the differences are generally less than 3°C at the end of the transient period. Figure 5.8 illustrates the change in temperature across the full duration of the transient period for the 120°C HT cable. It can be seen that initially the cable conductor temperature rises faster than that of the joint, however towards the end of the transient the rate of temperature rise in the joint passes that of the cable and the two lines begin to converge.

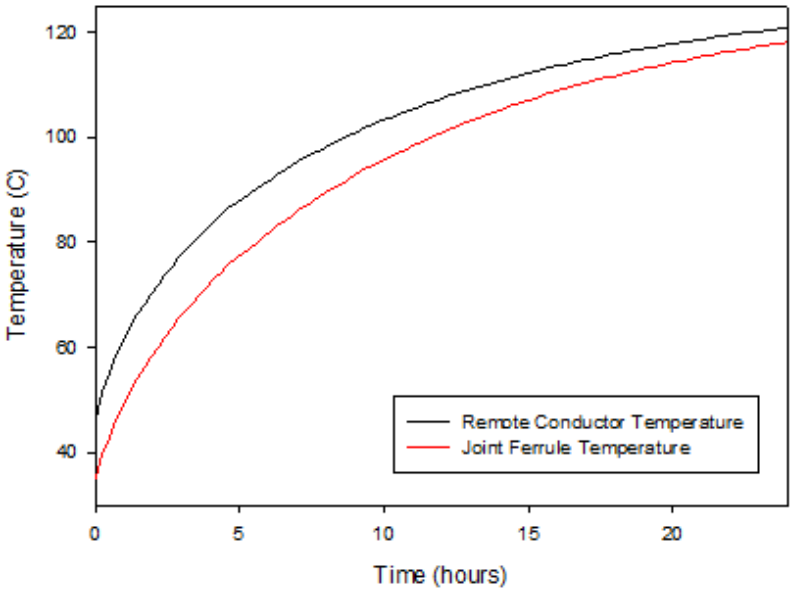

FIGURE 5.8: Temperature profile at 24hr rating (120°C)

Table 5.4 summarizes the difference between the joint and remote cable conductor temperatures under the 24 hour rating condition. From these results it is clear that over the longer transient period, the additional thermal capacity of the joint is almost offset by its higher radial thermal resistance. However it is clear that in this case the joint does not prove a limit on the 6 hour or 24 hour emergency rating of the cable circuit.

Cable	ΔT (t=0) (°C)	ΔT (t=24hrs) (°C)
XLPE	7.83	2.69
120°C HT	11.42	2.80
150°C HT	13.88	2.77

TABLE 5.4: Comparison of Joint and Remote Cable Temperatures at the start and end of 24hr rating period

Figure 5.9 shows the conductor temperature profile at the end of the 24 hour rating period for the 150°C HT cable. The red trace shows that the joint temperature for the outer phase has actually exceeded that of the remote cable, although the centre phase joint still operates 2.7°C cooler than the remote cable in the 3D model.

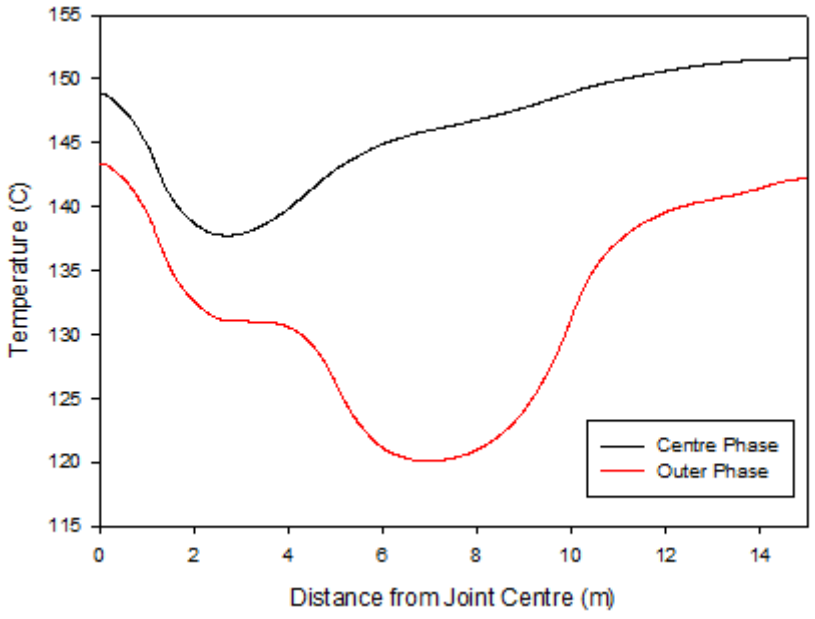

FIGURE 5.9: Conductor Temperature profile at end of 24hr rating period (150°C)

5.2.4.2 Staggered Joint Bay

The model described for the parallel spaced joint bay can easily be adapted to different joint bay configurations, for instance that shown in 5.10 where the centre joint is moved forward to further alleviate the effects of mutual heating. Such designs allow the core-core spacing to be reduced slightly, in this case to 80cm within the joint bay. This joint bay arrangement requires a smaller width of trench, hence may be preferred where the available space for the joint bay is limited. The total cable route length modelled for this installation is 25m, of which the 5m at either end of the model is a straight section of cable with the same geometric parameters as that shown in Chapter 4. All boundary conditions within this model are identical to those of the parallel spaced joint bay to permit comparison between the two designs.

FIGURE 5.10: Geometric Outline of Staggered Joint Bay

Solving the 3D model of the staggered joint bay yields similar conclusions to those from the study of the parallel bay model. Table 5.5 details the differences between the remote conductor temperature (in the 3D model) and the joint ferrule temperature. The joint ferrule temperature is substantially lower than that of the remote cable, again due to the impact of the greater core to core spacing at the joint and the larger CBS region in the joint bay. Figure 5.11 shows an example conductor temperature profile for the

120°C HT cable. The centre point of the joints are located at 10m (outer phase) and 14m (centre phase) on the conductor temperature profile plot. A small point of inflexion can be observed at these locations relative to the cable running into the joint bay but these are less than 5°C in magnitude.

Cable	Remote Conductor Temperature (°C)	Joint Ferrule Temperature (°C)
XLPE	88.54	72.46
120°C HT	120.57	98.22
150°C HT	145.92	110.56

TABLE 5.5: Comparison of Joint and Cable Temperatures (Staggered Joint Bay)

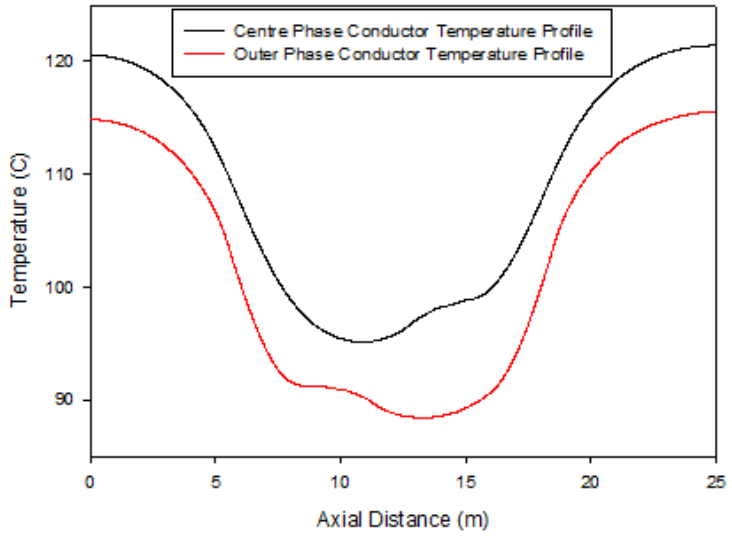

FIGURE 5.11: Conductor temperature profile through staggered joint bay, 120°C HT cable, 10% initial moisture content

Analysis of the 6hr ratings for the staggered joint bay shows similar conclusions to the parallel spaced joint bay. The conductor temperature variations summarized in Table 5.6 follow the same trend, with a greater temperature difference for the hottest cables and a reduction of at least 2°C in the temperature difference over the course of the six hour rating period. Figure 5.12 shows the change in cable and joint conductor temperature over the duration of the transient.

Cable	ΔT (t=0) (°C)	ΔT (t=6hrs) (°C)
XLPE	8.05	6.84
120°C HT	9.36	7.91
150°C HT	10.53	8.85

TABLE 5.6: Comparison of Joint and Remote Cable Temperatures at the start and end of 6hr rating period (staggered joint bay)

When compared with the parallel spaced joint bay, the peak in conductor temperature within the joint is much more obvious, as evidenced in Figure 5.13 at distances of 10m and 14m.

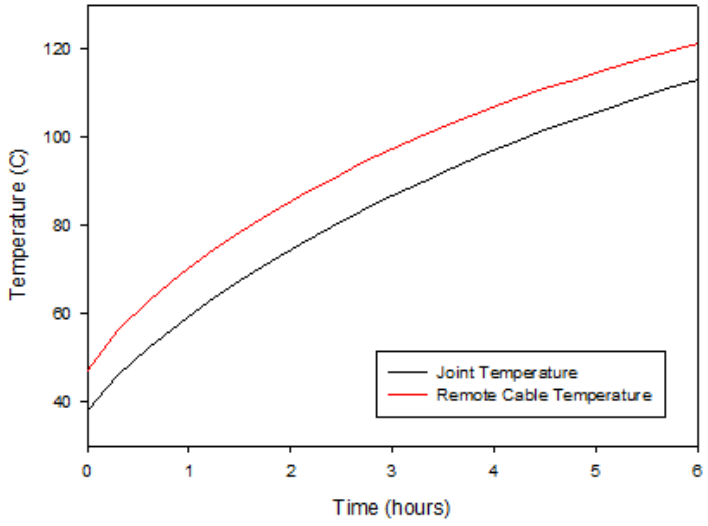

FIGURE 5.12: Comparison of cable and joint temperatures under 6hr rating conditions for staggered joint bay with 120°C HT cable

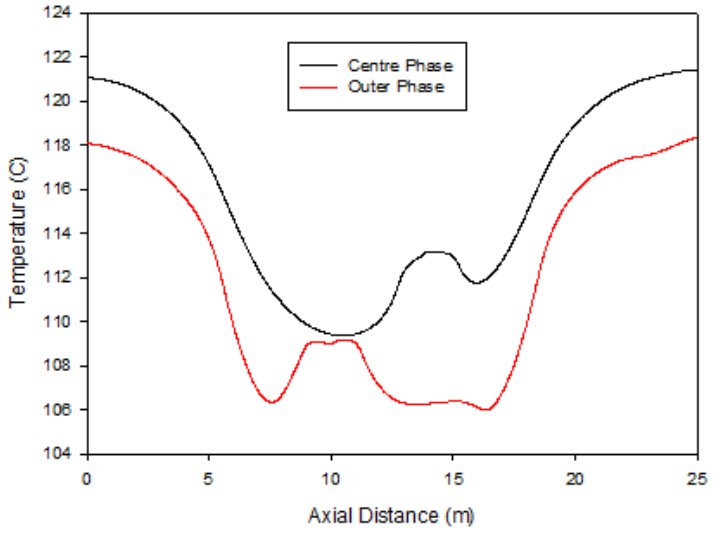

FIGURE 5.13: Conductor temperature profile at end of 6hr rating period for staggered joint bay with 120°C HT cable

The trends in the staggered joint bay results under 24hr ratings are again very similar to those of the parallel spaced joint bay. Table 5.7 demonstrates that the conductor temperatures of both joint and remote cable are similar at the end of the transient period, with a difference of only 1°C for the 150°C HT cable, as shown in Figure 5.14.

Cable	ΔT (t=0) (°C)	ΔT (t=24hrs) (°C)
XLPE	8.05	2.69
120°C HT	9.36	2.44
150°C HT	10.53	1.02

TABLE 5.7: Comparison of Joint and Remote Cable Temperatures at the start and end of 24hr rating period (staggered joint bay)

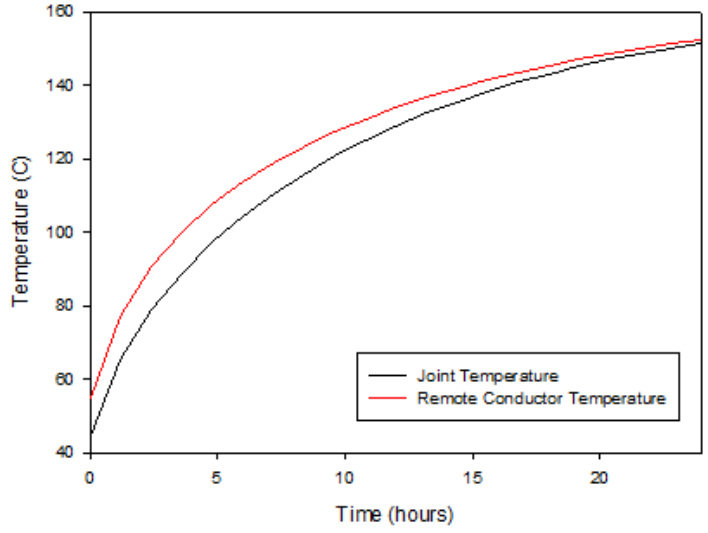

FIGURE 5.14: Comparison of cable and joint temperatures under 24hr rating conditions for staggered joint bay with 150°C HT cable

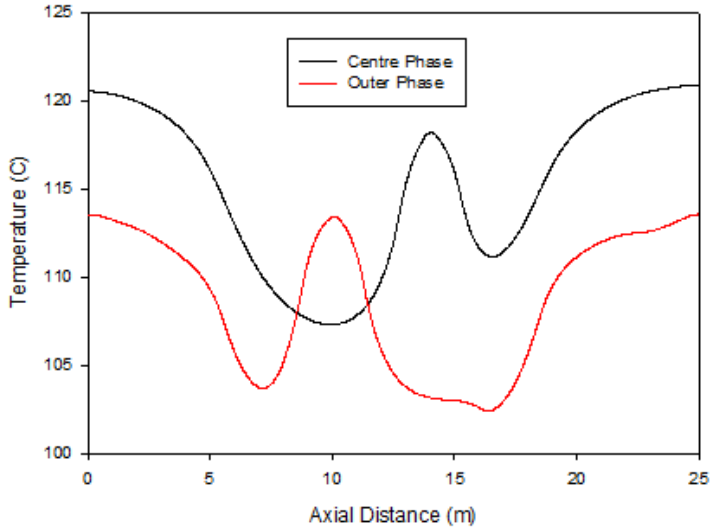

FIGURE 5.15: Conductor Temperature profile at end of 24hr rating period for staggered joint bay with 120°C HT cable

5.3 Forced-Cooled Installations

In order to meet higher ratings requirements in areas of high demand, approximately 16% of the transmission cable circuits in the UK are forced-cooled, either by means of forced air ventilation for those installed in tunnels or the installation of water cooling pipes within groups of buried cables. When calculating the rating of a buried force cooled cable circuit, an allowance is typically made for an increase in cable temperature across the joint bay through the use of a de-rating factor. This is used because water cooling is considered to be less effective on the joints than on the cables themselves [108]. The cable circuit is then rated using methods such as Electra 66 [23], with the use of a reduced maximum conductor temperature criterion. In order to obtain more

detailed temperature profiles for such circuits, the FEA techniques discussed previously for naturally cooled cable circuits are extended to include the effects of water cooling. The FEA models are used to obtain a circuit rating based on the thermally worst case joint bay location and a study has been performed to identify the factors which have the biggest effect on the size of the de-rating factor required.

5.3.1 Modelling of Water Cooling

The bulk of the modelling procedure for forced-cooled joint bays matches that of the previously addressed directly buried case. Modelling of the water cooling of the joint bay is achieved by placing a heat sink boundary possessing a constant heat transfer coefficient on the inner surface of the water pipe. In order to calculate h, knowledge of the water temperature is required. Within the joint bay the bulk water temperature is assumed constant, this argument is supported by calculating the coolant temperature rise obtained under the assumption that all heat generated by the cable circuit must be removed by the coolant, such that

$$\Delta T = \frac{V_c(W_c + W_s + W_d)}{f_c C_p m_c} \tag{5.3}$$

where V_c is the volume of coolant (m^3), W_c is the joule loss ($J.s^{-1}$), W_s is the sheath losses ($J.s^{-1}$), W_d is the dielectric losses ($J.s^{-1}$), f_c is the volumetric flow rate of the coolant ($m^3 s^{-1}$), C_p is the specific heat capacity of the coolant ($J.kg^{-1}K^{-1}$) and m_c is the mass of coolant within the system (kg). Performing this calculation yields a temperature rise of less than 0.1°C (based on a 2000A load current), judged to be an acceptable loss of precision.

5.3.2 Installation Properties

The cable circuit arrangement studied here is identical to that of Section 4.3. Outside the joint bay, the cables are installed in flat formation with four water cooling pipes around them. Inside the joint bay the water pipes loop such that each joint has one pipe either side of it, as shown in Figure 5.16. The water pipes are constructed of polyethylene and have an internal diameter of 66mm, with the water flowing through them at a rate of 1 litre per second per pipe, giving the cooling system a total throughput of 4 litres per second. All other thermal and electrical properties match the previously developed models, with the assumptions on boundary conditions, heat losses and soil thermal behaviour dealt with in the same way as for the uncooled buried joint bays.

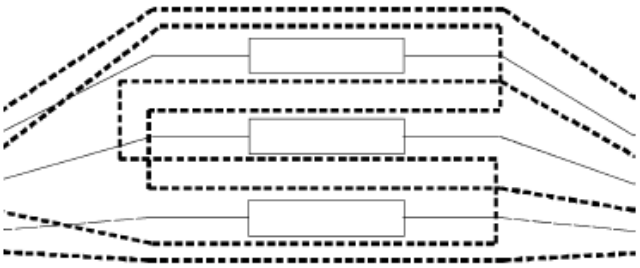

FIGURE 5.16: Water pipe layout in cooled joint bay

5.3.3 Results Obtained

To demonstrate the potential for the conductor temperature of the joint to exceed that of the remote cable temperature, the 3D model of the water-cooled joint bay has been solved for the 3% moisture initial condition with a load current of 2564A, the steady state rating found through the modelling in Chapter 4. The resulting conductor temperature profile is that shown in Figure 5.17, where the joint ferrule is located at 16.8m on the x axis. Two clear peaks can be seen in the centre phase conductor temperature profile, of which the highest is that associated with the joint itself. The maximum temperature in this case is not located at the ferrule (which benefits from a slightly lower ac resistance), but 50cm from the ferrule centre.

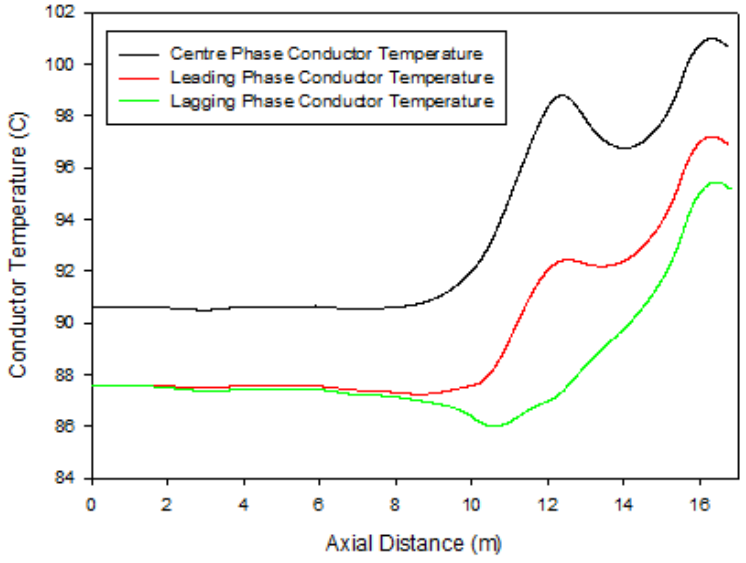

FIGURE 5.17: Conductor Temperature Profile for Cooled Joint Bay (remote cable temperature 90°C)

The conductor temperature profile for the lagging phase has a different shape due to the geometric location of the water pipes. It can be seen in Figure 5.18 that the water pipe passes over the cable on entry to the joint bay. As the cable is closer to the heat sink presented by the water pipe, the thermal resistance between the two is reduced resulting

in increased cooling of the cable in this location.

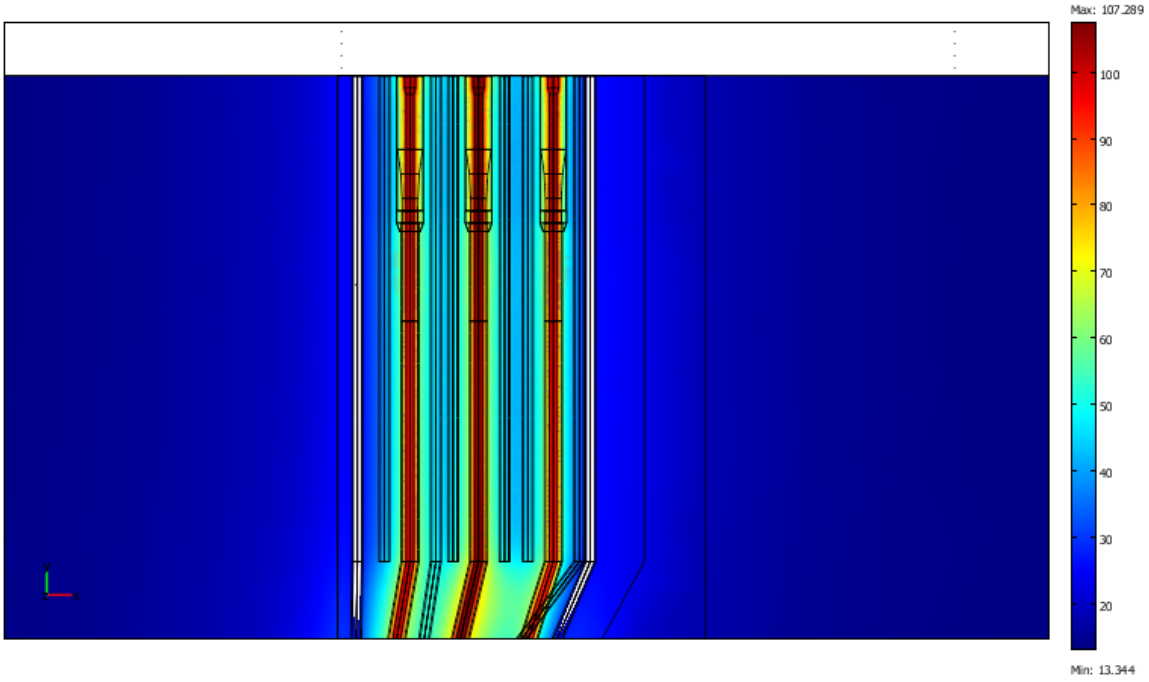

FIGURE 5.18: Slice plot of temperature through conductor axis

Previous application of this modelling technique to fluid filled paper impregnated cable circuits [102] found that the magnitude of the joint temperature offset (defined as the difference between the remote conductor temperature and the maximum temperature in the joint) varied strongly with load current. To examine the variation for the candidate water cooled system, the joint bay model has been solved for load currents of between 1500A and 3000A. The resulting joint temperature offset curve is plotted in Figure 5.19. It is clear that the magnitude of the joint temperature offset increases significantly as more load is applied, highlighting the issues with the present methodology of assuming a fixed value for the offset.

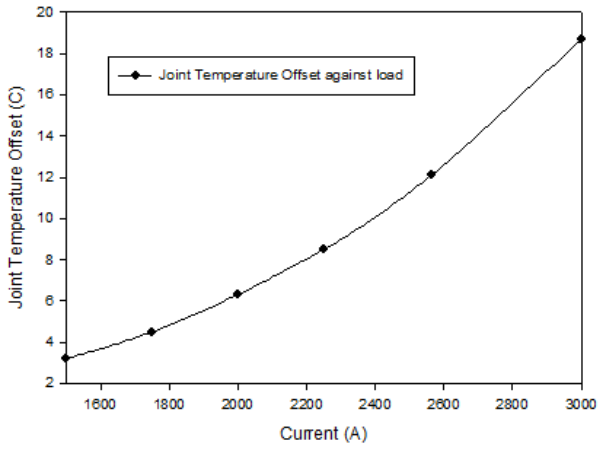

FIGURE 5.19: Joint Temperature Offset Plot

5.4 Viability of FEA Approach

The use of FEA has gained much interest from researchers wishing to calculate cable ratings. From the experience gained in developing the models described here, the use of 2D models and pseudo 3D models (where 2D slices are linked axially) is certainly viable for cable-rating calculations. For users with some experience of their chosen FEA package, models can be built quickly with solution times in the order of minutes. Where the FEA software allows interface with external code or numerical analysis packages, a good degree of automation can be achieved and large amounts of results can be acquired. However, 3D models present a larger burden in terms of build and solution times. For those presented here, build times are of the order of 20 hours and solutions can only be achieved within several hours where access to high-performance computer facilities is available. While this is likely to be acceptable for design studies, for on demand calculations, such lengths of time may not be available. Considering full transient models may also prove to be a challenge due to the substantial amounts of computational memory required to retain the solutions from intermediate computational steps.

5.5 Implications for Jointing High Temperature Circuits

The work presented in this Chapter broadly demonstrates that the thermal issues around the jointing of high temperature cables are similar to conventional XLPE technologies. Where sufficient core-core spacing between joints is provided, the mutual heating effects are sufficiently low that the parent cable operates at a higher temperature, particularly under continuous rating conditions, with the exception of the forced water cooled cable circuit. Even under emergency rating conditions where the load current is higher, the maximum temperature seen in the joint is less than that of the parent cable.

However, there are further concerns which would need to be investigated which fall beyond the scope of this thesis. One of the major design constraints on cable joints is in fact thermo-mechanical, due to the forces generated by the expansion and contraction of the conductor with changes in temperature. Allowing a greater operating temperature range will further increase such forces and may require additional mechanical reinforcement. Depending on the exact design required, this may worsen the thermal performance of the joint hence leading to the joint becoming a limiting factor on the cable circuit rating.

5.6 Summary

This Chapter has presented a new finite element method for calculating temperature profiles in joint bays. Initial models made use of the approximate axial symmetry of a single cable joint to allow modelling in two dimensions. These models demonstrated that

in isolation the conductor temperature in a single joint could be significantly higher than the parent cable. While such models are valuable in conducting a sensitivity analysis to geometrical features, three dimensional models are required to accurately represent real world joint bay installations. This is due to the importance of correctly specifying the remote boundary conditions for the installation environment.

By building on the axially symmetric modelling process, 3D models have been developed of two common directly buried joint bays. The first demonstrated that even where joints are installed in the parallel bay configuration, the joint conductor temperature will not exceed that of the parent cable where sufficient core to core spacing is provided. This verifies the commonly applied design assumption that joint temperatures can be controlled through careful consideration of mutual heating effects.

A more space efficient design is the staggered joint bay, which has been demonstrated to allow reduced core-core spacing (when compared with the parallel design) by moving the centre joint forward of the two outer phases. Again the conductor temperature in the joint remains below that of the parent cable for both continuous and short term emergency rating calculations.

The final joint bay modelled is that of the external pipe cooled joint bay, an important variation to consider given that the study in Chapter 4 showed that a cooled XLPE cable system still offered a higher continuous rating than a non-cooled 150°C HT cable. The results presented in this Chapter demonstrate that the joint temperature could reach 101°C for a 90°C remote cable temperature. The magnitude of the joint temperature offset was also seen to vary significantly with load current, meaning that the application of a fixed conductor temperature offset may prove inaccurate. If the temperature of the joint were to be constrained such that it must remain under the 90°C limit, this reduces the continuous rating of the water-cooled cable circuit. However, even after the rating reduction due to the joint bay, the 150°C HT cable still has a lower continuous rating.

Chapter 6

Cable Tunnel Installations

In Section 2.3.1, a number of shortcomings in the most commonly used cable ratings method for force ventilated cable tunnels were identified. Perhaps the most significant issue identified is that the method can only provide a rating for installations with multiple cable circuits where the circuits are of identical construction, voltage and load profile. This prevents the method being easily applied to mixed use tunnels (for instance transmission and distribution cables in the same tunnel space). The existing Electra 143 model is only applicable for conditions of turbulent air flow, although this is not a restriction in itself as the vast majority of forced air cooled tunnels are operated with a sufficiently high air velocity to yield turbulent flow. A second major issue is that there is no scope within the existing methodology to analyse the thermal implications of joint bays within the tunnel. As was observed in Chapter 5, it is clear that joints may operate at a higher temperature than the parent cable in some buried systems - it is hence clearly vital to determine the temperature profile of air cooled joints in tunnels.

The existing approach could also be made more flexible, for instance, by allowing multiple different sections of tunnel to be rated within one calculation by allowing variable geometrical parameters such as tunnel diameter. Finally, there is an outstanding issue to consider in the form of the convective heat transfer coefficients, to which the solution is sensitive. These points have been considered and some of them directly effect the operational requirements of utilities, for instance in the case of installation of both 132kV and 400kV XLPE circuits within the same tunnel [109]. At the time of the development of Electra 143 such needs had yet to be identified. The remaining points relate to the flexibility and validity of any new methods created through the course of this investigation, which should offer an improvement over the existing method. This Chapter outlines the approach by which these topics have been investigated, evaluates appropriate techniques, and presents the findings of this particular study.

6.1 Modelling Strategy

The overall aim of this Section of research work is to provide a revised standard method for the rating of cable circuits installed within ventilated tunnels which better allows for the presence of multiple circuits, some of which are capable of high temperature operation. A number of approaches are to be used to ensure that any new method is best suited to these requirements. To better inform the study of heat transfer, site visits have been made to three tunnels currently operated by National Grid for the purpose of gathering experimental data. The results gained from these studies are discussed in Section 6.2, before being contrasted with results from a number of numerical simulations (see Section 6.3). When combined, these two components inform the study of heat transfer coefficients which has been identified as a priority work area.

Once the heat transfer aspects have been examined, the study considered the structure of the rating method. Electra 143 has the clear benefit of being applicable to almost any tunnel arrangement without the need for altering the standard method - the algorithm has been built into a application named MORDEN [110] for use by National Grid, which can be set up and run in a matter of minutes, without reliance on other proprietary software. An incremental approach was taken in the development of the new model, with improvements being gradually introduced to ensure a reliable and robust calculation method. Once the framework for the new method has been obtained, a series of example scenarios have been analysed to determine the potential rating benefits of the introduction of a high temperature cable system.

6.2 Cable tunnel surveys

Although CFD modelling is a well established technique, it is always best practice to support the conclusions drawn from numerical models using experimental data. It is not possible to explicitly measure convective heat transfer in a tunnel, however, it was possible to measure the flow of air around the cable circuit to allow comparison with results from simulations. One of the principal cable tunnels on the National Grid network is the Dartford cable crossing which runs beneath the River Thames for interconnection between South East and North East London. The tunnel has recently been refurbished to include a double circuit of 400kV cables installed on wall mounted brackets, with a vertical core-core spacing of 500mm. A schematic including measurement locations is shown in Figure 6.1. Cooling is by means of force air ventilation from the Littlebrook shaft, which can be controlled by means of a computer from the Littlebrook head house to provide a nominal maximum flow rate of 5m/s.

Air flow measurements were made using an Airflow UA6 handheld ultrasonic anemometer, with a minimum of three measurements taken at 5 second intervals for each data

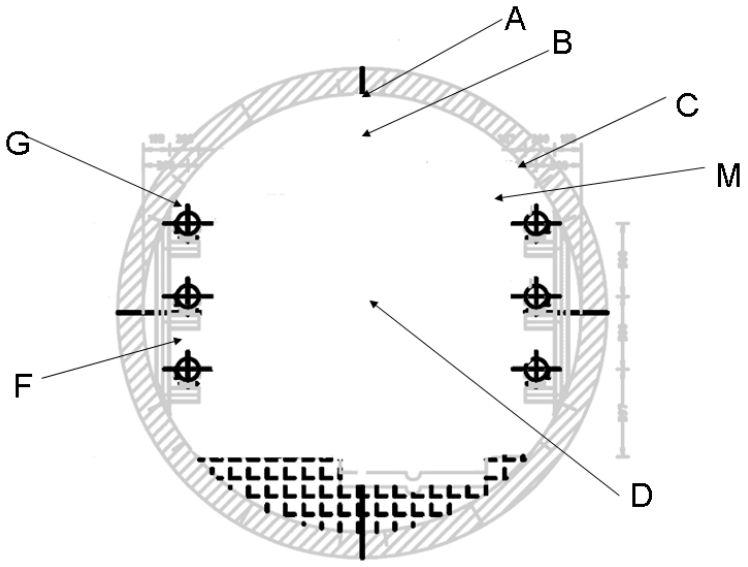

FIGURE 6.1: Schematic of cable layout and measurement locations within the Dartford tunnel

point. Measurements were taken at both ends of the tunnel to capture data from both developing turbulent flow (nearest the inlet) and fully developed turbulent flow at the outlet, with all measurements performed at both 50% and 100% fan speeds. The results of this survey are shown in Table 6.1 and Table 6.2, with all distances being quoted from the Littlebrook shaft.

Location	30m	60m	90m	120m	150m	2250m	2370m
C	1.65	1.85	1.68	1.90	1.72	1.53	1.87
M	1.75	2.29	2.11	2.15	2.26	1.87	2.35
D	2.82	3.00	2.84	2.85	2.88	2.42	2.20
E	1.61	1.46	1.21	1.71	1.38	1.75	1.80
F	2.15	0.91	1.49	1.89	1.45	1.32	1.21
G	1.31	1.82	1.52	1.58	1.73	1.77	2.14

TABLE 6.1: Dartford Tunnel Results (50% fan speed)

Location	30m	60m	90m	120m	150m	2250m	2370m
C	3.11	3.29	3.06	3.50	3.19	3.11	3.25
M	3.97	4.15	3.57	4.24	4.06	3.62	4.11
D	4.81	5.06	4.92	5.10	4.86	4.79	4.33
E	3.50	3.33	2.64	3.42	2.89	2.82	3.76
F	2.82	1.97	2.88	2.25	2.72	2.76	3.16
G	3.10	3.18	3.12	3.22	3.09	3.27	3.20

TABLE 6.2: Dartford Tunnel Results (100% fan speed)

An immediate conclusion from the tabulated data is that the fan system is not supplying a bulk velocity of 5m/s through the tunnel, with the tunnel centre point (theoretically that with the highest velocity) demonstrating a maximum of only 5.1m/s. Under both fan conditions the velocities recorded adjacent to the cable circuits are considerably

lower than the maximum values at point D. This result appears sensible - if the cable surface is considered as a wall then the air at the boundary between the cable and wall would be still (a no-slip condition). Moving further through the boundary layer towards the free stream flow will result in an increase in air velocity according to the expected turbulent flow profile. One major point of interest is that the values for convective heat transfer coefficient used in Electra 143 are based only on the bulk air velocity. The results presented in this Section suggest that this may be an over-simplification and this issue is further discussed in Section 6.4.1.

6.3 Modelling of Velocity Profiles

Whilst the experimental data discussed in Section 6.2 is valuable to this investigation, it is not possible to reliably derive heat transfer coefficients from this data. An alternative approach was taken involving the construction of numerical models of air flow within tunnels, with verification of their accuracy achieved through comparison with experimental data. This has been achieved through the use of finite volume analysis techniques, implemented using the commercial computational fluid dynamics code *Fluent*. Initial focus was been placed on tunnels with forced air cooling, owing to the greater number of these tunnels in present use within the UK and the likelihood of forced convection being necessary to remove the additional heat generated by high temperature cables.

6.3.1 Finite Volume Analysis technique

Whilst it is not possible to analytically derive a velocity profile for a full cable tunnel geometry, it is theoretically possible to obtain the complete velocity field for any given system, providing the appropriate boundary conditions can be well defined. This is possible through being able to discretize and solve the Navier Stokes equations with sufficient grid resolution to capture even the smallest eddies in turbulent flow and is known as Direct Numerical Simulation (DNS) [111]. However, there are limits to what can be achieved, even with the immense computational power available today. Such levels of detail are rarely required, meaning that some filtering of the numerical model of the flow can be undertaken, resulting in the derivation of the Reynolds Averaged Navier Stokes equations (RANS). This process has the disadvantage of yielding more variables than defining equations, hence requiring the use of a turbulence model to return to a closed equation system [112]. One of the most widely implemented turbulence models is the two equation $k-\epsilon$ model, which closes the Reynolds equations through the introduction of two extra equations for the turbulent kinetic energy k and the dissipation rate ϵ. This approach has been used for the work presented here.

As turbulence modelling is an enormous research field in its own right, discussion here will be kept to items of practical note which are required for the creation of stable

models. Solution techniques for laminar and turbulent flow are different owing to the change in fluid behaviour from a flow where different layers are able to slide past one another (laminar flow), to the turbulent case where different layers become mixed as the effect of the frictional forces reduces. Whilst the exact point at which a flow becomes turbulent is not well defined, a good approximation is that a flow can be considered turbulent once the magnitude of the Reynolds number, Re, exceeds 3000. The Reynolds number is defined as

$$R_e = \frac{\rho U_b D}{\mu} \tag{6.1}$$

where ρ is the density of the fluid (kgm^{-3}), U_b is the bulk velocity of the fluid (ms^{-1}), D is the characteristic diameter of the flow (m) and μ is the dynamic viscosity of the fluid ($kgm^{-1}s^{-1}$). For a cable tunnel with a typical diameter of 3m and a bulk air velocity of $5ms^{-1}$, the Reynolds number is in the region of 10^6 thus clearly turbulent. For the same tunnel the transition point between a turbulent and laminar flow occurs at around $0.015ms^{-1}$, hence it is clear that the turbulent regime should be considered for all models involving forced convection. The radial air velocity profile is not constant along the course of the tunnel and is instead dependant on axial position along the tunnel. This is due to the development of the boundary layers and velocity profile on entering the tunnel. On contact with the walls, the fluid nearest to the wall begins to slow through the effects of frictional forces. This causes drag on adjacent fluid layers, causing the radial velocity profile to change. Once the air has travelled sufficiently far down the tunnel the velocity profile becomes more uniform and remains so, provided there are no disturbances, for example due to obstructions. For turbulent flow this hydrodynamic entry length, L_h, can be approximated by,

$$\frac{L_h}{D} = 4.4Re^{1/6} \tag{6.2}$$

where D is the characteristic diameter of the tunnel under consideration [92].

6.4 Convective Heat Transfer Coefficients

Correctly specifying the convective heat transfer can have a large impact on the accuracy of any cable rating calculation for cables installed in tunnels, as convection can account for up to 90% of the heat transfer under high air velocities [51]. Electra 143 uses the experimentally derived heat transfer discussed in [56], which has not been thoroughly validated in a realistic cable tunnel environment. At the present stage it has not been possible to acquire sufficient data from operational circuits to validate these heat transfer relations. To provide a further insight, the tunnel airflow models discussed in Section 6.3.1 have been used to derive convective heat transfer coefficients for realistic cable arrangements. As the Dartford tunnel model is the most typical of modern designs it has formed the basis of this analysis.

The procedure adopted for obtaining the heat transfer coefficient in the numerical model is through the use of a wall function. Such an approach prevents the need for extremely high mesh resolution around the walls to ensure the correct calculation of the flow behaviour. This allows the heat transfer problem to be solved through the use of the analogy between momentum and heat transfer, with the full solution for momentum being obtained using the turbulence model as discussed in Section 6.3.1. The method used was originally proposed by Launder and Spalding [113]. It has also been possible to form comparisons against several other correlations for the Nusselt number, Nu [114], by using the fanning friction factor,f, obtained in the numerical model. In all of the equations described here, the characteristic dimension of the Reynolds number is taken to be the cable diameter, as would be the case for internal pipe flow. The first such correlation is the Reynolds Analogy, defined as

$$Nu = \frac{f}{2} RePr \tag{6.3}$$

where Pr is the Prandtl number of the working fluid. It assumes that momentum and heat are transferred in the same way, and that there exists a proportional relationship between heat transfer and the shear stress, τ_ω, defined as

$$\tau_\omega = 0.5 f \rho {U_m}^2 \tag{6.4}$$

where U_m is the mean linear velocity of the air (calculated by dividing the volumetric flow rate by the cross-sectional area). The quantities are related through the fanning friction factor, f, which can be found directly from the shear stress solution in the numerical model. It should be noted that the fanning friction factor has a magnitude four times smaller than the Darcy-Weisbach friction factor.

Some improvements have been suggested for the basic analogy given above. The Taylor-Prandtl Analogy attempted to account for the fluid flow at the tube wall by including the effect of the region of laminar flow close to the wall. Throughout this region heat transfer is through conduction alone, with the resulting Nusselt number correlation being given by

$$Nu = \frac{1}{2} \frac{fRePr}{1 + (u_L/U_m)(Pr - 1)} \tag{6.5}$$

where the quantity u_L represents the velocity at the outer region of the laminar sublayer, which can be found by calculating the velocity at which the Reynolds number is 2000. A further revision to this analogy was suggested by Von-K*árm*á*n* who introduced a buffer zone between the laminar sub-layer and the turbulent zone. This serves to increase the complexity of the relation, such that

$$Nu = \frac{0.5 fRePr}{1 + 5\sqrt{f/2}\left[(Pr - 1) + ln\left(\frac{5Pr+1}{6}\right)\right]} \tag{6.6}$$

Finally, the Colburn Analogy suggests that this level of detail might not be needed and

that instead a simpler correction to the Reynolds Analogy could be by stating

$$Nu = \frac{f}{2} RePr^{1/3} \tag{6.7}$$

For further comparison of methodologies there are also methods which do not require the friction factor to be computed, instead working directly on the Reynolds and Prandtl numbers [115]. Original work by Nusselt suggested that the Nusselt number could be determined according to

$$Nu = 0.024 Re^{0.786} Pr^{0.45} \tag{6.8}$$

Similar work by Dittus and Boelter yielded the relationship

$$Nu = 0.023 Re^{0.8} Pr^{0.4} \tag{6.9}$$

The convective heat transfer coefficients given by these equations are compared to the results of the friction factor methods (where the friction factor is determined by CFD analysis) in Section 6.4.1.

6.4.1 Tunnel Convective Heat Transfer

In order to investigate the predicted values of the convective heat transfer coefficient, the model of the Dartford tunnel has been solved for a range of velocities to allow the heat transfer coefficient to be calculated. All values obtained are averaged along the length between 100m and 200m to ensure that fully developed flow is being considered. The results of the analogy used by the numerical model are compared to the analogies listed in equations (6.3) to (6.7) and also to the correlation used in the Electra 143 equation,

$$Nu = C\,(Re)^{0.65} \;\; [W/m^2K] \tag{6.10}$$

These results can be seen in Figure 6.2. It is clear that the correlation used in Electra 143 provides a much higher value for the convective heat transfer coefficient than those derived from the shear stress solution in the CFD model. These analogies provide similar predictions of the heat transfer coefficient to those predicted by the CFD wall function, with the best fit provided by Von-K*árm*ans' relation. Analysis of the model suggests that this analogy may in fact best approximate the behaviour seen at the wall, as the y+ values derived from the model are in the region of $10 < y+ < 15$, which is just inside the buffer layer (linear relations for laminar flow are used for values of $y+ < 11.225$). However examining the empirical relations of Nusselt and Dittus-Boelter, which do not rely on the prior calculation of the friction factor, a much closer correlation can be seen with the Electra 143 result.

In order to examine the reasons for the differences between the calculations, a numerical model of the experiment discussed in [56] has been created. The original experiments

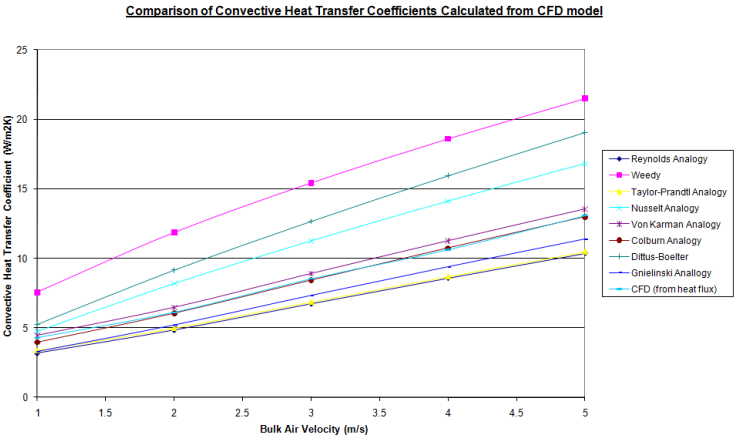

FIGURE 6.2: Comparison of heat transfer calculations

were conducted in a square tunnel of width 66cm and height 61cm, with a length of 8m. Instrumented dummy cables of 5cm to 12cm diameter were used during the tests, with the measurement area being between 2m and 6m along the cable length. One concern with this experimental set up is that it does not appear to account for the hydrodynamic entry length (after which flow would be fully developed). Calculating this quantity using equation (6.2) yields a value of approximately 24m for a bulk air velocity of 5m/s at room temperature. Clearly this would suggest that the velocity profile around the cable groups had not entirely developed, giving the potential for overestimating the true value of the convective heat transfer coefficient.

To verify this hypothesis, a numerical model of the experimental arrangement, complete with a straight unsupported cable of the same dimensions as those installed within the Dartford tunnel, was constructed. The cable section was subdivided five times such that the surface area averaged heat transfer coefficient could be calculated for the regions related to the original experiment, and also for an 8m region beyond 24m from the inlet where the flow was fully developed. The resulting velocity profiles are shown in Figure 6.3.

It is clear that the low velocity areas underneath the cables have not fully developed within 6m of the inlet, which was specified as a uniform velocity of 5m/s. Examining the resulting values of the convective heat transfer coefficient shows a clear trend; for the section measured by the original experiment of Weedy, the convective heat transfer coefficient is $16.70 Wm^{-2}K^{-1}$. For the 8m section in fully developed flow, the average value is reduced to $13.36 Wm^{-2}K^{-1}$. This result suggests that the convective heat transfer coefficient in current use is not sufficiently accurate for use in new methods developed in this study.

Despite the possibility that the existing correlation provides optimistic values for the cable surface convective heat transfer coefficient, it is also likely that the values obtained from the friction factor based correlations are excessively conservative. This is because

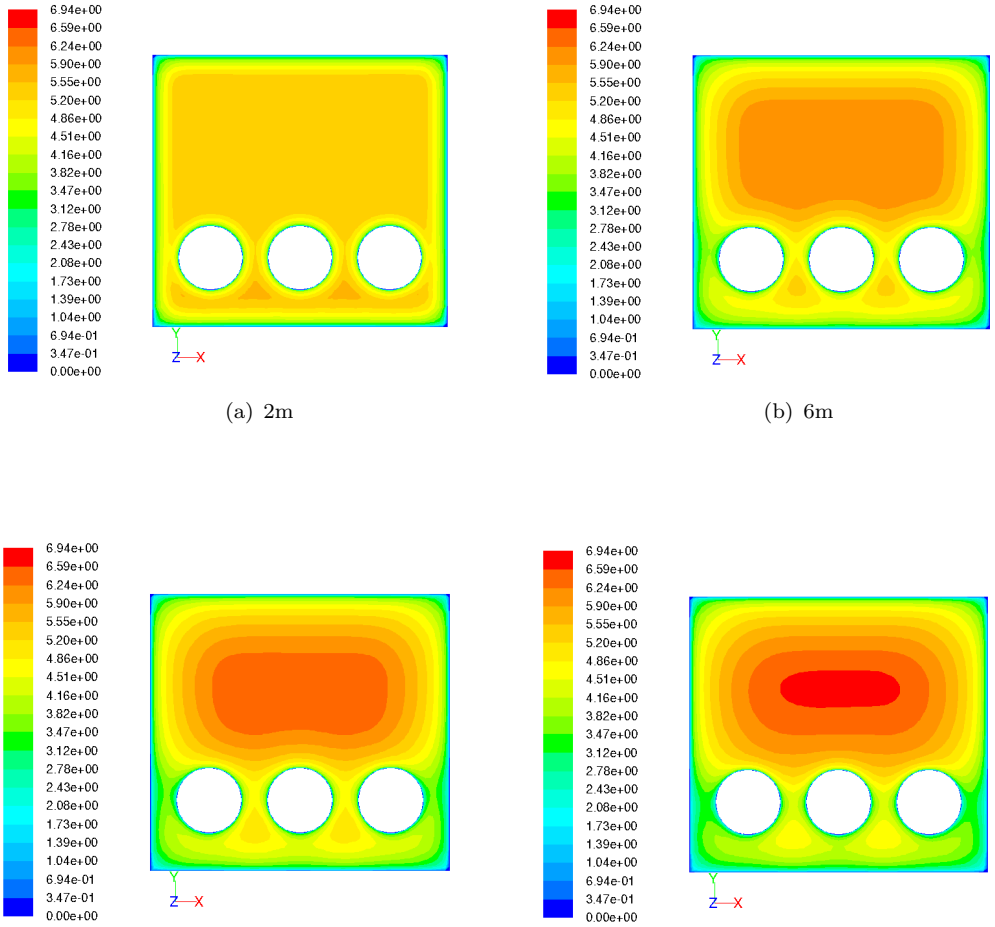

(a) 2m

(b) 6m

(c) 8m

(d) 24m

FIGURE 6.3: Velocity profiles for 2m, 6m, 8m and 24m from inlet of trough

the CFD model represents an overly idealized cable environment, with no brackets, cleats or other obstructions to break up the boundary layers around the cables. The treatment of the cable surfaces as being entirely smooth will also add a small amount of conservatism. These two factors combined could over-estimate the size of the laminar part of the boundary layer, hence it is likely that the true coefficient lies between that of Electra 143 and the CFD based results. Further experimental verification in operational tunnels would be necessary to fully validate this case.

6.5 New Model Construction

In essence, the recommended design for the thermal network is largely similar to that of [50]. Several important changes are needed in order to fulfill the requirements for modelling multiple independent cable circuits, each of which are discussed in detail in the following Sections.

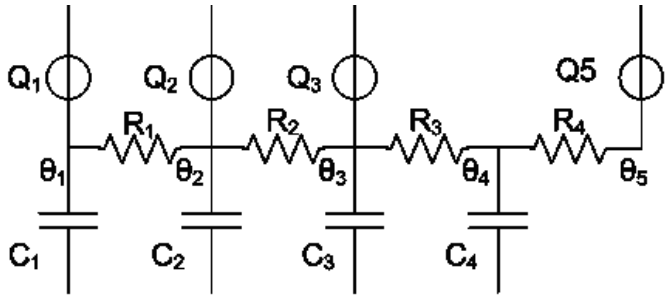

FIGURE 6.4: Thermal network to represent one cable

6.5.1 Cable Model

It is possible to represent the majority of single core cables using a five node thermal network shown in Figure 6.4. The location of these nodes is as follows:

1. Conductor (assumed isothermal)
2. Log mean radius of the dielectric
3. Centre of cable sheath (assumed isothermal)
4. Log mean radius of the oversheath
5. Outer surface of the cable.

The four nodes which are internal to the cable have a thermal capacitance associated with them. In addition, the first three nodes have heat sources due to the conductor, dielectric and sheath losses at these locations. The equations which define the resistances illustrated in Figure 6.4 are as shown in [50], but with the parameter N=1, as each cable is modelled individually. Whilst this model is simple, a comparison with a steady state finite element model has demonstrated that it is also very accurate (agreement between the two models at both cable surface and the conductor was found to be 0.1°C). Where short duration transients or cyclic load variations are to be modelled, it can be beneficial to subdivide the dielectric region into a number of layers to increase the precision of the model. Unlike the Electra 143 model which uses a constant a.c. resistance, in this model the a.c. resistance of the conductor is implemented as a function of temperature. The most accurate way in which the resistance may be calculated is to use the procedure outlined in [18]. The only change is the addition of a source term Q5,

$$Q_{5,y} = \pi D_e \Delta x \epsilon_{cab} \sigma \sum_{c=1}^{N} F_{cc(y,c)} \left[\theta_{5A(y)}^4 - \theta_{5A(c)}^4 \right] \tag{6.11}$$

which permits direct transfer of radiation either between cables, or between cables and other heat sources or sinks. Note that y denotes the cable under consideration and

$F_c c(y, c)$ is the view-factor between cables y and c. View-factors may be calculated in a number of ways, with the simplest being that of cross strings [116]. For more complex geometries it may be necessary to use a full contour integral solution [117] or finite element methods if the maximum possible accuracy is required.

Consideration must also be given to the values of cable surface convective heat transfer which are specified in the model. Where cables are located close to the wall, the relation in present use [56] proves optimistic. Due to the way in which all individual cables are modelled, it is possible to specify different coefficients for each cable group. Where this is felt to be appropriate, it is frequently necessary to use computational fluid dynamics methods to determine improved values as was illustrated in section 6.4.1.

6.5.2 Tunnel Model

In order to meet the requirements for the new model, significant changes must be made to the way in which heat transfer from the cables to the tunnel environment is modelled. Since multiple cables are modelled explicitly, the thermal network must allow for the summation of the individual contributions to the rise in air temperature (node 6) and tunnel wall temperature (node 7). There is no limit to the number of cable circuits for which a temperature distribution can be obtained. This is achieved by defining a number of thermal resistances $R_{5(n)}$,

$$R_{5(n)} = \frac{1}{\pi D_e \zeta h_{cab} \Delta x} \tag{6.12}$$

This models convective transfer from the cable surface to the air, arranged in a star point configuration around node 6. Additionally each cable surface (node 5) is connected directly to the tunnel wall by a thermal resistance $R_{r(n)}$,

$$R_{r(n)} = \frac{1}{\sigma F_{cw} D_e \epsilon_{cab} \Delta x (\theta_{5A}^2 + \theta_{7A}^2)(\theta_{5A} + \theta_{7A})} \tag{6.13}$$

which represents heat transfer by radiation. Convection heat transfer to the tunnel wall is accounted for by

$$R_6 = \frac{1}{\pi D_{tun} h_{wall} \Delta x} \tag{6.14}$$

The applicable values of the convective heat transfer coefficient are a function of the particular installation and ventilation parameters.

Axial heat transfer between slices is permitted between adjacent air nodes (due to the movement of air through the tunnel system) and can be characterized using

$$R_f = \frac{1}{c_{pf} V A_f} \tag{6.15}$$

Heat transfer within the soil or rock surrounding the tunnel is easily solved using the

method of Electra 143 [50]. This requires the region to be split into annular rings, with a thermal capacitance and resistance assigned to each. The only point at which an alternative method must be considered is if significant moisture migration is expected away from the tunnel region. In this case it may be necessary to use a finite element technique with Philip and de Vries equations to model the thermal behaviour of the surrounding soil [66].

6.5.3 Riser Shafts

At present, the Electra 143 model does not include the riser shafts at either end of the tunnel. If the shaft cross-sectional area is greater than that of the tunnel this may limit the rating of the circuit. Only minor modifications to the algorithm are required to integrate the temperature calculations for the shaft into the overall tunnel section. The modelling of the cable remains the same, but clearly the different dimensions of the shafts must be accounted for (in the majority of UK tunnels, the shaft diameter is at least double that of the main tunnel section). This also means that the bulk air velocity in the shaft section must be adjusted to take account of the effect of the increased cross-sectional area through which the air may flow. Where the velocity over the cable surface is reduced, different cable surface convective heat transfer coefficients need to be specified.

6.5.4 Solution Procedure

Under the Electra 143 scheme, it is only necessary to solve one set of matrix equations to determine the nodal temperature at each slice. However, where more than one cable model is used this is not feasible and the solution must be split into sequential steps. Initially the five matrix equations describing cable temperatures,

$$(\frac{C_1}{\Delta T} + \frac{1}{R_1})\theta_{i,1}^{m+1} - \frac{1}{R_1}\theta_{i,2}^{m+1} = Q_1(\theta_{i,1}^m) + \frac{C_1}{\Delta T}\theta_{i,1}^m \tag{6.16}$$

$$-\frac{1}{R_1}\theta_{i,1}^{m+1} + (\frac{1}{R_1} + \frac{1}{R_2} + \frac{C_2}{\Delta T})\theta_{i,2}^{m+1} - \frac{1}{R_2}\theta_{i,3}^{m+1} = Q_2 + \frac{C_2}{\Delta T}\theta_{i,2}^m \tag{6.17}$$

$$-\frac{1}{R_2}\theta_{i,2}^{m+1} + (\frac{1}{R_2} + \frac{1}{R_3} + \frac{C_3}{\Delta T})\theta_{i,3}^{m+1} - \frac{1}{R_3}\theta_{i,4}^{m+1} = Q_3(\theta_{i,1}^m) + \frac{C_3}{\Delta T}\theta_{i,3}^m \tag{6.18}$$

$$-\frac{1}{R_3}\theta_{i,3}^{m+1} + (\frac{1}{R_3} + \frac{1}{R_4} + \frac{C_4}{\Delta T})\theta_{i,4}^{m+1} - \frac{1}{R_4}\theta_{i,5}^{m+1} = \frac{C_4}{\Delta T}\theta_{i,4}^m \tag{6.19}$$

$$-\frac{1}{R_4}\theta_{i,4}^{m+1}+(\frac{1}{R_4}+\frac{1}{R_5}+\frac{1}{R_r})\theta_{i,5}^{m+1}=Q_5+\frac{1}{R_5}\theta_{i,6}^{m}+\frac{1}{R_r}\theta_{i,7}^{m} \tag{6.20}$$

are assembled into the form of

$$[K][\theta]=[S] \tag{6.21}$$

where [K] is a matrix of coefficients consisting of R and C terms, $[\theta]$ is the column vector of temperatures to be calculated and [S] is a column vector of source terms and those which depend on the temperature at a previous time-step. These are solved to obtain $[\theta]$, with the surface temperature data passed into a second set of matrix equations, described by 6.22 - 6.25,

$$\left(\frac{1}{R_f}+\frac{1}{R_6}+\frac{C_6}{\Delta T}\right)\theta_{i,6}^{m+1}-\frac{1}{R_6}\theta_{i,7}^{m+1}=\sum_{c=1}^{N}\left(\frac{(\theta_{i,5(c)}^{m+1}-\theta_{i,6}^{m})}{R_{5(c)}}\right)+\frac{1}{R_f}\theta_{i-1,6}^{m+1}+\frac{C_6}{\Delta T}\theta_{i,6}^{m} \tag{6.22}$$

$$-\frac{1}{R_6}\theta_{i,6}^{m+1}+\left(\frac{1}{R_6}+\frac{1}{R_7}+\sum_{c=1}^{N}\frac{1}{R_{r(c)}}\right)\theta_{i,7}^{m+1}-\frac{1}{R_7}\theta_{i,8}^{m+1}=\sum_{R_{r(c)}}^{1}\theta_{i,5}^{m+1} \tag{6.23}$$

$$-\frac{1}{R_{j-1}}\theta_{i,j-1}^{m+1}+\left(\frac{1}{R_{j-1}}+\frac{1}{R_j}+\frac{C_j}{\Delta T}\right)\theta_{i,j}^{m+1}-\frac{m+1}{i,j+1}=\frac{C_j}{\Delta T}\theta_{i,j}^{m} \tag{6.24}$$

$$-\frac{1}{R_{n+7}}\theta_{i,n+6}^{m+1}+\frac{1}{R_{n+7}}\theta_{i,n+7}^{m+1}=0 \tag{6.25}$$

which contain the nodal equations for the tunnel. This allows the contribution of each cable to the tunnel temperature rise to be summed at the tunnel air and wall nodes.

In the steady state case it may be assumed that all of the capacitance terms can be set to zero. An iterative solution process can be adopted whereby the calculation progresses along the length of the tunnel, each time comparing the change in nodal temperatures with the last iteration. The ac resistance of each cable is also updated with the conductor temperature from the previous time-step to ensure accurate calculation of cable losses. Once the temperature difference between two iterations becomes less than a set convergence criterion (typically 0.01°C), the solution is complete. For most tunnel configurations tested, steady state convergence was achieved in less than 20 iterations along the tunnel length.

When obtaining a transient solution, it is important to select a suitable time-step for the calculations such that an accurate solution is obtained, but without excessively extending computational time. Where particularly long transients are to be analysed, the most accurate method is to use a two stage solution. Due to the hugely different time constants of the cable circuit and the tunnel environment, most of the temperature change in the cable circuit will occur within the first 24 hours of operation at a set level of load current, whilst the tunnel wall temperature responds over a period of years. To

best capture this behaviour, it was found that the first few days have to be resolved using a time-step no larger than one hour. After this a one day time-step is more appropriate due to the large time constant of the tunnel wall. Small time steps of less than one hour or less are required where factors such as daily cyclic variation in inlet temperatures are to be modelled.

6.5.5 Benchmarking

In order to validate the revised solution procedure, a series of comparisons have been undertaken against the original Electra 143 methodology. The sample tunnel used for the benchmarking tests is that reported in [118]. In order to make a straight comparison, one 3 phase cable circuit is modelled, with all heat transfer data being identical between the two tests. Testing across a range of inlet air velocities for the steady state case with 2000A load current, the largest temperature difference observed (for cable, tunnel air or tunnel wall temperatures) is 0.01°C. Checks on the transient performance were undertaken for the case of a step application of 2000A load current for 24 hours. In this case the agreement between the two methods is within 0.05°C. As both implementations provide consistent answers (when provided with the exact same input conditions), the use of the revised network is entirely reasonable for steady state and transient conditions where circuits are identical.

6.5.6 Modelling of Cable Joints

The developed model allows for improved consideration of multiple different cable circuits within one tunnel, however, it does not tackle the key issue identified in Chapter 2, namely the thermal implications of cable joints within tunnels. The study presented in Chapter 5 demonstrated that it is not always possible to ignore the presence of joints. Based on experience gained from this it is clear that similar FEA techniques could be adopted for the case of tunnels. While the use of two different techniques makes model integration more challenging, it has the simultaneous benefit of allowing much better modelling of the cable joints themselves. Although there would be some value in modelling each of the joints within the tunnel, in reality it is only necessary to consider the thermal impact of the joint situated closest to the air outlet (hence surrounded by the warmest air).

Where a tunnel is forced ventilated, the temperature of the air around the surface of the joint can be considered approximately constant over both the length and radius. As a result, it is not considered necessary to construct full 3D models of the joint, but instead to make use of the 2D axially symmetric modelling initially presented in Section 5.2.3. The 2D FEA model is constructed outside of the main tunnel rating algorithm, with the air and wall temperatures at the joint bay location being passed to it. Where

transient simulations are undertaken, both of these parameters will be time variant. This approach permits the thermal effect of the joint to be modelled without giving rise to a significant increase in computational time.

6.6 Calculation of Ratings for High Temperature Cables

This Section details the application of the developed method to a complex cable tunnel arrangement. Continuous and emergency rating calculations are undertaken for a number of operational configurations, allowing the potential of the new cables to be assessed.

6.6.1 Tunnel Arrangement Considered

The tunnel under consideration is shown in Figure 6.5; it is a 4m diameter tunnel with a total of 5 cable circuits installed. Circuits 1 and 2 are 400kV high temperature circuits with two cables per phase, while circuits 3, 4 and 5 are 132kV XLPE cable circuits installed in trefoil configuration.

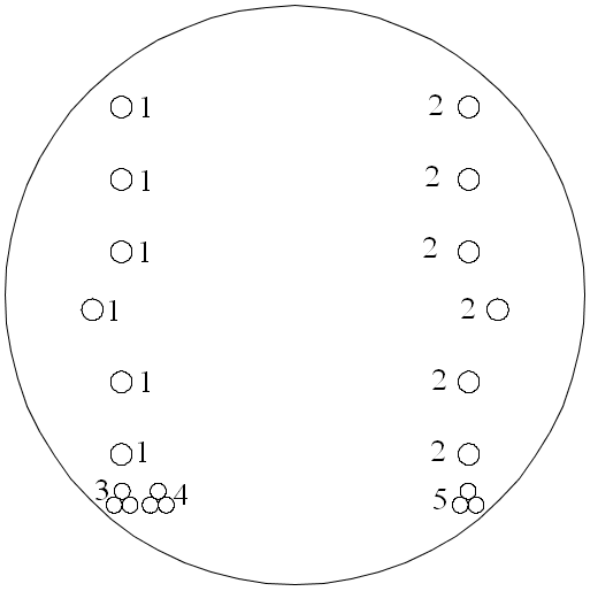

FIGURE 6.5: Arrangement of cable circuits for tunnel calculations

As the convective heat transfer coefficients have been identified as a key variable to consider, a computational fluid dynamics analysis similar to that discussed in 6.3 has been undertaken. This allows the convective heat transfer coefficients to be obtained and compared with the standard values. Figure 6.6 illustrates the simulation result for an inlet velocity of $62.8m^3/s$, equivalent to a bulk velocity of 5m/s in the tunnel.

Circuit Number	h_{cab} min (W/m^2K)	h_{cab} mean (W/m^2K)	h_{cab} max (W/m^2K)
1	9.58	10.73	11.36
2	9.53	10.78	11.38
3	2.30	3.98	6.17
4	4.59	7.28	8.82
5	2.51	5.63	7.29

TABLE 6.3: Convective heat transfer coefficients from CFD model (minimum, maximum and average values are based on the circumferential average of each cable circuit)

Geometric Parameters	400kV cable	132kV cable
Conductor Cross Sectional Area (mm^2)	2500	1600
Conductor Diameter (mm)	64	53
Dielectric Thickness (mm)	31	20.5
Outer Spaced Copper Wire Screen Diameter (mm)	132	101
External Diameter (mm)	148	110
Phase Separation (mm)	500	110
Thermal Parameters	**400kV cable**	**132kV cable**
Dielectric Thermal Resistivity (Km/W)	3.5	3.5
Serving Thermal Resistivity (Km/W)	3.5	3.5
Volumetric Specific Heat Capacity of Conductor (J/m^3K)	$3.45x10^6$	$3.45x10^6$
Volumetric Specific Heat Capacity of Dielectric (J/m^3K)	$2.4x10^6$	$2.4x10^6$
Volumetric Specific Heat Capacity of Spaced Copper Wire Screen (J/m^3K)	$3.45x10^6$	$3.45x10^6$
Volumetric Specific Heat Capacity of Serving (J/m^3K)	$2.4x10^6$	$2.4x10^6$
Cable Surface Emissivity	0.9	0.9
Conductor Temperature Limit (°C)	90/120/150	90
Electrical Parameters	**400kV cable**	**132kV cable**
Resistivity of conductor Ωm	$1.7241x10^{-8}$	$1.7241x10^{-8}$
Conductor temperature coefficient of resistance $(°C^{-1})$	0.00393	0.00393
ks coefficient	0.62	0.62
kp coefficient	0.8	0.8
Screen Loss Factor	0.0152	0
Dielectric relative permittivity	2.4	2.4
System Frequency (Hz)	50	50
Phase to Earth Voltage (V)	230940	76210
Tangent of dielectric loss angle	0.001	0.001

TABLE 6.4: Parameters of Tunnel Cables

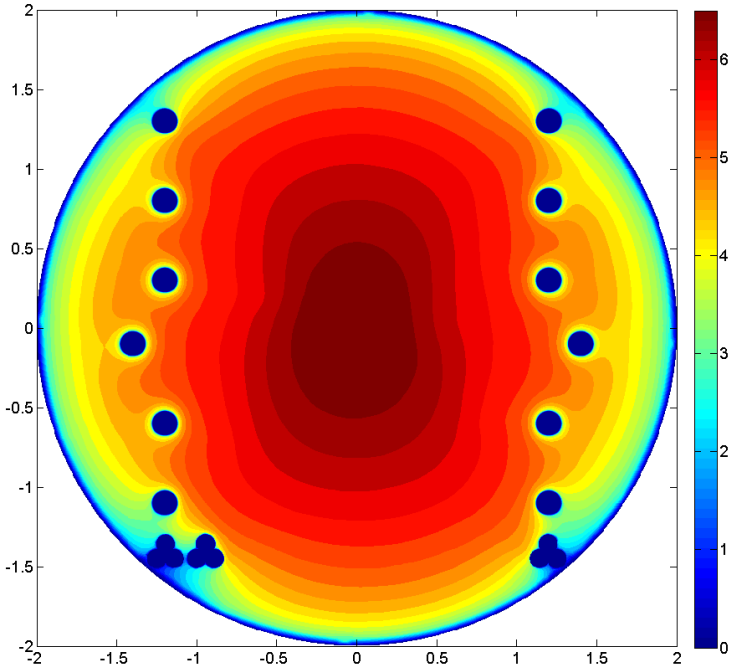

FIGURE 6.6: Velocity profile for 5m/s inlet

Examination of Figure 6.6 reveals similar trends to those observed during the study of the Dartford tunnel in Section 6.4.1. The 400kV cables closer to the walls (those at the top and bottom of the formation) are surrounded by slower moving air than those in the middle of the formation, yielding an impact on the heat transfer coefficients as shown in Table 6.3. The values presented in Table 6.3 are based on the circumferential averages of convective heat transfer coefficient on each cable within the circuit. These values are significantly lower than the standard results of [56] would suggest, ideally requiring verification on an operational cable system. It is likely that in a real tunnel additional obstructions to the airflow would break up the boundary layers, slightly improving the value of h_{cab}.

6.6.2 Calculation of Continuous Ratings

Analysis of the continuous rating is greatly simplified by trading off the rating of the cable circuits in groups, in this case by voltage. In order to illustrate the effect of the values of h_{cab} used on the circuit rating, two sets of results are obtained. The first is for the standard values of [56], while the second uses the maximum value derived from the CFD analysis (see Table 6.3). The resulting rating curves are plotted in Figure 6.7, examination of which suggests that the optimum trade-off between the rating of the 132kV and 400kV circuits is found where the rating of the 132kV circuits is approximately 1000A. There is little to gain by limiting the rating of the 132kV circuits to less than 1000A as the increase in 400kV circuit rating is low, while increasing the rating of the 132kV circuits above 1500A requires such a substantial de-rating of the 400kV

circuits that it would never be operationally viable. The relationship between the two ratings is non-linear due to the joule losses being a function of current squared.

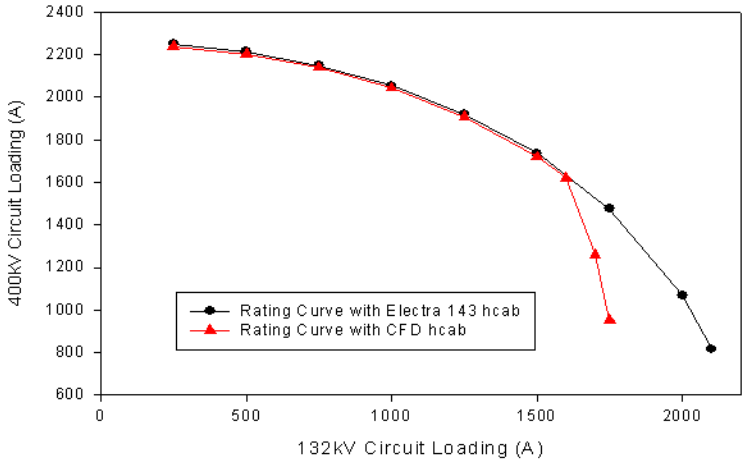

FIGURE 6.7: Continuous Rating Trade-off

The shape of the curves in Figure 6.7 is partly determined by the results shown in Figures 6.8 and 6.9. It is apparent that for 132kV circuit ratings below 1500A the choice of h_{cab} does not have a significant impact on the result. This arises from the effect of the 50°C air outlet limit, which is actually the limiting criterion on the overall circuit ratings. As the conductor temperature is below its maximum threshold, the shift in conductor temperature does not have a huge effect on the rating overall.

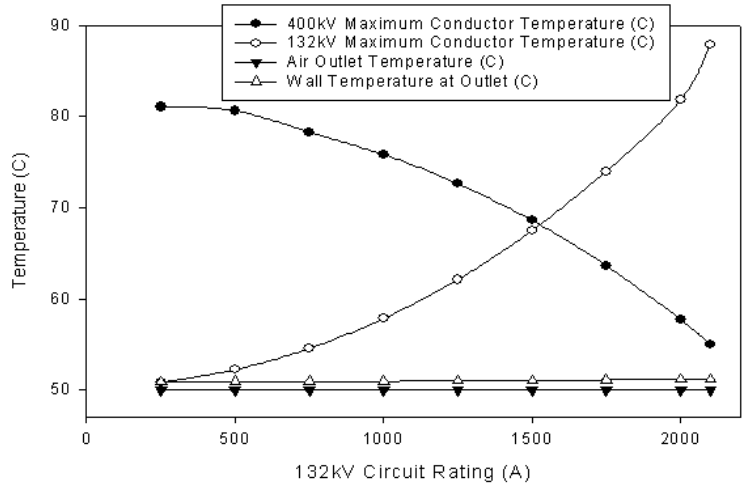

FIGURE 6.8: Temperature Curves at Continuous Ratings (Electra h_{cab})

The small reduction seen when the CFD h_{cab} values are used is due to the slightly increased joule losses caused by the increase in conductor temperature, which serve to increase the temperature of the air beyond what would otherwise be expected. However, there is a marked difference in the rating curve above 1500A, the cause of which is identifiable in Figure 6.9. As circuit 3 is closest to the wall it sees a significant reduction

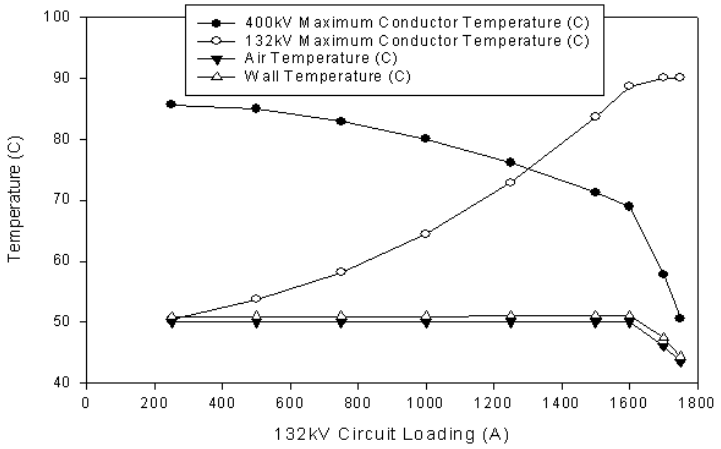

FIGURE 6.9: Temperature Curves at Continuous Ratings (CFD h_{cab})

in convective heat transfer coefficient when the CFD values are used, leading to its conductor temperatures rising much more quickly. Simultaneously it is also subject to the highest mutual heating by radiation due to its proximity to the adjacent 400kV cable.

Figure 6.10 illustrates the difference between the maximum temperature at the joint for both of the heat transfer cases studied. In both cases the fact that the air temperature limit governs the rating prevents the joint temperature exceeding the cable temperature by more than 7°C. An example joint temperature profile is shown in Figure 6.11, which clearly demonstrates that the thermal effect of the joint cannot be ignored. This is especially true for two cases - the first where the joint bay is very close to the outlet of the tunnel and the second being where the conductor temperature is the limiting factor on the circuit rating (which is common for shorter circuits).

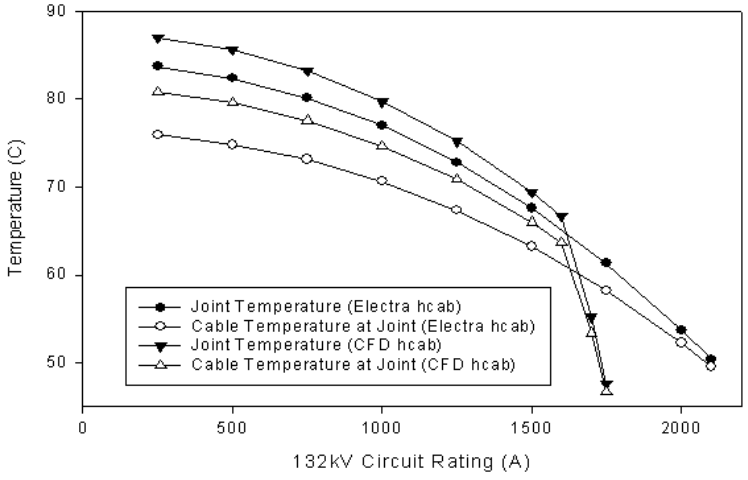

FIGURE 6.10: Maximum Joint Temperatures under Continuous Rating

Perhaps the most significant conclusion from Figures 6.7 to 6.11 is that there is no real benefit to the continuous rating in this case from using a high temperature cable. As

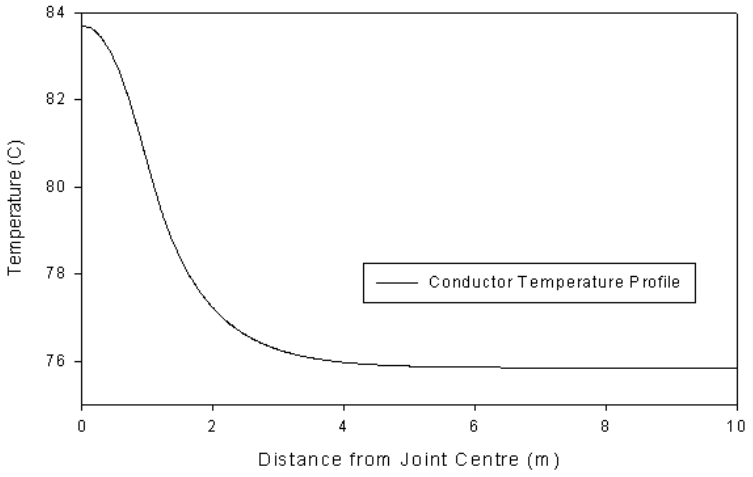

FIGURE 6.11: Example Joint Temperature Profile

the air temperature is the limiting factor the peak joint temperature remained below 90°C for all cases studied, as is frequently the case for longer tunnels. However, the true benefit may arise from the ability to attain emergency ratings significantly above those of overhead lines, effectively removing the cable as the limiting factor over the 6 hour rating period. A full study into these effects is presented in Section 6.6.3.

6.6.3 Calculation of Emergency Ratings

The most commonly used post-fault rating on the UK transmission network is a six hour rating, defined as the maximum step load of six hours duration which can be applied to a circuit given operation at a set percentage of its continuous capability (defined as pre-fault load). Using the revised method presented here, it is possible to investigate the post-fault rating capability of one circuit against the thermal background of other circuits continuing to operate as normal due to the explicit calculation of all conductor temperatures. If individual instantaneous conductor temperatures are not known, it is impossible to accurately calculate the rating. This is because the limiting factor on the magnitude of the emergency rating is the initial cable temperature.

The first example considers the requirement to elevate the rating of both 400kV circuits simultaneously. The 132kV circuits are presumed to be operating independently at a constant loading of 1000A throughout the pre-fault and post-fault periods (a potentially important assumption if these cables are operated by a separate utility). Figure 6.12 illustrates the resulting ratings when the pre-fault loading on the 400kV circuits is varied between 20% and 90% of the continuous rating (2054A in this case), with a conductor temperature limit of 90°C. The initial condition is specified by solving the steady state calculation for the pre-fault loading conditions and setting this as the initial temperature distribution for the first time-step in the transient calculation. The flexibility afforded by the method allows for instantaneous cable temperatures to be derived for the different

loadings within the same tunnel environment, the results of which may be found in Figure 6.13.

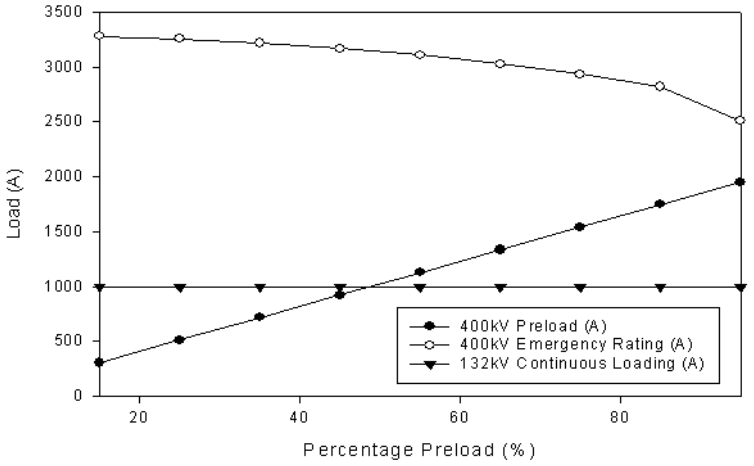

FIGURE 6.12: 6hr cable rating with 90°C conductor temperature limit

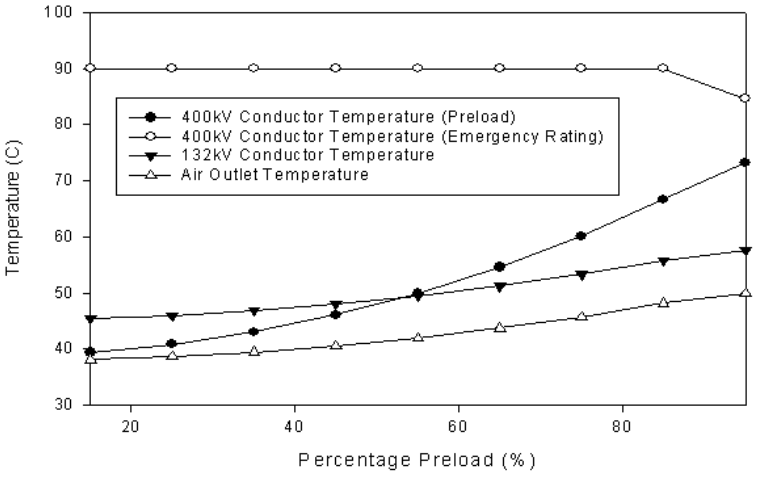

FIGURE 6.13: Cable temperatures for 6hr ratings at 90°C

It is immediately apparent that there are two different regimes present in Figure 6.13, with the far right hand side of the plot limited by the air temperature, and the remainder by the conductor temperature limit. However, the analysis above does not consider the potential effects of the cable joints. Transferring the air and wall temperatures to a transient model of the cable joint illustrates the necessity of this additional model step, as shown in Figure 6.14.

Above the 55% preload it can be seen that the joint temperature exceeds the maximum temperature criterion, in this case 90°C. Were these ratings to be deployed on an operational cable system this issue would be vital to consider. However, due to the additional thermal capacitance of the joint, the thermal limit is not exceeded until the end of the 6hr period, as shown in Figure 6.15. As transmission network operators must, by their nature, tolerate only very small risks of failure, it would be necessary to introduce a

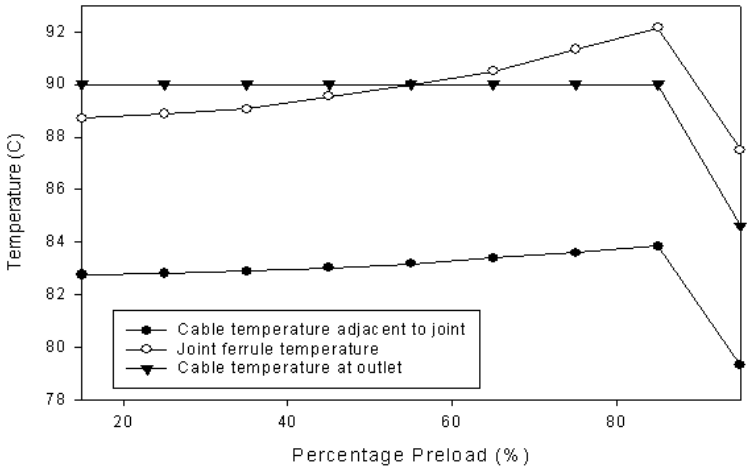

FIGURE 6.14: Peak joint ferrule temperatures

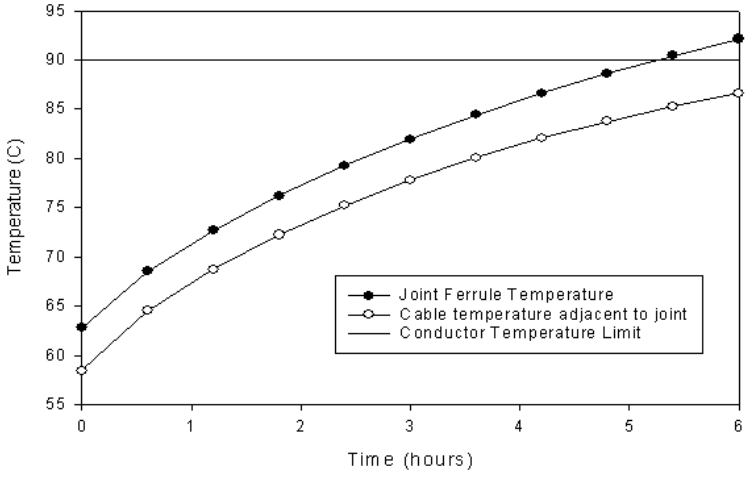

FIGURE 6.15: Increase in joint temperature during emergency period

de-rating factor to prevent the joint temperature exceeding its limit.

Having ascertained the performance of the standard 90°C cable the model has been solved for the higher conductor temperature limits (Figure 6.16). At lower preloads (where the initial air temperature is lower) there is a clear benefit to the use of the 150°C cable system. However, as the preload increases the initial air temperature increases such that the additional heat generated by the cables during the emergency period causes the air outlet limit to be exceeded, constraining the rating. In this case the 120°C cable would be sufficient to gain maximum available benefit. Finally consideration must be given to the presence of other limiting factors within the circuit, notably circuit breakers. At present, the majority of circuit breakers deployed on the National Grid network are rated to 4kA. Overhead lines are frequently constrained to similar conductor currents, as the level of sag would otherwise cause clearance distances to be breached. As such, it is possible that the full capability of the 150°C cable system might not be utilized in a modern transmission circuit.

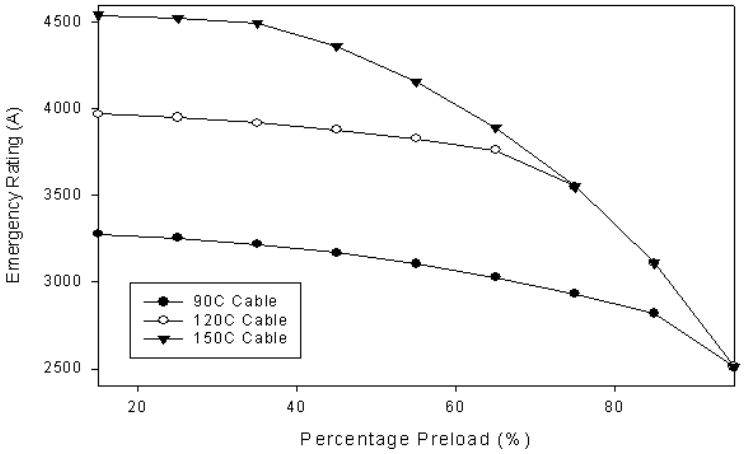

FIGURE 6.16: Comparison of emergency ratings for 90°C, 120°Cand 150°C cables

The final consideration regarding emergency ratings is whether the high temperature cable has the potential to extend a conventional 6hr rating from an XLPE cable circuit to a duration of 24 hours, as seen in the directly buried case (Section 4.4.2). To investigate this issue further, the emergency rating calculations discussed above have been repeated for the case of an emergency rating being applied to both 400kV circuits for a duration of 24 hours. As per the previous analysis, the 132kV circuits continue to operate at a load of 1000A per phase throughout the pre-fault and post-fault periods. Figure 6.17 summarises the ratings available for the XLPE and 120°C cables, with no rating benefit being gained from operation at temperatures higher than 120°C due to the limit imposed on the air outlet temperature.

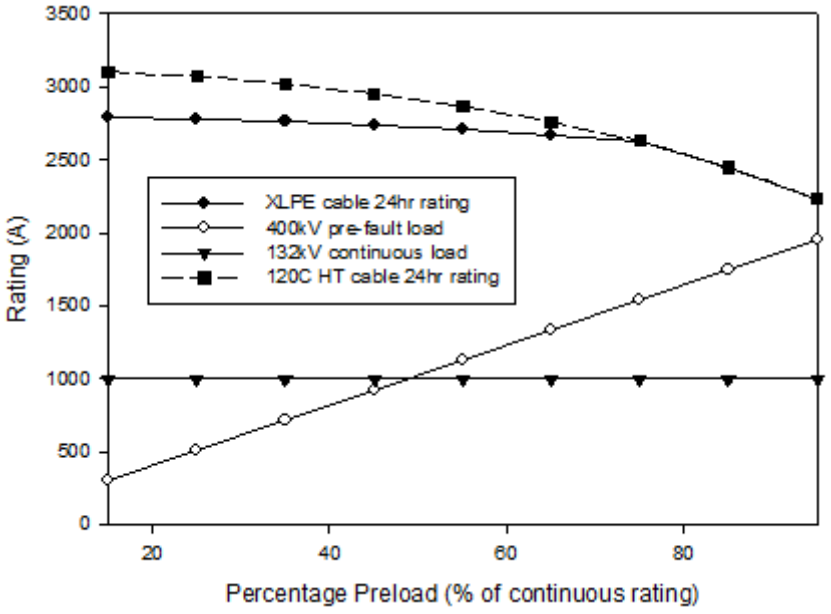

FIGURE 6.17: 24hr Emergency Rating for both 400kV circuits

Considering the results it is clear that for this particular application the attainable 24hr

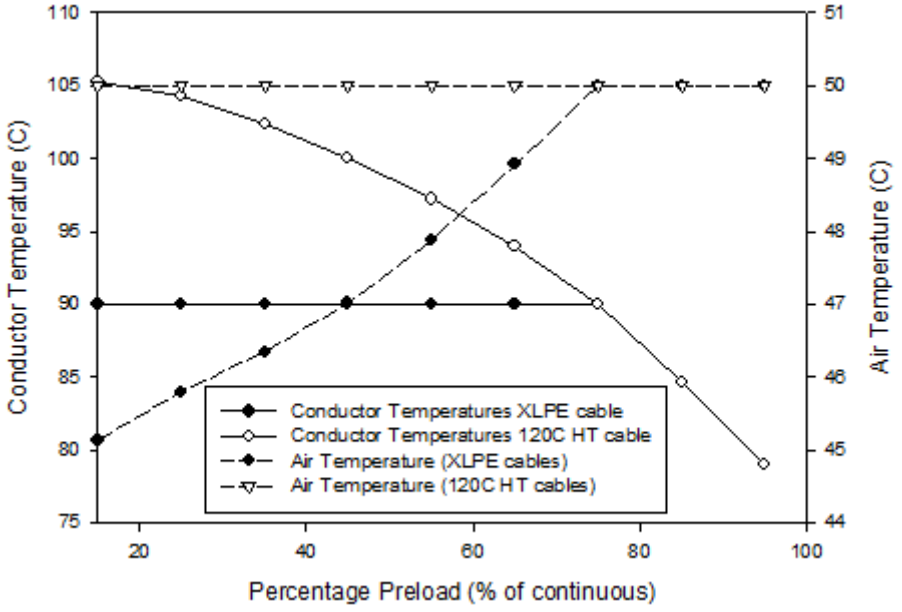

FIGURE 6.18: Conductor and air temperature profiles for 24hr ratings

ratings are considerably lower than in the buried cable case. This is mainly due to the requirement to maintain an air outlet temperature lower than 50°C. Given the number of 132kV cables present in the tunnel, the background heat generation is quite high, restricting the thermal headroom of the 400kV cables. As such, the benefits of high temperature operation will be much higher in tunnels containing only 400kV cables. The data for air and conductor temperatures in Figure 6.18 demonstrate that the high temperature cable in this example never attains 120°C under 24hr rating conditions. This is because the air temperature always reaches 50°C at the outlet prior to the conductor temperature becoming the limiting factor.

6.7 Summary

This Chapter has presented solutions to a number of issues with the present Electra 143 rating methodology. The co-location in tunnels of cable circuits of differing voltages, potentially operated by different utilities, required a new approach to the calculation of the circuit rating. Key to this issue is that there is no longer a single maximum value of current. Indeed, depending on the tunnel configuration and the operational requirements of the circuits, a whole range of different theoretical maximum ratings can be specified, as evidenced by Figure 6.7. By using the method presented here, it is possible to examine a wide variety of potential loading constraints and analyze the impact of each on the conductor temperature of each cable circuit. The ability to access the full temperature profile means that a wider range of circuit rating trade-offs can be investigated, enabling the cable engineer to undertake an optimisation process between

the continuous and short-term rating requirements of each individual circuit. As a result, the cable section can be operated in a way which best meets the operational needs of the network operator.

Through applying this method the potential applications of high temperature cables have been illustrated, along with some of the drawbacks. While the benefit to the continuous rating is likely to be limited due to the tendency of the air temperature to limit the rating, real benefits can be achieved under emergency rating conditions. The calculation methodology presented here has subsequently been published in [119] and is to be submitted to the Cigre cable rating working group for consideration as a replacement to Electra 143.

Chapter 7

Rating of Cables in Surface Troughs

Through the review of the literature presented in Section 2.4, it was noted that cable trough installations, although frequently short in length, can often present critical links in a transmission circuit. Two basic types of trough installation are used in the UK, the first being backfilled troughs and, second, air cooled troughs. Previous work has highlighted the importance of considering moisture migration [63] and ground surface effects [62] for backfilled troughs. This could be easily achieved through the application of the techniques for buried cables presented in Chapter 4. However, the majority of such installations in the UK tend to date from the early years of the construction of the 400kV supergrid, and it is no longer common practice to install cables in this manner. As a result, this Chapter will focus on the modelling techniques applicable to air filled cable troughs, which are commonly used to link cable tunnel environments (as presented in Chapter 6) with adjacent overhead lines.

Three different forms of ventilation will be considered to determine the most appropriate method for use with high temperature cables. The first is a traditional unventilated installation where the troughs are covered by solid concrete lids and the system can be considered to be sealed, i.e. there is no exchange of warm air inside the trough with cooler ambient air. In recent years it has been necessary to increase the rating of some cable circuits which were previously installed in this manner, for which a common solution has been the use of partial ventilation. Here some of the solid concrete lids, typically one in four, are replaced by a grille or mesh to permit the circulation of air into and out of the troughs. This increases the circuit rating without the need to install mechanical ventilation. For very high operating temperature cables, such as the 150°C example considered in this thesis, it may be necessary to increase the rate of ventilation further by using fans to force air through the trough.

7.1 Modelling Strategy

The modelling strategy adopted for the cable trough installations is in part similar to that used for cable tunnels. Computational fluid dynamics models will be constructed to model the convective flow induced by the heat from the cable, however, for cable troughs it is possible to fully couple the fluid dynamics equations with the solution of the heat equations. The reason for this is that the overall model size is considerably smaller as the maximum length considered is 50m for the ventilated trough case, compared to several kilometres for the tunnel case. Throughout the Chapter the results gained from the numerical models are compared with existing published methods.

7.1.1 Unventilated Trough Modelling

For the unventilated troughs, a rating method is presented in IEC 60287 which uses an empirically derived function to determine the air temperature rise in the trough, $\Delta\theta_{tr}$, such that

$$\Delta\theta_{tr} = \frac{W_{TOT}}{3p} \tag{7.1}$$

where W_{TOT} is the heat generated by the cables per metre of installed trough and p is part of the trough perimeter which is effective for heat dissipation (m). Any part of the perimeter which is subject to solar radiation is excluded from the distance p. The rating is then calculated as if the cable were installed in free air, but with the ambient temperature increased by the value of $\Delta\theta_{tr}$. Taking such an approach has one clear disadvantage, namely, that it fails to consider the impact of the ground around the outside of the trough. Work by Anders has suggested that this method is conservative and a new equation was proposed [120]. Instead of calculating an effective air temperature rise, the thermal resistance of the trough and ground is calculated explicitly by

$$T_t = \frac{\rho_e}{0.3907 + H_c + \phi_b} \tag{7.2}$$

where ρ_e is the thermal resistivity of the soil, H_c is defined by

$$H_c = \frac{H_s B \rho_e}{a\rho_c H_s + B} \tag{7.3}$$

where ρ_c is the thermal resistivity of the trough cover, B is the internal trough width (m), and a is the cover thickness (m). ϕ_b is calculated by

$$\phi_b = 2.13\left(\frac{a}{A} + 0.05\right)^{-0.39}\left(\frac{B}{A}\right)^{0.065} \tag{7.4}$$

with A defined as the internal height of the trough (m). The value of T_t is then added to the conventional T_4 value in the IEC 60287 free air calculation to determine the correct

rating for the trough. Both methods will be considered against the CFD implementation to benchmark their performance for both conventional and high temperature cables.

7.1.2 Ventilated Trough Modelling

At the time of writing no formal standard has been developed for the rating of partially ventilated troughs. Discussion with a number of cable engineers has determined that the common practice is to treat such installations as having a rating of 90% of that of the IEC free air rating, with no additional allowance made for a possible increase in trough air temperatures. Despite undertaking a comprehensive search of the technical literature it has not been possible to find any validation of this method. As a result, a 3D CFD model has been developed and the possibility of deriving a modified method for use with analytical calculations has been considered.

The situation is similar for the case of forced ventilated troughs, where no clear international standard method exists for calculating the ratings. One method which has been previously used is that described in [20] which effectively assumes that all of the heat from the cables must be removed from the trough via the outlet air. The calculation is straightforward, with the total volumetric airflow requirement, Q, derived by

$$Q = \frac{\sum \left(P_i^{'} + P_d^{'}\right) l}{c_p \Delta \vartheta_{ku}} \tag{7.5}$$

where $P_i^{'}$ represents the current dependent losses, $P_d^{'}$ the dielectric losses, l the length of the trough (m), c_p the specific heat capacity of air ($Jm^{-3}K^{-1}$) and ϑ_{ku} is defined by

$$\vartheta_{ku} \leq \vartheta_{Lr} - \vartheta_U - (\vartheta_{Lr} - 30)\left(\frac{I_b}{I_r}\right)^2 \tag{7.6}$$

where ϑ_{Lr} represents the operating temperature of the hottest cable, ϑ_U represents the ambient temperature, I_b represents the operating current (A) and I_r represents the rated current. This method is inherently conservative as no heat transfer through the wall is considered and the potential for variation in the ac resistance with temperature cannot be easily modelled. As a result, it will prove a useful benchmark case for consideration against the CFD models developed in this Chapter.

7.1.3 Trough Geometry Considered

As with all rating calculations within this study, a common cable design has been used (Table 6.4), the only difference here is a change in the sheath loss factor due to the change in the cable spacing, with a value of 0.0725 for the centre cable and 0.0191 for the outer cables. The cables are installed 15cm above the trough base (measured from

the centre of the conductor) with a core-core spacing of 25cm. The trough is constructed of concrete with a thermal conductivity of $1 W.m^{-1}K^{-1}$ with the wall thickness being 8cm. The lid is 5cm thick and is considered to be installed flush to the ground surface, as outlined in Figure 7.1.

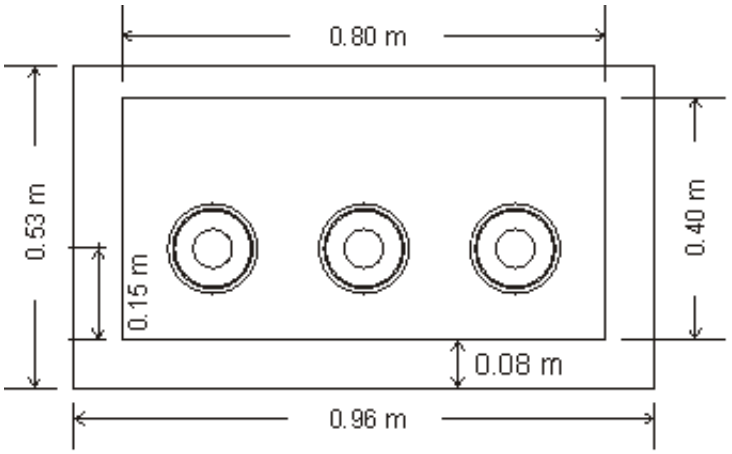

FIGURE 7.1: Cross sectional geometry of cable trough

7.2 Unventilated Troughing

The most common type of cable trough installation in the UK is the traditional unventilated installation with sealed lids. Although this type of installation does not offer the highest rating and is less likely to be suited to high temperature cables, it is the installation considered by IEC 60287 and several other research papers including [120]. As a result it is to be used as a benchmark for the performance of the ventilated trough options and a useful comparator to standard methods.

7.2.1 CFD Model Development

Of the three trough installations considered in this Chapter, the unventilated case is the simplest to model, as, given that the trough has constant dimensions and burial depth along its length and that there is no longitudinal flow of air, a 2D slice model is appropriate. Further simplification is possible as the physics of the problem are symmetric about a plane through the centre phase cable, meaning that only half of the problem needs to be modelled, as shown by the mesh in Figure 7.2. The image shown represents the main detail, with the mesh coarsening as it moves towards the external boundaries at a distance of 10m from the centre line and 7m down from the ground surface. The level of mesh refinement is increased at the cable surface by applying a thin boundary layer mesh. This increased mesh resolution provides a more accurate

solution for the turbulent boundary layer above the cable which is critical for the accurate determination of the convective heat transfer coefficient.

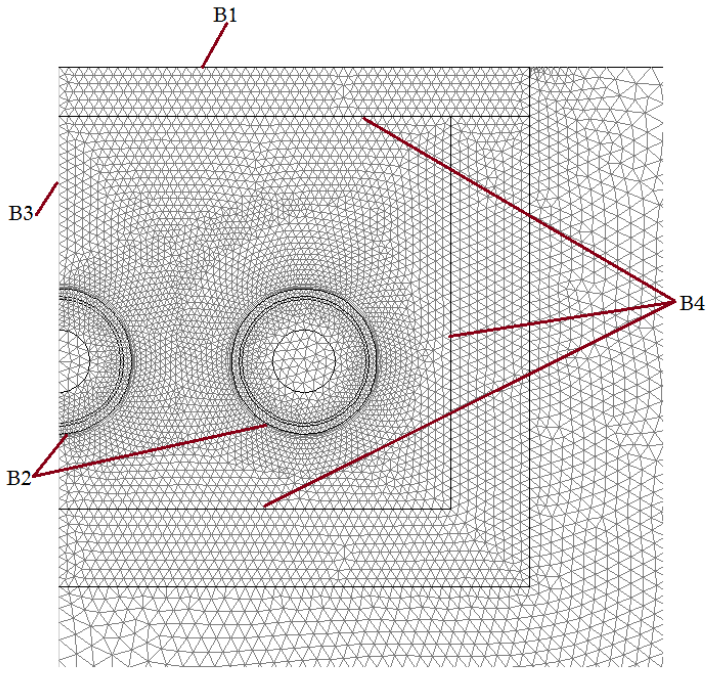

FIGURE 7.2: 2D triangular mesh for Unventilated Trough Model

Many of the boundary conditions applied are common to the previous finite element based models, however, there are important differences as additional boundary conditions are required at the interfaces between the fluid (air) and solid domains. The appropriate conditions are summarised in Table 7.1. Where a boundary condition is stated as coupled convective, the heat transfer coefficient on the surface for each cell is evaluated using the local shear stress solution. This then determines the rate at which the heat will enter the air from the cable surface, hence impacting back on the buoyant convection.

Boundary	Thermal Condition	Fluid Condition
Ground Surface (B1)	Still air convection	n/a
Cable Surface (B2)	Coupled Convective	Smooth Wall, No slip
Centre line (B3)	Symmetry	Symmetry
Trough inner walls (B4)	Coupled Convective	Smooth Wall, No slip
Remote soil (7m depth)	Temperature = 12°C	n/a
Remote soil (side)	Insulation	n/a

TABLE 7.1: 2D slice model boundary conditions

The fluid velocities in this model are solved using the $k-\epsilon$ turbulence model. Although the flow is not turbulent throughout, initial tests with a laminar flow model failed to converge due to the presence of faster moving air currents above the cables and close to

the walls. Tests were also carried out with a turbulence model designed for transition flow ($k - kl - \omega$) however the change in the solution was considered negligible against the increased solution time.

7.2.2 Continuous Rating Results

Solutions for the continuous ratings in the covered trough environment have been found from three models, namely the 2D CFD model, the empirical IEC 60287 and the analytical method published by Anders. The first set of results obtained is for a baseline calculation, thus moisture migration is neglected and the soil thermal resistivity is assumed constant at $1.872 K m W^{-1}$. Examining the results from all three models in Table 7.2, a number of trends are immediately apparent. Firstly the IEC rating appears to be the most conservative in all cases, with the Anders model yielding ratings 2.6% higher on average. This trend is in agreement with the data reported in [120]. The differences between the Anders model and the CFD models are of a similar order, with the magnitude varying according to the air temperature. In the hottest season the CFD model gives a rating 3.3% higher, while the two models agree to within 1.8% in the winter season.

Rating Season	Rating from IEC 60287 (A)	Rating from Anders [120] (A)	Rating from 2D CFD model
Summer	1886	1934	1999
Spring/Autumn	2053	2106	2159
Winter	2208	2265	2305

TABLE 7.2: Continuous Ratings for Covered Trough at 90°C

Two main factors account for the CFD model giving a higher rating. The first reason for this lies in the difference between the air temperature (considered by both analytical models as the global ambient) and the remote soil temperature. Within the CFD model it is possible to model both conditions explicitly. As a result, more heat is dissipated to the local ground below the trough during the hotter seasons in the CFD model than is the case with the analytical models. Secondly, the use of a full temperature dependent ac resistance value means that the outer phases do not attain the 90°C temperature limit, instead reaching around 88°C, thus slightly reducing the total heat generation in the model. Figure 7.3 illustrates the trough temperature profile generated by the CFD model for the winter season. Clear evidence of the air circulation within the trough can be seen in Figure 7.4, which plots colour-scaled velocity vectors. A region of faster moving air can be seen around the top half of the cable, caused by the density variation between this warm air and the cooler air elsewhere in the trough. As this air rises it is cooled on contact with the trough surface and eventually sinks back below the cables via the side wall.

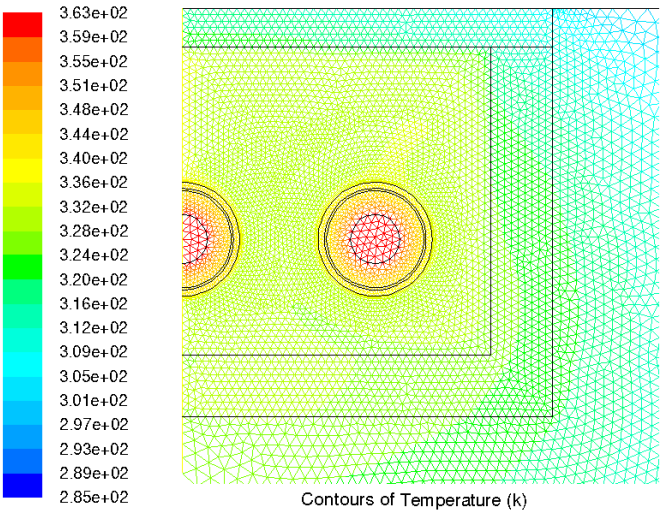

FIGURE 7.3: Trough Temperature Profile

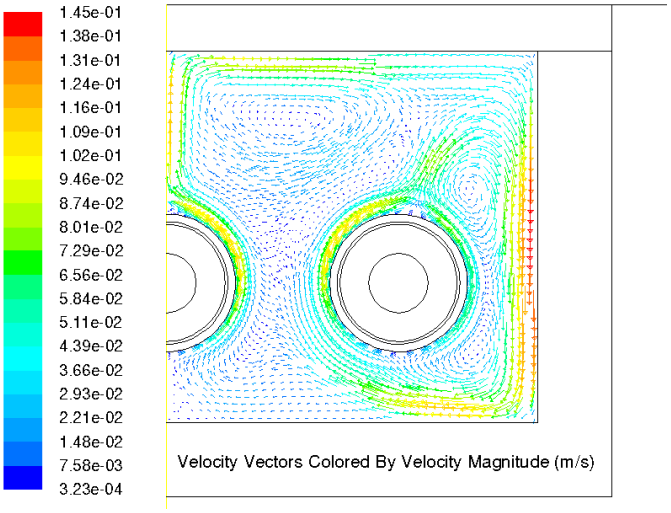

FIGURE 7.4: Velocity Vector plot for Covered Trough

Table 7.3 displays a full set of ratings from the three different models considered across both the XLPE and HT cables. In these results the representation of the backfill in the 2D CFD model is amended to give the two zone approximation for moisture migration at 3%, as discussed in Section 4.2.2. The rating reduction seen for the CFD calculations is small, at less than 100A, demonstrating that the rating for air filled troughs is less sensitive to the ground thermal resisitivity than is the case for buried cables. This explains the acceptable performance of the IEC 60287 model across the conductor temperature range considered. However, even with the 2 zone modelling of the soil around the trough, the Anders model still matches the CFD calculations to within 50A.

The performance of the two analytical models is perhaps surprising given that they both assume an isothermal ground surface, including the trough lid section. Analysis of the results for the summer season at 90°C demonstrates that the peak temperature on the

trough lid could reach 49.4°C, considerably higher than the 30°C air temperature. Were all other conditions to be the same, this would make the analytical models considerably more optimistic than the CFD model. This is not the case due partly to the enhanced model of heat transfer within the trough in the CFD model, and partly due to the greater heat transfer through the trough and into the ground in the CFD model, as a result of the remote temperature assumptions discussed previously.

Rating Season	Conductor Temperature (°C)	Rating from IEC 60287 (A)	Rating from Anders [120] (A)	Rating from 2D CFD model
Summer	90	1886	1954	1904
Spring/Autumn	90	2053	2106	2057
Winter	90	2208	2265	2222
Summer	120	2294	2355	2318
Spring/Autumn	120	2428	2492	2440
Winter	120	2529	2623	2573
Summer	150	2588	2682	2647
Spring/Autumn	150	2703	2799	2756
Winter	150	2815	2912	2868

TABLE 7.3: Continuous Ratings for Covered Trough with 2 Zone Soil Representation

In the case of the covered trough the continuous rating increase from the use of the high temperature cables is significant, with a maximum increase of 39% for the switch from 90°C to 150°C in the summer season, higher than the 34% increase seen for buried cables. One significant issue which would need to be addressed is the potential for very high temperatures exceeding 50°C on the trough lids during the summer season. While this may be permissible in a substation where access can be strictly controlled, it would clearly be less suitable for any public area.

7.2.3 6hr Rating Results

Having assessed the continuous rating performance of the unventilated trough, the model can easily be extended to consider the applicable emergency ratings. Within the CFD models, this can easily be calculated by solving the steady state model for the given preload (in this case 60% of the continuous current rating) and setting the result as the initial condition of a transient solution. A transient solver is then used to calculate the cable temperature rise over the course of the 6 hour period, with the maximum time step in this case set to 18 minutes. The results of this analysis are shown in Table 7.4, with all data being for the CFD model including the 2 zone backfill representation.

Comparing the results in Table 7.4 to those shown in Figure 4.12 it can be seen that the 6hr ratings are very similar to those for the buried cable at 3% moisture content. The increase in the rating at higher conductor temperatures follows the same trends as were

Rating Season	Rating (90°C)	Rating (120°C)	Rating (150°C)
Summer	2815	3340	3804
Spring/Autumn	2940	3526	3961
Winter	3243	3740	4152

TABLE 7.4: 6hr Ratings for Covered Trough Model

observed for the continuous rating, with the maximum increase in rating being 35% for the summer season using the 150°C HT cable.

7.3 Partially Ventilated Troughs

The work presented here on the traditional covered trough design has demonstrated that the CFD models compare well to existing analytical techniques. This provides confidence that the technique will be suitable for the rating of partially ventilated troughs, for which no equivalent analytical solution is available.

7.3.1 CFD Model Development

Unlike the covered trough model, it is not possible to treat the partially ventilated trough as a 2D model due to the induced longitudinal air flows around the inlet grilles. As a result, a 4m long 3D model is constructed and use is made of the periodic symmetry along the route between inlets. The outline geometry is shown in Figure 7.5.

The majority of boundary conditions are specified as per the covered trough model, however, two additional groups are required to model the additional flow boundaries. Boundaries labeled as B5 are modelled as pressure inlet boundaries, with the external pressure set to 1 atmosphere. This allows the warm air at a lower relative density to rise out of the trough and be replaced by cooler air at ambient temperature. The final boundary group contains those labelled B6, which includes all of the end boundaries on both solid and fluid domains. A periodic condition is set such that the values of the independent variables (such as temperature and velocity) are constrained to match, effectively ensuring symmetry between the two ends of the model.

7.3.2 Continuous Rating Results

Results are obtained for the three rating seasons using the same parameters as for the covered trough model, with the first set of results displayed in Table 7.5 being for the XLPE cable and a uniform ground thermal resistivity of $1.872 K m W^{-1}$. A comparison to the standard IEC 60287 free air (solar shielded) rating is also given. Analysis of

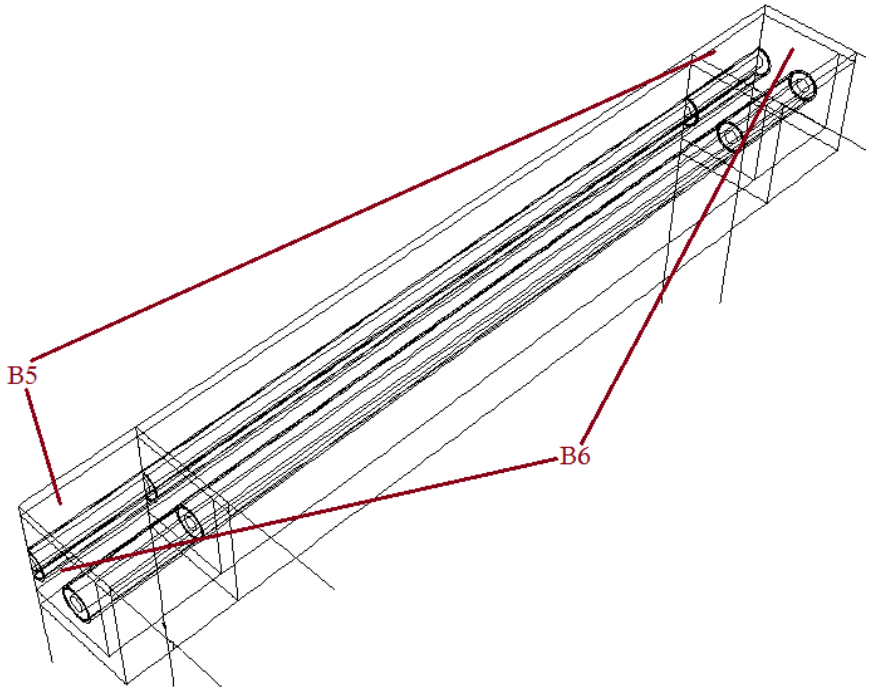

FIGURE 7.5: Geometry of partially ventilated trough model

the data clearly demonstrates that the additional ventilation provided by the grilles has significantly up-rated the cables by up to 31% over the traditional covered design. However, as would be expected the rating of the cable in free air (solar shielded) is higher.

Rating Season	Rating in Free Air IEC 60287	Rating from 3D CFD model	CFD Model Covered Trough Rating
Summer	2686A	2564A	1999A
Spring/Autumn	2926A	2790A	2159A
Winter	3150A	3020A	2305A

TABLE 7.5: Continuous rating for standard cable in partially ventilated trough

One of the main drivers for the increased rating is the reduction in air temperature in the trough. Table 7.6 summarises the volume averaged air temperature data from both the covered and partially ventilated trough models. It is clear that the air temperatures have been reduced significantly, especially in the region just below the grille where the air circulation is most effective.

Rating Season	PV model, air below inlet	PV model, air below lid	Covered Trough Air
Summer	36.7°C	42.7°C	61.5°C
Spring/Autumn	27.6°C	34.1°C	57.0°C
Winter	17.1°C	24.7°C	52.5°C

TABLE 7.6: Comparison of air temperatures

Figure 7.6 shows a slice plot of the velocity magnitudes at different axial locations along the model. As would be expected the velocity is at its highest near to the inlet grilles.

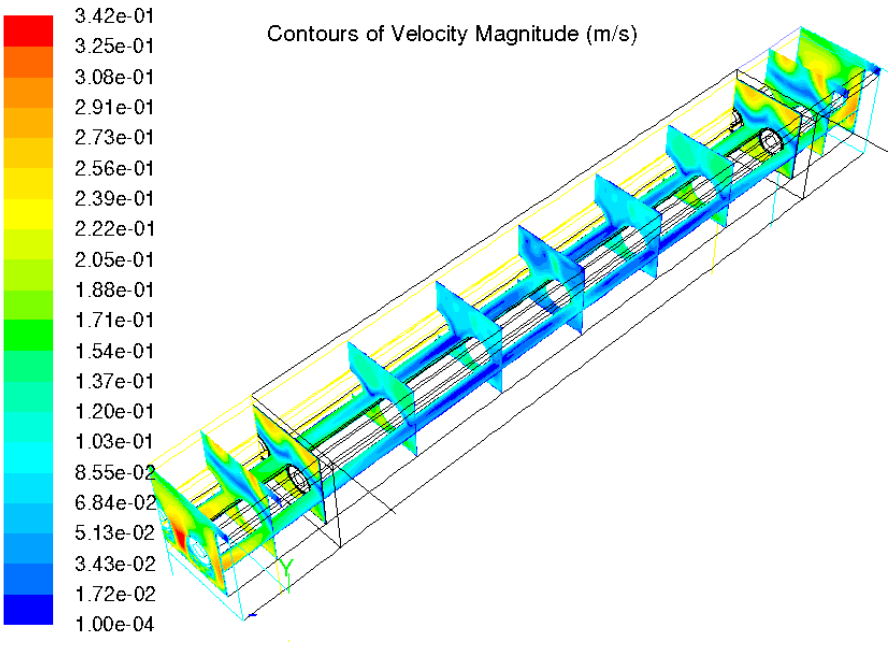

FIGURE 7.6: Slice plot of velocity in the partially ventilated trough (summer season, XLPE cable)

The impact of the reduced air circulation under the lid can be seen in Figure 7.7 which plots the conductor temperatures along the model length. For the example shown of the spring season, the conductor temperature beneath the inlet grille is 4.3°C lower than the model centre (equidistant from the two inlets). This effect illustrates the requirement to consider this problem in a full 3D model.

Having examined the trends for the standard XLPE cable, the technique has been applied to the high temperature cable designs, with the results generated being detailed in Table 7.7. The same trends are evident across the full temperature range, with the partially ventilated trough rating being lower than the free air rating by 6-8%. The key significance in this result is that a 'common rule of thumb' among cable engineers has been to rate the partially ventilated trough at 90% of the IEC 60287 free air rating. The results generated here show that this approximation would be only slightly conservative for all combinations of season and conductor temperature tested.

By removing one in four of the trough lids the induced naturally convective air currents increase the continuous rating by up to 41%. For the 150°C cable the ratings are becoming close to the conventional busbar rating limit of 4kA, meaning that it may now be possible to match a conventional overhead line rating with a high temperature cable. This could prove particularly valuable in cable tunnels, where the partially ventilated trough installation provides the link between the sealing end and the cable tunnel itself.

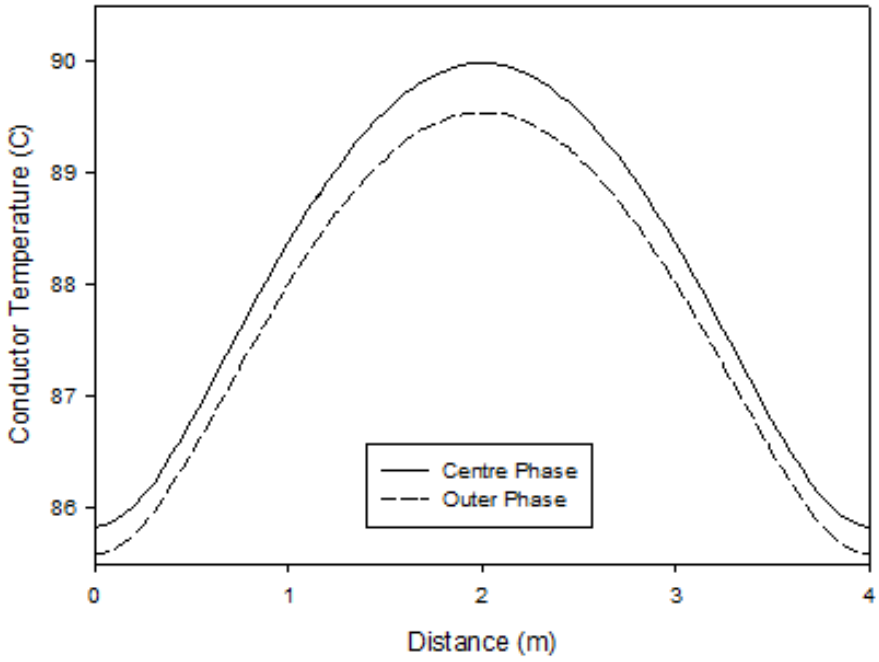

FIGURE 7.7: Variation of conductor temperature along trough (XLPE cable, spring season)

Rating Season	Conductor Temperature (°C)	IEC 60287 Free Air(A)	Partially Ventilated CFD Model (A)	Rating from 2D CFD model
Summer	90	2684	2549	1904
Spring/Autumn	90	2924	2780	2057
Winter	90	3148	2987	2222
Summer	120	3271	3112	2318
Spring/Autumn	120	3465	3282	2440
Winter	120	3650	3476	2573
Summer	150	3731	3548	2647
Spring/Autumn	150	3897	3706	2756
Winter	150	4057	3837	2868

TABLE 7.7: Continuous Ratings for Covered Trough with 2 Zone Soil Representation

7.3.3 6hr Rating Results

Having assessed the continuous rating performance of the partially ventilated trough, the model can easily be extended to consider the applicable emergency ratings. The solution procedure is identical to that outlined for the covered trough, with the steady state solution at 60% of the continuous rating used as the input to the transient solver. Table 7.8 illustrates the results for the conventional XLPE cable design at 90°C with a uniform backfill resistivity.

As would be expected, the 6 hr ratings from the partially ventilated trough are higher than the traditional covered trough, however, the increase is much smaller at around

Rating Season	6hr Rating (Covered)	6hr Rating (PV)	T_{ci} Covered	T_{ci} PV
Summer	2793A	2983A	52.24°C	52.83°C
Spring/Autumn	3030A	3236A	45.56°C	46.25°C
Winter	3248A	3484A	38.95°C	39.03°C

TABLE 7.8: 6hr Ratings for Conventional XLPE cable

7% than was found for the continuous rating (where the rating increase was up to 31%). This occurs as the main influencing factor on a 6hr rating of a 400kV cable is the conductor temperature at the start of the transient. The data in Table 7.8 shows that the initial temperatures were similar in both troughs (although the loading is higher in the partially ventilated case). As the cable time constant is similar in duration to the transient length, the thermal environment around the cable has much less impact on the overall ratings.

Table 7.9 summarises the 6hr rating data for the high temperature cables, including the two zone representation of the backfill. Comparison with the figures in Table 7.8 reveals that the sensitivity to the change in the backfill representation is very low, leading to a rating decrease of only 13A in the summer season at 90°C. This is due to the majority of the heat leaving the trough in the form of warm air rising out of the inlet grilles. The ratings seen at high temperatures are again similar to those seen for buried cables in Section 4.4.1, although the absolute magnitude of the preload is higher.

Rating Season	Rating (90°C)	Rating (120°C)	Rating (150°C)
Summer	2970A	3602A	4090A
Spring/Autumn	3229A	3816A	4222A
Winter	3528A	3988A	4490A

TABLE 7.9: 6hr Ratings for Partially Ventilated Trough Model

7.4 Forced-cooled Troughs

The two trough installations considered so far have both relied upon naturally induced convective heat transfer to cool the cables within them. In some cases where very high continuous ratings are required, it may be preferable to install forced ventilation to guarantee a minimum rate of air flow through the troughs. This may also be necessary where the rating from a conventional covered trough would not be sufficient, but the location does not permit grilles to be installed to allow partial ventilation. The main principles of the CFD modelling technique are the same, however, some changes are necessary as described in Section 7.4.1.

7.4.1 CFD Model Development

From a survey of the route records for a number of substations operated by National Grid, the longest typical trough length is 50m from a sealing end to the top of a cable tunnel, hence 50m is the length adopted here. The cross-sectional layout of the trough is the same as has been used for all other models within this Chapter, but in order to determine the air temperature rise it is necessary to model the full 50m of the trough. The air is assumed to enter the trough vertically downwards from an inlet of 0.8m in width by 0.5m in length, with a bulk linear flow through the trough of $3ms^{-1}$. An outlet boundary of the same size is specified at the trough lids at the end of the 50m run. All other boundary conditions on the cable and trough surfaces are as per the previous naturally ventilated models. In order to accurately characterise the airflow as it enters the trough, the mesh density is increased by a factor of 2.5 in the regions around the inlets and outlets. Figure 7.8 illustrates the developed turbulent air velocity profile through the troughs. The velocity profile here differs to that shown in Chapter 6 as the air enters the trough from above, rather than through the main flow cross section.

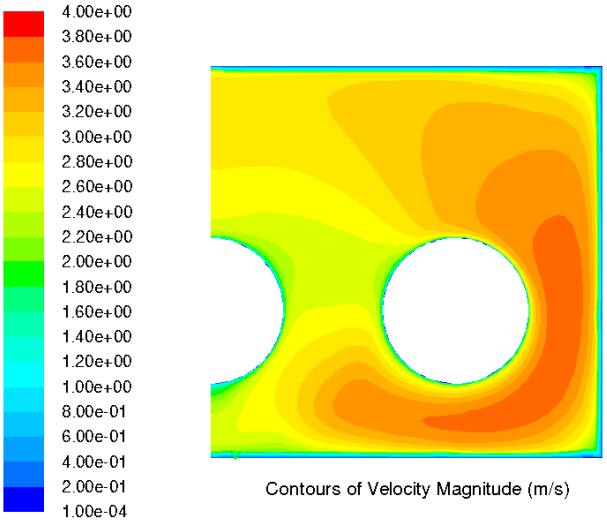

FIGURE 7.8: Velocity Profile through Forced Ventilated Trough

7.4.2 Continuous Rating Results

Results are obtained for the three rating seasons using the same parameters as for the covered trough model, with the results displayed in Table 7.10 being for the XLPE cable with the 2 zone backfill model. Tests with the constant backfill resistivity found only an 8A increase in rating due to the relative insensitivity of the conductor temperature to the external environment. This is because heat transfer by convection into the air is by far the dominant mode, with the high air velocity meaning that this heat is removed from the trough at the outlet rather than dissipating through the trough walls, as was the case with the covered trough.

Rating Season	Rating of XLPE Cable (A)	Rating of 120°C HT Cable (A)	Rating of 150°C HT Cable (A)
Summer	2775 (2549)	3316 (3112)	3738 (3548)
Spring	2994 (2780)	3493 (3282)	3888 (3706)
Winter	3207 (2987)	3667 (3476)	4040 (3837)

Table 7.10: Forced-cooled Trough Continuous Ratings

Examining the data in Table 7.10, the percentage increase in continuous rating from the deployment of the 150°C cables is a maximum of 34% in the summer rating season, reducing to 26% in the winter season. The values shown in brackets are the continuous ratings for the partially ventilated cable trough with the same combination of cable type and season. It is immediately clear that the introduction of forced cooling has not greatly increased the continuous rating when compared to the partially ventilated design, with the largest gain being in the summer season at 8.8%. Analysis shows that the air temperature is again a key factor.

Figure 7.9 shows the conductor temperature variation for the 90°C cable in the spring season between the inlet and the outlet. The conductor temperature rise is seen to be 17°C for the centre phase, which compares to a rise in air temperature of 14.3°C between the inlet and outlet. Using the analytical temperature rise calculation of equation 7.5 obtains a value of 16.4°C for the air temperature rise. Further analysis of the results from the numerical model show that the area weighted average of heat flux leaving the lid surface is $30.1 W m^{-2}$. When added to the heat leaving the trough through the external walls this explains why the analytical method gives such a conservative result. Were the trough run to be longer than 50m, it would actually be more beneficial to use the partially ventilated design if practicable. This eliminates the risk to the cable circuit from a cooling outage, as were the forced ventilation to fail, the continuous rating of the forced ventilated system would reduce immediately back to that of the conventional covered design.

7.4.3 6hr Rating Results

The solution methodology for the 6hr ratings remains the same as for the partially ventilated troughs, however, no results are calculated for the case where the ground thermal resistivity is uniform due to the very small differences between the assumptions. Data obtained are presented in Table 7.11, with the results given in brackets being those for the partially ventilated trough.

The trends observed in the 6hr rating data are very similar to those seen for the continuous rating, with the ratings for the forced ventilated troughs being at most 6.6% higher, although in the majority of cases the improvement in rating was of a smaller magnitude.

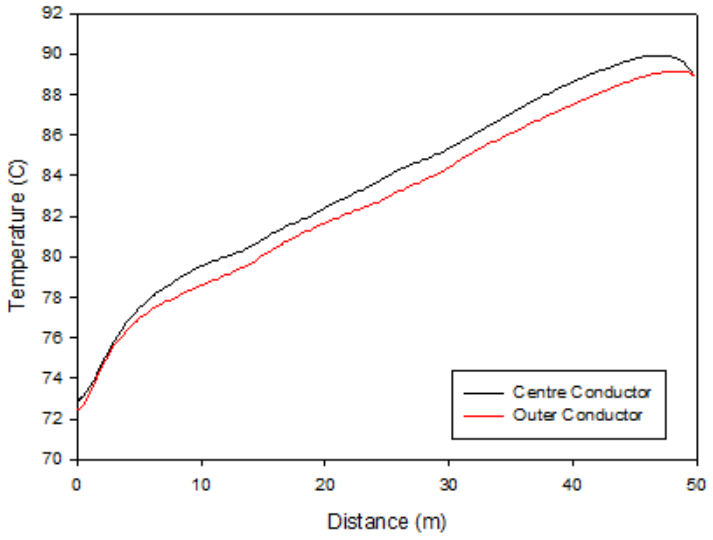

FIGURE 7.9: Conductor Temperature Variation for 90°C conductor in Spring season

Rating Season	Rating of XLPE Cable (A)	Rating of 120°C HT Cable (A)	Rating of 150°C HT Cable (A)
Summer	3095 (2970)	3723 (3602)	4223 (4090)
Spring	3443 (3229)	3933 (3816)	4400 (4222)
Winter	3596 (3528)	4136 (3988)	4578 (4490)

TABLE 7.11: Forced-cooled Trough 6hr Ratings (Partially ventilated data in brackets)

7.5 Implications for HT Cables in Troughs

The results presented in this Chapter demonstrate that installing high temperature cables in troughs would prove a viable option. The continuous ratings obtained for the trough with HT cables are almost 40% higher for each of the three designs, which fits in with the trends seen for buried cable installations. One particularly notable feature of the results is that the rating with the 150°C HT cable in the traditional covered trough design is only 128A lower than that for the conventional XLPE cable in the forced ventilated trough study. In more remote substations where short cable links are installed, the high temperature cable could remove the need for forced ventilation and the associated electrical infrastructure. Were the price of the cable to be similar to existing designs, this technology could deliver a significant cost saving for the utility.

Examining the transient performance of the 150°C HT cable over the 6hr emergency rating period, the permissible load flows are approaching 4000A which would allow the cable to match the post fault continuous rating of the majority of UK overhead lines. Achieving this aim through the use of HT cable would remove the need for installing two cables per phase on many transmission circuits, an extremely valuable option for environments where the additional footprint of the second cable group is not an option.

7.6 Summary

This Chapter has presented a new approach to calculating the ratings of cables in air-filled troughs through the use computational fluid dynamics. The new method has been benchmarked against two existing analytical calculations for the traditional covered trough design and has been demonstrated to give more accurate results by removing some of the conservative assumptions demanded by the analytical approaches. By moving from 2D modelling into 3D, it has been possible for the first time to directly rate partially ventilated cable troughs, with the rating results obtained being considerably higher than the traditional covered troughs but only up to 10% lower than the IEC free air rating. Finally the 3D modelling techniques have been applied to the case of forced ventilated troughs, which has further illustrated the potential application of the partially ventilated trough layout owing to the similarity of the continuous ratings obtained. The methods developed suit high conductor temperature cables without further need for modification.

Chapter 8

Conclusions

This thesis has presented a series of new cable circuit rating techniques which are applicable to future cable designs capable of operating at conductor temperatures of up to 150°C. Although existing methods were fully considered to determine their potential applicability, the majority are analytical methods whose accuracy is constrained by the assumptions necessary to make their solution viable. This has led to the adoption of two numerical techniques; finite element analysis and computational fluid dynamics, which have been demonstrated to be both applicable and reasonably practical for use. All methods have been applied to an example high temperature cable circuit based on an existing XLPE cable design, with both continuous and emergency ratings calculated to assess the potential operational benefits that such a technology might offer to a Transmission System Operator. This Chapter summarises the contribution made by this work, draws out the key results, and discusses the implications for future cable technologies.

8.1 Research Contribution

The work presented in this thesis forms a significant contribution to the literature in the field of cable system engineering. Throughout the thesis a comprehensive analysis of the rating of high temperature cables has been conducted, however, each of the methods presented is also applicable to more conventional cable system designs. The dynamic backfill model presented in Chapters 3 and 4 has illustrated that the partial drying methodology within IEC 60287 does not suit all backfills as the moisture migration behaviour is a function of the initial moisture content, not just the temperature. This result demonstrates that care should be taken in applying the partial drying algorithm within IEC 60287 as there is a danger of over-rating the cable circuit under certain environmental conditions. Through using the Philip and de Vries method for modelling moisture migration this thesis has proved that deploying HT cables can offer significant increases in both the continuous and emergency ratings for buried cables.

A further contribution to the technical state of the art has been made by the development of finite element models for buried cable joints, particularly in regard to forced-cooled joint bays. This work has demonstrated that National Grid's existing thermal allowance of 15°C is not always sufficient for high coolant flow rates in buried systems or for high air velocities in cable tunnels. The work presented here has been applied to a number of up-rating schemes of operational transmission cable tunnels and has proved invaluable in identifying the rating impact of joint bays in these cases. As a result, circuit rating practices have been updated within National Grid to ensure that joints are fully considered in the circuit design process. Discussions of the model development processes and the application of the method to conventional cable circuits were published in [102].

The revised cable tunnel rating methodology presented in Chapter 6 has also been deployed in both up-rating and design studies on the transmission network and has recently been published in [119]. This work has proved particularly timely given the need to conduct rating studies for new cable tunnels in London where 400kV and 132kV cables are to be installed in the same tunnel environment. At the time of writing the method is being considered as a potential update to Electra 143 by Cigré Committee B1, following a recommendation by the Cigré Task Force B1-35 to convene a working group on cable ratings.

Despite the majority of cable circuits installed in troughs being short in length, they form critical links in many transmission circuits and this thesis has made a number of contributions to rating best practice in this area. The development of CFD models for traditional unventilated troughs has demonstrated that the relevant IEC 60287 method proves conservative and that the analytical method proposed by Anders offers a better approach due to its consideration of the external ground thermal resistance. The method presented for rating partially ventilated cable troughs is the first bespoke method for this application and is currently being applied to trough installations on a transmission cable replacement project. Taken together, this thesis and its associated work has been summarised in 8 peer reviewed papers. A full list of conference and journal publications, including those awaiting editorial decisions, may be found in Appendix A.

8.2 Benefits of HT Cable Technologies

Throughout this thesis, circuit rating methods have been developed for the most common deployment cases from the point of view of a transmission system operator. While there are evidently a number of benefits to using this technology, they do not necessarily represent a revolution in cable technology. As would be expected, the continuous rating of the HT cables was higher than the XLPE benchmark, however, the magnitude of the increase was limited to around 30% for buried systems and 40% for air filled troughs. For the candidate cable tunnel there was no increase in the continuous rating as the

thermal limit was actually the air outlet temperature and not the cable. However, for a shorter tunnel, with less cable circuits, where the air temperature limit was not reached there would be scope for enhanced continuous ratings using HT circuits.

While this is a positive development, three mitigating conditions exist which may restrict the overall benefit. The first consideration is that of energy losses from the cable system. As the ac resistance of the conductor increases with temperature, the overall efficiency of transmission is reduced. In the UK at present there is no financial penalty for system losses, however utilities in other parts of Europe have to account for such losses financially. Where the losses represent a cost to the utility the benefit of a higher continuous rating per physical cable might be diminished compared to the option of installing two conventional cables per phase with a significant reduction in overall losses. The second consideration is that the continuous rating of the buried circuits at 150°C was significantly lower than that of a water-cooled XLPE system, meaning that conventional technologies may still give higher ratings overall.

The third key implication for the continuous rating potential is the possible thermal limit posed by cable joints. In reality the maximum delivery length of 400kV cable is unlikely to exceed approximately 1km owing to the difficulty of transporting such large drums of cable. Thus, in most real world cable circuits (excepting short links in substations) the rating of the cable joints must be considered. The results presented in Chapter 5 have demonstrated that for uncooled buried systems the rating of the joint is not an issue where core-core spacing can be increased in the joint bay. However, where forced water cooling is installed it is vastly more effective on the cables than on the joints, mainly due to the higher radial thermal resistance of the joint. This will act to reduce the overall rating of a water-cooled cable circuit, however, it will still possess a higher continuous rating than the equivalent uncooled circuit.

Across all of the installation options, with the exception of the tunnel, the HT cable proved to perform well under emergency rating conditions. Were such a cable system to be produced, it is under these conditions that the true benefits would be realised. Assuming that the HT cable is operated to a maximum continuous temperature of 90°C as per an XLPE cable, the ability to further increase the conductor temperature means that very high emergency ratings are available even from substantial preloads. For a transmission system operator this can be key in ensuring that the cable 6hr rating can match the post-fault continuous rating of the overhead line, potentially removing the requirement to install 2 cables per phase on some circuits. This was particularly true for the cable trough deployment option, where the emergency ratings from the partially ventilated cable trough option at 150°C were easily sufficient to match the typical circuit breaker rating of 4kA. This is especially significant as it removes the need for forced cooling and the associated operational costs.

In summary, although HT cable does not represent a huge leap forward in performance

over existing XLPE systems it does offer significant benefits in a number of application areas. The largest gains are available when the cable is installed in air filled troughs as both the continuous and emergency ratings are up to 40% higher than for an XLPE system. That said, the emergency ratings of all the deployment scenarios increased where HT cable circuits were used, providing valuable additional flexibility for transmission system operators in times of high demand.

8.3 Recommendations for Further Work

Despite the contribution made by this thesis, a number of areas have been identified which merit further work. The topic representing the greatest challenge relates to the development of the dynamic backfill model presented in Chapters 3 and 4. The work presented here only relates to one candidate backfill, although it is that which exhibits the most obvious moisture migration due to the low levels of energy required to extract moisture from the soil pores. However, in order to comprehensively assess the applicability of the IEC 60287 partial drying method, it will be necessary to conduct a similar analysis on numerous soil types. This should include those such as clay, which will exhibit very different moisture migration patterns due to the different shape of their soil water characteristic curve. Carrying out this work will allow the identification of whether the initial moisture content affects the rate of moisture migration across all soils, from which it may be possible to make recommendations on the applicability of the present IEC 60287 method, which considers only the soil temperature.

The growth of the number of cable tunnels on the UK transmission network has reinforced the importance of being able to accurately rate such cable assets. Two key issues have been identified as worthy of further research effort in this field, the first of which is experimental validation. Although the revised method for cable tunnels has been benchmarked against other methods, there is still a case for an attempt at quantifying how well the method performs against real experimental data. In particular, this would address the issues identified around the convective heat transfer coefficients. However this is not a trivial task - as the overwhelming majority of cable tunnels operate with less than 50% of rated current, it would be necessary to find a heavily loaded tunnel which could be instrumented for a period of several years in order to gather sufficient data. The second component of the work on tunnels is a detailed study of cable tunnel ventilation strategy. High ventilation flowrates are financially costly to achieve and operation at 100% duty cycle is rarely necessary. Having established a method which permits thermal modelling of cables on numerous different load cycles, it is feasible to apply this to ventilation control methodology to identify the best compromise between minimising operational costs and maximising system availability. One transmission system operator has identified this as a top research priority and as such work is anticipated to commence in mid 2011.

Although the CFD modelling techniques identified for partially and forced ventilated troughs represent the most accurate technique available to rate these installations, they do require both specialist knowledge and additional time to apply. For many cable engineers this will not be practical and a benchmarked analytical or simple numerical method would be preferred. The most likely approach to take here would be to build on the thermal analogue model used for cable tunnels, as the conductor temperature variation seen along the trough length does not lend itself well to an analytical model.

The topics discussed thus far all relate to the model development aspect of this project, however, the study conducted in this thesis of high operating temperature cables also brings about considerations as to the best way in which to design cable systems with higher ratings. Although the prospect of higher operating temperature clearly merits consideration, advances in polymer science may allow gains of a similar or even larger scale from other improvements in material properties. Examples of such improvements would be to reduce the thickness of the dielectric through improving the breakdown strength or improving the thermal conductivity of the dielectric material itself in order to aid the flow of heat away from the conductor. It is recommended that the techniques presented here are used to examine the sensitivity of the cable circuit rating to such improvements in material properties (and their resulting impacts on cable design). This would help to provide clearer direction as to which research breakthroughs offer the most utilisable gains for transmission network operators.

Appendices

Appendix A

List of Published Papers

A.1 Refereed Conference Papers

The following papers have been presented at International Conferences and have been subject to peer review. Papers are listed in chronological order.

Pilgrim, J. A., Swaffield, D. J., Lewin, P. L. and Payne, D. (2008) "An investigation of thermal ratings for high voltage cable joints through the use of 2D and 3D finite element analysis." IEEE International Symposium on Electrical Insulation, 8-11 June 2008, Vancouver, Canada. pp 543-546.

Pilgrim, J. A., Swaffield, D. J., Lewin, P. L. and Payne, D. (2009) "Use of finite element analysis to obtain thermal ratings for high voltage cable joint bays." IEEE Electrical Insulation Conference, 31 May - 3 June 2009, Montreal, Canada. pp 224-227.

Pilgrim, J. A., Swaffield, D. J., Lewin, P. L., Larsen, S. T., Waite, F. and Payne, D. (2010) "Thermal rating implications of the co-location of HV cable circuits in tunnels." IEEE International Symposium on Electrical Insulation, 6 - 9 June 2010, San Diego, California, USA. CD-ROM

The following 3 papers have been accepted for presentation at forthcoming international conferences:

Pilgrim, J. A., Swaffield, D. J., Lewin. P. L. and Payne. D. (2011) "Rating methods for cables installed in unventilated and partially ventilated surface troughs." IEEE Electrical Insulation Conference, 5 - 8 June 2011, Annapolis, Maryland, USA.

Pilgrim, J. A., Swaffield, D. J., Lewin, P. L., Swingler, S. G., Waite, F. and Payne, D. (2011) "Impact of moisture migration on the current rating of high operating temperature cables." Jicable 8th International Conference on Insulated Power Cables, 19 - 23 June 2011, Versailles, France.

Pilgrim, J. A., Swaffield, D. J., Lewin, P. L., Swingler, S. G., Waite, F. and Payne, D. (2011) "Investigation into the benefits of installing high operating temperature cables in tunnels." Jicable 8th International Conference on Insulated Power Cables, 19 - 23 June 2011, Versailles, France.

A.2 Peer Reviewed Journal Papers

The following papers have been published in peer reviewed academic journals.

Pilgrim, J. A., Swaffield, D. J., Lewin. P. L., Larsen, S. T. and Payne. D. (2009) "Assessment of the impact of joint bays on the ampacity of high voltage cable circuits." IEEE Transactions on Power Delivery, vol. 24, no. 3, pp1029-1036.

Pilgrim, J. A., Swaffield, D. J., Lewin. P. L., Larsen, S. T., Waite, F. and Payne. D. (2010) "Rating independent cable circuits in forced-ventilated cable tunnels." IEEE Transactions on Power Delivery, vol. 25, no. 4, pp. 2046-2053.

The following papers were under production/awaiting decisions at the point of submission of the thesis:

Pilgrim, J. A., Lewin, P. L., Waite, F. and Payne, D. "Calculations of the ampacity of high voltage cable circuits in partially and fully ventilated surface troughs using computational methods" Intended for submission to IEEE Transactions on Power Delivery.

Pilgrim, J. A., Lewin, P. L., Waite, F. and Payne, D. Investigation of thermal rating benefits from high voltage cables capable of higher conductor temperatures" Intended for submission to IEEE Transactions on Power Delivery.

References

[1] Operating instructions for the cat. no. 1600 5 bar pressure plate extractor. Technical report, Soilmoisture Equipment Corp, Santa Barbara, California, 2000.

[2] D. P. Hauser. System costs and the location of new generating plant in England and Wales. *Transactions of the Institute of British Geographers*, 54:101–121, November 1971.

[3] Cigré WG B1. Statistics of ac underground cable in power networks. *Electra*, 235:43–55, December 2007.

[4] J. D. Endacott. Underground power cables. *Philosophical Transactions of the Royal Society of London. Series A, Mathematical and Physical Sciences*, 275(1248):193–203, 1973.

[5] F. J. Miranda and H. W. Holdup. Development of 400kV cable in Great Britain. *IEEE Transactions on Power Apparatus and Systems*, 86(5):604–611, May 1967.

[6] J. Becker and C. Chatterjee. Development and evaluation of 400kV XLPE cable system. In *Proceedings of the 1996 IEEE Power Engineering Society Transmission and Distribution Conference*, pages 508–514, Los Angeles, September 1996. Institution of Electrical and Electronics Engineers.

[7] E. H. Ball, M. Reilly, D. J. Skipper, and J. B. Yates. Connecting Dinorwic pumped-storage power station to the grid system by 400kV underground cables. *Proceedings of the Institute of Electrical Engineers*, 126(3):239–245, March 1979.

[8] D. E. Williams. Natural and forced cooling of HV underground cables: UK practice. *Proceedings of the Institution of Electrical Engineers, Part A*, 3:137–161, 1982.

[9] C. K. Haswell. Thames cable tunnel. *Proceedings of the Institution of Civil Engineers*, 47:255, 1970.

[10] C. K. Haswell. Tunnel under the Severn and Wye estuaries. *Proceedings of the Institution of Civil Engineers*, 54(1):451–486, 1973.

[11] R. West and S. T. Larsen. Kentish town project [power cable laying]. Technical report, IEE Seminar, London, 2000.

[12] S. Sutton, R. Plath, and G. Schroder. The St Johns Wood - Elstree Experience - testing a 20km long 400kV XLPE insulated cable system after installation. In *Jicable '07*, Versailles, France, 2007.

[13] M. Knights, J. Mathews, and B. Marshall. Revealed: London's network of power tunnels. *Proceedings of ICE*, 144:121–127, 2001.

[14] G. Robinson. Ageing characteristics of paper-insulated power cables. *Power Engineering Journal*, 4(2):95–100, 1990.

[15] A. Motori, F. Sandrolini, and G. C. Montanari. A contribution to the study of ageing of XLPE insulated cables. *IEEE Transactions on Power Delivery*, 6(1):34–42, January 1991.

[16] I. L. Hosier, S. Reaud, A. S. Vaughan, and S. G. Swingler. Morphology, thermal, mechanical and electrical properties of propylene-based materials for cable applications. In *Proceedings of the 2008 IEEE International Symposium on Electrical Insulation*, pages 502–505, Vancouver, BC, June 2008.

[17] A. E. Kennelly. The current carrying capacity of electric cables submerged, buried or suspended in air. *The Electrical World*, 22:183, 1893.

[18] IEC. Electric cables - calculation of the current rating - part 1-1: Current rating equations (100% load factor) and calculation of losses - general. Technical report, International Electrotechnical Commission, 2006.

[19] G. J. Anders. *Rating of Electric Power Cables in Unfavourable Thermal Environment*. IEEE Press series on Power Engineering. John Wiley & Sons Inc, Hoboken, NJ, 1st edition, 2005.

[20] L. Heinhold. *Power Cables and their Application*. Siemens, 3rd edition, 1970.

[21] F. H. Buller. Artificial cooling of power cable. *Transactions of the American Institute of Electrical Engineers*, 71:634–641, August 1952.

[22] J. H. Neher and M. H. McGrath. The calculation of the temperature rise and load capability of cable systems. *Transactions of the American Institute of Electrical Engineers*, 76(3):752–772, October 1957.

[23] Cigré. The calculation of continuous ratings for forced-cooled cables. *Electra*, 66(4):59–84, October 1979.

[24] Cigré WG B1. Technical bulletin 272: Large conductors and composite screens. Technical Report TB272, Cigré, 2005.

[25] IEC. Electric cables - calculation of the current rating - part1-3: Current rating equations (100% load factor) and calculation of losses - current sharing between parallel single core cables and calculation of circulating current losses. Technical report, International Electrotechnical Commission, 2002.

[26] IEC. Electric Cables - Calculation of the Current Rating - Part 2: Thermal Resistance - Section 2.1 Calculation of thermal resistance. Technical report, International Electrotechnical Commission, 1994.

[27] IEC. Electric cables - Calculation of the Current Rating - Part 2: Thermal Resistance - Section 2.2 A method for calculating reduction factors for groups of cables in free air, protected from solar radiation. Technical report, International Electrotechnical Commission, 1995.

[28] D. J. Swaffield, P. L. Lewin, and S. J. Sutton. The use of finite element analysis modelling to improve the precision of high voltage cable ratings. In *The 10th INSUCON International Electrical Insulation Conference*, pages 155–161, Birmingham, UK, May 2006.

[29] IEC. Calculation of the cyclic and emergency current rating of cables: Part 2: Cyclic rating of cables greater than 18/30 (36) kv and emergency ratings for cables of all voltages. Technical Report IEC853-2, International Electrotechnical Commission, 1989.

[30] H. Goldenberg. The calculation of cyclic rating factors for cables laid direct or in ducts. *Proceedings of the Institution of Electrical Engineers Part C*, 104:154–166, 1957.

[31] G. J. Anders and M. A. El-Kady. Transient ratings of buried power cables, part 1: Historical perspective and mathematical method. *IEEE Transactions on Power Delivery*, 7(4):1724–1754, October 1992.

[32] C. R. Gane and D. R. Soulsby. Extensions to MOBEC, a model for externally-cooled buried cable circuits, to include cable straight joints. Technical Report TPRD/L/2243/N82, CERL, 1982.

[33] Cigré. Forced cooled cables - calculation of thermal transients and cyclic loads. *Electra*, 104, 1986.

[34] C. R. Gane, A. Hitchcock, J, and D. R. Soulsby. Digital computation methods for the determination of EHV cable transient ratings. In *Cigré 1980 Session*, number Paper 21-07, 1980.

[35] Cigré. Computer method for the calculation of the response of a single core cable to a step function thermal transient. *Electra*, 87:41–64, March 1983.

[36] N. Flatabø. Transient heat conduction problems in power cables solved by the finite element method. *IEEE Transactions on Power Apparatus and Systems*, 92(1):56–63, January 1973.

[37] D. J. Swaffield, P. L. Lewin, and M. LeBlanc. Investigation into the conservatism of high voltage cable ratings methods: A comparison between IEC 60287 and finite

element analysis. In *Proceedings of the XIVth International Symposium on High Voltage Engineering*, Beijing, China, 2005.

[38] J. J. Walker. Modelling of power cables for thermal finite element computer simulations. In *XVth International Symposium on High Voltage Engineering*, number T11-239, Ljubljana, Slovenia, August 2007.

[39] F. Aras, C. Oysu, and G. Yilmaz. An assessment of the methods for calculating ampacity of underground power cables. *Electric Power Components and Systems*, 33(10):1385–1402, October 2005.

[40] D. J. Swaffield, P. L. Lewin, D. Payne, and S. T. Larsen. Effects of modelling assumptions on the rating calculation for externally forced cooled high voltage cables. *IET Generation, Transmission and Distribution*, 3(5):496–507, 2009.

[41] G. J. Anders and H. S. Radhakrishna. Power cable thermal analysis with consideration of heat and moisture transfer. *IEEE Transactions on Power Delivery*, 3(4):1280–1288, October 1988.

[42] R. J. Preece and J. A. Hitchcock. Simultaneous diffusion of heat and moisture around a normally buried E.H.V. cable system. In *IEE Conference Publication 176*, pages 262–267, 1979.

[43] S. T. Larsen, C. L. Ong-Hall, and P. L. Stephenson. Cable rating methods applied to a real-time cable system monitor. In *Third International Conference on Power Cables and Accessories 10kV - 500kV*. IEE, November 1993.

[44] G. J. Anders. Advanced modelling techniques for dynamic feeder rating systems. *IEEE Transactions on Industrial Applications*, 39(3):619–626, May 2003.

[45] G. J. Anders and H. Brakelmann. Improvement in cable rating calculations by consideration of dependence of losses on temperature. *IEEE Transactions on Power Delivery*, 19(3):919–925, July 2004.

[46] G. Nokes. Optimising power transmission and distribution networks using optical fibre distributed temperature sensing systems. In *Proceedings of IEE Seminar on Asset Management of Cable Systems*, pages 4/1 – 4/9. IEE, February 2002.

[47] J. Downes and H. Y. Leung. Distributed temperature sensing: Worldwide power circuit monitoring applications. In *International Conference on Power Systems Technology*. IEEE, November 2004.

[48] J. A.. Williams, J. H. Cooper, T. J. Rodenbaugh, G. L. Smith, and F. Rorabaugh. Increasing cable rating by distributed fiber optic temperature monitoring and ampacity analysis. In *Transmission and Distribution Conference*, volume 1, pages 128–134, New Orleans, 1999.

[49] D. J. Swaffield, P. L. Lewin, and S. J. Sutton. Methods for rating directly buried high voltage cable circuits. *IET Generation, Transmission and Distribution*, 2(3):393–401, 2008.

[50] Cigré. Calculation of temperatures in ventilated cable tunnels. *Electra*, 143:38–59, 1992.

[51] B. M. Weedy and H. M. El-Zayyat. The current carrying capacity of power cables in tunnels. *IEEE Transactions on Power Apparatus and Systems*, 92(1):298–307, 1973.

[52] J. A. Giaro. Temperature rise of power cables in a gallery with forced ventilation. *Cigré*, (Paper 213), 1960.

[53] K. Kitagawa. Force cooling of power cables in Japan: Its studies and performance. *Cigré*, (Paper 213), 1964.

[54] G. J. Anders. Rating of cables on riser poles, in trays, in tunnels and shafts - a review. *IEEE Transactions on Power Delivery*, 11(1):3–11, January 1996.

[55] S. M. King. Heat transfer calculation methods for cables in tunnels. Technical Report 4-19, IEE Seminar, 2000.

[56] B. M. Weedy and H. M. El-Zayyat. Heat transfer from cables in tunnels and shafts. Paper to IEEE Summer Meeting, 1972.

[57] T. Endersby. Ratings of cables in tunnels-the hea(r)t of the matter. Technical report, IEE Seminar, 2000.

[58] P. Slaninka. External thermal resistance of air installed power cables. *Proceedings of the Institute of Electrical Engineers*, 116(9):1547–1552, September 1969.

[59] V. T. Morgan. External thermal resistance of aerial bundled cables. *IEE Proceedings Part C*, 140(2):65–72, March 1993.

[60] T. E. Hoover, W. W. Hitchcock, W. D. Kennedy, and J. W. Guinan. Computer simulation of subway environment. *Transportation Journal - Proceedings of the American Society of Civil Engineers*, 99(1):53–72, February 1973.

[61] B.M. Weedy. Thermal assessment of surface troughs for 400kv cables with air, backfill and water fillings. *Electric power systems research*, 16:53–61, 1989.

[62] P. L. Lewin, J. E. Theed, A. E. Davies, and S. T. Larsen. Methods for rating power cables buried in surface troughs. *IEE Proceedings: Generation, Transmission and Distribution*, 146(4):360–364, July 1999.

[63] E. J. Brooks, C. H. Gosling, and W. Holdup. Moisture control of cable environment with particular reference to surface troughs. *Proceedings of the Institution of Electrical Engineers*, 120(1):51–60, January 1973.

[64] G. T. Symm. External thermal resistance of buried cables and troughs. *Proceedings of the Institute of Electrical Engineers*, 116(10):1695–1698, October 1969.

[65] J. Karlstrand and G. Henning. Modern FEM tools - an example of cables installed in duct banks. In *Jicable'07 - 7th International Conference on Insulated Power Cables*, pages 664–669, Versailles, June 2007.

[66] J. R. Philip and D. A. de Vries. Moisture movement in porous materials under temperature gradients. *Transactions of the American Geophysical Union*, 38(2):222–232, April 1957.

[67] N. S. Hudi-Jahit. *Hydrological Effects and Avoidance of Thermal Runaway.* PhD thesis, Faculty of Engineering, Science and Mathematics, University of Southampton, July 2005.

[68] W. Powrie. *Soil Mechanics: Concepts and applications.* Spon Press, 1st edition, 1997.

[69] L. A. Ramdas. Some new instruments and experimental techniques developed in the agricultural meteorology section at Poona. *Journal of Scientific and Industrial Research*, 7:16–29, 1948.

[70] K. Mochlinski. Assessing ground ambient temperature. *Electrical Times*, pages 42–46, 9th July 1971.

[71] A. G. Milne and K. Mochlinski. Characteristics of soil affecting cable ratings. *Proceedings of the Institution of Electrical Engineers*, 111(5):1017–1039, May 1964.

[72] F. Donazzi, E. Occhini, and A. Seppi. Soil thermal and hydrological characteristics in designing underground cables. *Proceedings of the Institution of Electrical Engineers*, 126(6):506–516, 1979.

[73] A. N. Arman, D. M. Cherry, L. Gosland, and P. M. Hollingsworth. Influence of soil moisture migration on power rating of cables in h.v. transmission systems. *Proceedings of the Institution of Electrical Engineers*, 111(5):1000–1016, 1964.

[74] H. Rennie, K. Turner, and D. Sollitt. Auckland power supply failure 1998, the report of the ministerial inquiry into the Auckland power supply failure. Technical report, Ministry of Economic Development, New Zealand, Auckland, New Zealand, June 1998.

[75] T. J. Marshall and J. W. Holmes. *Soil Physics.* Cambridge University Press, 1979.

[76] P. C. Carman. Properties of capillary held liquids. *Journal of Physical Chemistry*, 57:56–64, 1953.

[77] D. A. Rose. Water movement in porous materials: Part 1 isothermal vapour transfer. *British Journal of Applied Physics*, 14:256–262, 1963.

[78] D. A. Rose. Water movement in porous materials: Part 2 the separation of the components of water movement. *British Journal of Applied Physics*, 14:491–496, 1963.

[79] S. A. Taylor and J. W. Cary. Linear equations for the simultaneous flow of matter and energy in a continuous soil system. *Soil Science Society of America Proceedings*, 28:167–172, 1964.

[80] D. Hillel. *Fundamentals of Soil Physics*. Academic Press Inc, 1980.

[81] D. K. Cassel, D. R. Nielsen, and J. W. Biggar. Soil water movement in response to temperature gradient. *Soil Science Society of America Proceedings*, 33:493–500, 1969.

[82] V. Dakshanamurthy and D. G. Fredlund. A mathematical model for predicting moisture flow in an unsaturated soil under hydraulic and temperature gradient. *Water Resources Research*, 17:714–722, 1981.

[83] P. C. Milly. Moisture and heat transport in hysteretic inhomogeneous porous media: A matric head formulation and a numerical model. *Water Resources Research*, 18(3):489–498, 1982.

[84] M. Sophocleous. Analysis of water and heat flow in unsaturated-saturated porous media. *Water Resources Research*, 15(5):1195–1206, 1979.

[85] J. G. Hartley and W. Z. Black. Transient simultaneous heat and mass transfer in moist unsaturated soils. *Transactions of the ASME*, 103:376–382, 1981.

[86] G. Koopmans, G. M. L. M. van de Wiel, L. J. M. van Loon, and C. L. Palland. Soil physical route survey and cable thermal design procedure. *IEE Proceedings Part C*, 136:341–346, 1989.

[87] D. S. Freitas, A. T. Prata, and A. J. de Lima. Thermal performance of underground power cables with constant and cyclic currents in presence of moisture migration in the surrounding soil. *IEEE Transactions on Power Delivery*, 11(3):1159–1170, 1996.

[88] C. Venkatramaiah. *Geotechnical Engineering*. New Age International, 2006.

[89] R. J. Wiseman and R. W. Burell. Soil thermal characteristics in relation to underground power cables. *AIEE Committee Report*, 1:792–815, 1960.

[90] D. G. Fredlund and A. Xing. Equations for the soil-water characteristic curve. *Canadian Geotechnical Journal*, 31:521–531, 1994.

[91] H. S. Radhakrishna. Heat flow and moisture migration in cable backfills. Technical Report Ontario Hydro Research Quarterly, 2nd quarter, Ontario Hydro, 1968.

[92] C. A. Long. *Essential Heat Transfer*. Pearson Education Limited, Harlow, England, 1st edition, 1999.

[93] A. Klute. *Laboratory Measurement of Hydraulic Conductivity of Saturated Soil*. American Society of Agronomy, 3 edition, 1973.

[94] D. G. Fredlund, A. Xing, and S. Huang. Predicting the permeability function for unsaturated soil using the soil water characteristic curve. *Canadian Geotechnical Journal*, 31:533–546, 1994.

[95] R. J. Preece. The measurement and calculation of physical properties of a cable bedding sand: Part 1: Suction and hydraulic conductivity. Technical Report RD/L/N/230/74, Central Electricity Research Laboratories, 1975.

[96] B. A. Kimball, R. D. Jackson, R. J. Reginato, F. S. Nakayama, and S. B. Idso. Comparison of field-measures and calculated soil heat fluxes. *Soil Science Society of America Journal*, 40:18–24, 1976.

[97] IEEE Power Engineering Society. IEEE std 442:1981 IEEE guide for soil thermal resistivity measurements, 1981.

[98] O. Johansen. *Thermal conductivity of soils*. PhD thesis, Trondheim, Norway, 1975.

[99] V. R. Tarnawski, W. H. Leong, and K. L. Bristow. Developing a temperature dependent kersten function for soil thermal conducitivity. *International Journal of Energy Research*, 24:1335–1350, 2000.

[100] O. Farouki. Thermal properties of soils. Technical Report CRREL Monograph 81-1, US Army Corps of Engineers, 1981.

[101] V. Gnielinski. New equations for heat and mass transfer in turbulent pipe and channel flow. *International Chemical Engineering*, 16:359–368, 1976.

[102] J. A. Pilgrim, D. J. Swaffield, P. L. Lewin, S. T. Larsen, and D. Payne. Assessment of the impact of joint bays on the ampacity of high voltage cable circuits. *IEEE Transactions on Power Delivery*, 24(3):1029–36, July 2009.

[103] M. M. Abdel-Aziz and H. Riege. Thermal analysis of cable joints. In *Second International Conference on Progress in Cables and Overhead Lines For 220 KV and above*, pages 268–272, London, September 1979.

[104] B. M. Weedy and J. P. Perkins. Steady-state thermal analysis of a 400kV-cable through joint. *Proceedings of the Institute of Electrical Engineers*, 114(1):109–115, January 1967.

[105] S. Nakamura, S. Morooka, and K. Kawaski. Conductor temperature monitoring system in underground power transmission XLPE cable joints. *IEEE Transactions on Power Delivery*, 7(4):1688–1697, 1992.

[106] C. R. Gane and D. R. Soulsby. A numerical scheme for predicting transient temperature distributions in forced-cooled, buried cable joint assemblies. In *Proceedings of the 2nd International Conference on Numerical Methods in Thermal Problems*, Venice, July 1981.

[107] Cigré. The steady state thermal behaviour of accessories for cooled cable systems. *Electra*, 128:64–98, 1990.

[108] A. E. Crockett and G. Yates. Cooling of accessories of high voltage cable systems. In *2nd International Conference on Progress in Cables and Overhead Lines for 220kV and above*, pages 256–261. Institution of Electrical Engineers, September 1979.

[109] D. Payne and S.J. Sutton. National Grid R&D project proposal form - ratings of cables in tunnels. Technical report, National Grid plc, June 2006.

[110] P. L. Stephenson. MORDEN5 - an enhanced version of the MORDEN cable tunnel program. Technical report, National Power, March 1993.

[111] M. Griebel, T. Dornseifer, and T. Neunhoeffer. *Numerical Simulation in Fluid Dynamics*. Society for Industrial and Applied Mathematics, 1998.

[112] J. H. Ferziger and M. Perić. *Computational Methods for Fluid Dynamics*. Springer, 2002.

[113] B. E. Launder and D. B. Spalding. The numerical computation of turbulent flows. *Computer methods in applied mechanics and engineering*, 3:269–289, 1974.

[114] S. Kakaç and Y. Yener. *Convective Heat Transfer (Second edition)*. CRC Press, 1994.

[115] S. Kakaç, R. K. Shah, and W. Aung. *Handbook of Single-Phase Convective Heat Transfer*. John Wiley and Sons, 1987.

[116] W. A. Gray and R. Muller. *Engineering Calculations in Radiative Heat Transfer*. Pergamon Press, 1974.

[117] E. M. Sparrow and R. D Cess. *Radiation heat transfer*. Wadsworth Publishing, 1966.

[118] Cigré. Calculation of temperatures in ventilated cable tunnels - part 2. *Electra*, 144:97–105, October 1992.

[119] J. A. Pilgrim, D. J. Swaffield, P. L. Lewin, S. T. Larsen, D. Payne, and F. Waite. Rating independent cable circuits in forced ventilated cable tunnels. *IEEE Transactions on Power Delivery*, 25(4):2046–2053, October 2009.

[120] G.J. Anders, M. Coates, and M. Chaaban. Ampacity calculations for cables in shallow troughs. *IEEE Transactions on Power Delivery*, 25(4):2064–2072, October 2010.